METHOD OF MOMENTS ANALYSIS OF MICROSTRIP ANTENNAS IN CYLINDRICALLY STRATIFIED MEDIA USING CLOSED-FORM GREEN'S FUNCTIONS

A DISSERTATION SUBMITTED TO

THE DEPARTMENT OF ELECTRICAL AND ELECTRONICS

ENGINEERING

AND THE GRADUATE SCHOOL OF ENGINEERING AND SCIENCES

OF BILKENT UNIVERSITY

IN PARTIAL FULFILLMENT OF THE REQUIREMENTS

FOR THE DEGREE OF

DOCTOR OF PHILOSOPHY

By

Şakir Karan

July, 2012

I certify that I have read this thesis and that in my opinion it is fully adequate, in scope and in quality, as a dissertation for the degree of doctor of philosophy.

Assoc. Prof. Dr. Vakur B. Ertürk (Advisor)

I certify that I have read this thesis and that in my opinion it is fully adequate, in scope and in quality, as a dissertation for the degree of doctor of philosophy.

Prof. Dr. Ayhan Altıntaş

I certify that I have read this thesis and that in my opinion it is fully adequate, in scope and in quality, as a dissertation for the degree of doctor of philosophy.

Prof. Dr. Gülbin Dural

I certify that I have read this thesis and that in my opinion it is fully adequate, in scope and in quality, as a dissertation for the degree of doctor of philosophy.

Assoc. Prof. Dr. Lale Alatan

I certify that I have read this thesis and that in my opinion it is fully adequate, in scope and in quality, as a dissertation for the degree of doctor of philosophy.

Assoc. Prof. Dr. M. Özgür Oktel

Approved for the Graduate School of Engineering and Sciences:

Prof. Dr. Levent Onural
Director of Graduate School of Engineering and Sciences

ABSTRACT

METHOD OF MOMENTS ANALYSIS OF MICROSTRIP ANTENNAS IN CYLINDRICALLY STRATIFIED MEDIA USING CLOSED-FORM GREEN'S FUNCTIONS

Şakir Karan
Ph.D in Electrical and Electronics Engineering
Supervisor: Assoc. Prof. Dr. Vakur B. Ertürk
July, 2012

Numerical methods based on Method of Moments (MoM) have been widely used for the design and analysis of planar microstrip antennas/arrays and printed circuits for various applications for many years. On the other hand, although the design and analysis of similar antennas/arrays and printed circuits on cylindrical structures are of great interest for many military, civil and commercial applications, their MoM-based analysis suffers from the efficiency and accuracy problems related with the evaluation of the Green's function representations which constitute the kernel of the regarding integral equations. In this dissertation, novel closed-form Green's function (CFGF) representations for cylindrically stratified media, which can be used as the kernel of an electric field integral equation (EFIE) are developed. The developed CFGF representations are used in a hybrid MoM/Green's function solution procedure.

In the course of obtaining the CFGF representations, first the conventional spectral domain Green's function representations are modified so that all the Hankel (Bessel) functions are written in the form of ratio with another Hankel (Bessel) function. Furthermore, Debye representations for the ratio terms are used when necessary in order to avoid the possible overflow and underflow problems. Acceleration techniques that are present in the literature are implemented to further increase the efficiency and accuracy of the summation and integration. Once the acceleration techniques are performed, the resultant expressions are transformed to the space domain in the form of discrete complex images (DCIM) with the aid of the generalized pencil of function (GPOF) method and the final CFGF expressions are obtained by performing the resultant space domain integrals analytically.

The novel CFGF expressions are used in conjunction with MoM for the investigation of microstrip antennas on cylindrically stratified media. The singular terms in mutual impedance calculations are treated analytically. The probe-fed excitation is modeled by implementing an attachment mode that is consistent with the current modes that are used to expand the induced current on the patches. In the course of modeling the probe-fed excitation, the probe-related components of CFGF representations are also derived for the first time in the literature and MoM formulation is given in the presence of an attachment mode. Consequently, several microstrip antennas and two antenna arrays are investigated using a hybrid MoM/Green's function technique that use the CFGF representations developed in this dissertation. Numerical results in the form of input impedance of microstrip antennas in the presence of several layers as well as the mutual coupling between two microstrip antennas are presented and compared with the available results in the literature and the results obtained from the CST Microwave Studio.

Keywords: Cylindrically stratified media, closed-form Green's function representations, discrete complex image method, generalized pencil of function method, Method of Moments, input impedance, mutual coupling.

ÖZET

KAPALI FORMDA GREEN'İN FONKSİYONLARINI KULLANARAK SİLİNDİRİK KATMANLI YÜZEYLERDE MİKROŞERİT ANTENLERİN MOMENTLER METODU İLE ANALİZİ

Şakir Karan
Elektrik ve Elektronik Mühendisliği, Doktora
Tez Yöneticisi: Vakur B. Ertürk
Temmuz, 2012

Uzun yıllar boyunca değişik uygulamalar için düzlemsel mikroşerit anten/dizi ve devrelerin analiz ve tasarım çalışmaları için Momentler Metodu'na dayalı nümerik metodlar kullanılmıştır. Öte yandan benzer anten/dizi ve devrelerin silindirik yapılardaki analiz ve tasarım çalışmaları birçok askeri, sivil ve ticari uygulamalar için ilgi odağı olsa da Momentler Metod'una dayalı analizler ilgili integral denkleminin çekirdeğinde yer alan Green'in fonksiyonunun doğruluğundan ve etkinliğinden yoksundur. Bu doktora tezinde, elektrik alan integral denkleminin çekirdeğini oluşturabilecek yeni kapalı-formda Green'in fonksiyonları elde edilmektedir. Elde edilen kapalı-formdaki ifadeler birleşik Momentler Metodu/ Green'in fonksiyonu çözümünde kullanılmıştır.

Kapalı-formdaki ifadeleri elde ederken, öncelikle izgel uzaydaki Green'in fonksiyonları değiştirilerek her Hankel (Bessel) fonksiyonu bir diğer Hankel (Bessel) fonksiyonu ile oran şeklinde yazılmıştır. Ayrıca, aşırı azalan ve artan problemlerini çözmek için oran terimleri için Debye ifadeleri kullanılmıştır. Toplamın ve integralin etkinliğini ve doğruluğunu arttırmak için literatürde hazır olan hızlandırma teknikleri kullanılmıştır. Hızlandırma teknikleri uygulandıktan sonra uzamsal uzaydaki ifadeler genelleştirilmiş kalem fonksiyonu metodu ile ayrık kompleks imgeler şekline dönmüştür ve en son kapalı-formdaki ifade uzamsal uzaydaki integrallerin analitik olarak alınması ile elde edilmiştir.

Yeni kapalı-formdaki ifadeler mikroşerit antenlerin silindirik katmanlı ortamda analizi için Momentler Metodu ile kullanılmıştır. Karşılıklı etkileşim hesabında tekil ifadeler analitik olarak hesaplanmıştır. Prob ile beslemeyi modellemek için yama anten üzerindeki akımları açmak için kullanılan akım modları ile uyumlu ek

akım modu tanımlanmıştır. Prob ile beslemeyi modellemek için kullanılan prob ile ilgili terimler literatürde ilk defa verilmiştir ve Momentler Metodu formulasyonu ek akım modunun varlığında tanımlanmıştır. Sonuç olarak bu doktora tezinde elde edilen kapalı-formdaki Green'in fonksiyonları kullanılarak birleşik Momentler Metodu/Green'in fonksiyonu yardımı ile değişik anten ve ikili dizi antenler incelenmiştir. Nümerik sonuç olarak birkaç katmanın olduğu durumda şerit antenlerin giriş empedansları ve iki şerit anten arasındaki karşılıklı etkiletişim sonuçları verilmiş, literatürde yer alan ve CST Microwave Studio programından elde edilen sonuçlar ile karşılaştırılmıştır.

Anahtar sözcükler: Silindirik katmanlı ortamlar, kapalı-formda Green'in fonksiyonu gösterimleri, ayrık kompleks imge metodu, genelleştirilmiş kalem fonksiyonu metodu, Momentler Metodu, giriş empedansı, karşılıklı etkileşim.

To the spirit of my father

To my son

To my wife

To my mother

who are

the answers to all my how's and why's

Acknowledgement

I would like to express my sincere gratitude to my advisor Assoc. Prof. Dr. Vakur B. Ertürk for his instructive comments and continuing support in the supervision of the dissertation.

I would like to express my special thanks and gratitude to Prof. Dr. Ayhan Altıntaş , Prof. Dr. Gülbin Dural and Assoc. Prof. Dr. Lale Alatan for showing keen interest to the subject matter, their useful comments during the study and accepting to read and review the dissertation.

I would like to thank to Assoc. Prof. Dr. M. Özgür Oktel for showing keen interest to the subject matter and accepting to read and review the dissertation.

I would like to especially thank to my dear wife, Sema, for her endless love and patience throughout the years of this study. I hope she will accept my apologies for sometimes leaving her alone with the responsibility of our little child, Kaan. Also thanks to Kaan for leaving the keyboard in one piece during the typing of this dissertation.

Finally I would like to thank Aselsan Inc. for letting me to involve in this Ph.D. study.

Contents

List of Figures

List of Tables

Chapter 1

Introduction

Numerical methods based on Method of Moments (MoM) have been widely used for the design and analysis of planar microstrip antennas/arrays and printed circuits for various applications for many years [1]-[2]. In general the structures of interest are open geometries. Hence, an integral equation (IE) is usually set up and the closed-form Green's function (CFGF) representations are used as the kernel of this IE [3]-[7]. Then the IE is solved using the MoM based algorithms. On the other hand, although the design and analysis of similar antennas/arrays and printed circuits on cylindrical structures are of great interest for many military, civil and commercial applications, their MoM based analysis suffers from the efficiency and accuracy problems related with the evaluation of the available Green's function representations that can be used for cylindrically stratified media.

A number of studies regarding the Green's functions in cylindrically stratified media have been reported before [8]-[25]. More references on the conventional spectral domain and asymptotic Green's function representations particularly for single layer dielectric deposited on a perfectly conducting cylinder can be found in [15] and [16]. However, a vast majority of the above mentioned Green's function representations (derived for cylindrically stratified media) are not in closed form. Besides, convergence of these expressions become an important issue from the accuracy and efficiency point of views for antenna and/or mutual coupling problems. On the other hand, most of the studies on the subject of

CFGF for cylindrically stratified media have the CFGF expressions that are valid when the source and observation (or field) points are on different radial distances from the axis of the cylinder [17]-[21]. Therefore, these expressions are useful for radiation/scattering problems, provided that the current distribution on the radiating structure is known. However, they cannot be used in conjunction with a MoM based algorithm to find the input impedance of an antenna and/or the mutual coupling between antennas.

Closed-form expressions that can be used in MoM-based algorithms to investigate cylindrically conformal microstrip antennas and arrays are given in [22]. However, provided closed-from expressions are for the impedance matrix elements and the voltage vector elements (using entire domain basis functions) rather than the Green's functions. In [23], CFGF expressions to be used in the mixed potential integral equation (MPIE) have been presented. Although, these CFGF expressions (provided in [23]) are valid when the source and the observation points are located at the same radial distance from the axis of the cylinder, the final expressions are not valid along the axial line (defined as $\rho = \rho'$ and $\phi = \phi'$) as well as on a certain region of the cylinder surface where the source and field points are very close to each other (will be referred to as the "source region" thereafter). Recently, novel CFGF representations that can be used in MoM-based algorithms for the solution of an IE have been presented in [25]-[28] to rigorously analyze antenna problems on cylindrically stratified media. However, presented CFGF representations in these studies are not valid on the source region. Therefore, an alternative representation must be used for the evaluation of the MoM impedance matrix entries that represent the interaction of two current modes when they partially or fully overlap with each other.

In this dissertation, an efficient and accurate space domain hybrid MoM/Green's function method [29]-[31] is developed, which combines the MoM with the novel CFGF representations provided again in this dissertation. As the first step of this method, an electric field integral equation (EFIE) is formulated that uses the aforementioned novel CFGF representations as its kernel. Basically, for a probe-fed microstrip patch antenna element on a dielectric coated perfect

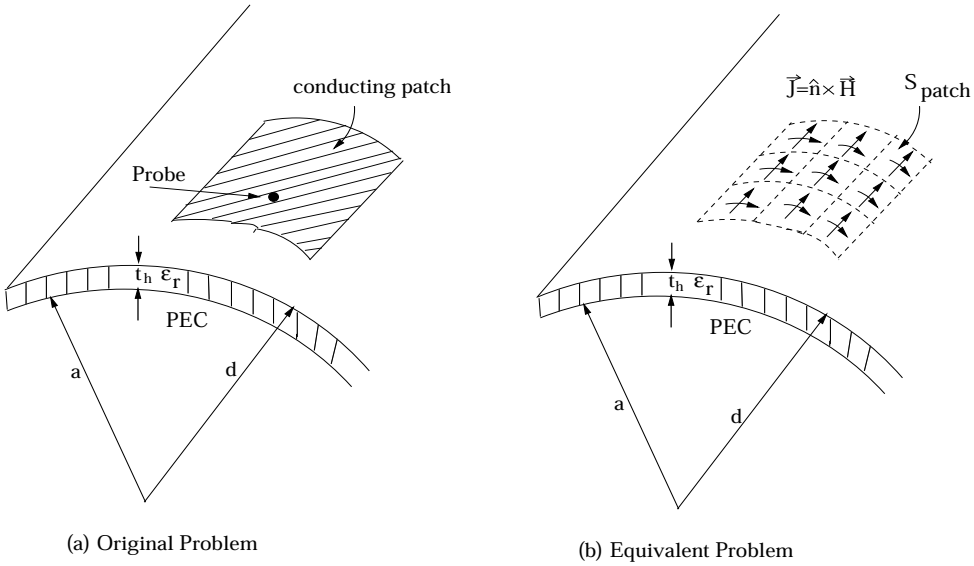

Figure 1.1: Equivalence principle

electric conducting (PEC) circular cylinder (see Fig. 1.1(a)), an equivalent problem (see Fig. 1.1(b)) is formed such that the conducting patch is replaced with the unknown equivalent induced currents making use of the surface equivalence principle. The total electric field, $\underline{E}(\bar{r})$, is written as

$$\underline{E}(\bar{r}) = \underline{E}^i(\bar{r}) + \underline{E}^s(\bar{r}) \tag{1.1}$$

where $\underline{E}^i(\bar{r})$ is the field produced by a known probe current density $\underline{J}^i(\bar{r}\,')$ in the presence of a dielectric coated PEC cylinder and its generic form is given by

$$\underline{E}^i(\bar{r}) = \int\int\int_{V_{source}} \underline{\underline{G}}(\bar{r}/\bar{r}\,') \cdot \underline{J}^i(\bar{r}\,')dv' \tag{1.2}$$

where $\underline{\underline{G}}(\bar{r}/\bar{r}\,')$ denotes the dyadic form of the CFGF representations involving the probe-related components with primed and unprimed coordinates representing the source and observation points, respectively. Similarly, $\underline{E}^s(\bar{r})$ is the scattered field and its generic form can be expressed as

$$\underline{E}^s(\bar{r}) = \int\int_{S_{antenna}} \underline{\underline{G}}(\bar{r}/\bar{r}\,') \cdot \underline{J}^s(\bar{r}\,')ds' \tag{1.3}$$

where $\underline{\underline{G}}(\bar{r}/\bar{r}\,')$ denotes the dyadic form of the CFGF representations involving the tangential components and $\underline{J}^s(\bar{r}\,')$ is the unknown induced current to be

determined at the end of the MoM procedure. An EFIE is established by setting the tangential components of the total electric field (1.1) to zero on the conducting surface of the patches leading to

$$\hat{n} \times \underline{E}(\bar{r}) = \hat{n} \times [\underline{E}^i(\bar{r}) + \underline{E}^s(\bar{r})] = 0 \qquad \text{on} \qquad S_{\text{patch}} \tag{1.4}$$

where $\hat{n}$ is $\hat{\rho}$ for this problem.

The second step is the MoM solution procedure and starts by expanding the induced current $\underline{J}_s$ on each conducting patch shown in Fig. 1.1(a) in terms of a finite set of subsectional basis functions. For each patch $\underline{J}_s$ is expanded as follows:

$$\underline{J}_s(\bar{r}') = \sum_{n=1}^{N} a_n \underline{J}_n(\bar{r}') \tag{1.5}$$

where

$$\underline{J}_n(\bar{r}') = \begin{cases} f_p(\bar{r}')\hat{z}, & p = 1, ..., P \quad \text{on each patch} \\ g_k(\bar{r}')\hat{\phi}, & k = 1, ..., K \quad \text{on each patch} \end{cases} \tag{1.6}$$

with $N = P + K$ as shown Fig. 1.1(b). In (1.5) a_n's are the unknown coefficients to be solved at the end of the MoM procedure, and $\underline{J}_n(\bar{r}') \neq 0$ only if $\bar{r} \in S_n$; $U_{n=1}^{N} S_n = S_{\text{patch}_i}$; $i = 1, ...,$ # of patches.

First substituting (1.2) and (1.3) into (1.4) and then substituting (1.5) and (1.6) into the resultant equation, a single equation with N unknowns (for each patch) can be obtained. Using a set of weighting (testing) functions denoted by $w_m(\bar{r}_m)$ $(m = 1, ..., N)$, the following matrix equation is obtained

$$\underline{\underline{Z}}\ \underline{I} = \underline{V} \tag{1.7}$$

where

$$Z_{mn} = \int\int_{S_m} ds_m w_{m_u}(\bar{r}_m) \int\int_{S_n} ds_n G_{uv}(\bar{r}_m / \bar{r}_n) J_{n_v}(\bar{r}_n) \tag{1.8}$$

$$I_n = a_n \tag{1.9}$$

$$V_m = -\int\int_{S_m} ds_m w_m \cdot \underline{E}^i(\bar{r}_m) \tag{1.10}$$

with $m, n = 1, ..., N$. In this dissertation, piecewise sinusoidal (PWS) functions are used for both expansion and testing functions. Because testing and expansion functions are selected to be the same, this testing method is called Galerkin's method.

The efficiency and accuracy, which are the major issues in this hybrid method, are mainly determined by the computation of the Green's function representations which should be accurate for arbitrary source and observation locations. Therefore, we provide novel CFGF representations to be used as the kernel of the EFIE. The derivation of these novel CFGF representations starts by expressing the conventional spectral domain Green's function representations in a different form by (i) recognizing the Fourier transform based relations between the spectral domain variables and the space domain variables, and (ii) writing the special cylindrical functions, such as Bessel and Hankel functions, in the form of ratios (i.e., each Hankel (Bessel) function is written in ratio form with another Hankel (Bessel) function). Furthermore, these ratios are evaluated directly and Debye representation (given in Appendix A) of these special functions is used when necessary during the evaluation of the ratios. Therefore, possible overflow/underflow problems in the numerical calculations of these functions are completely avoided. Then, the summation over the cylindrical eigenmodes, n, is performed in the spectral domain. Numerical evaluation of large n values that appear in the orders of special functions (Hankel and Bessel functions), especially for electrically large cylinders, do not create numerical problems due to the aforementioned way of expressing the spectral domain Green functions and due to Debye approximations used when necessary. Furthermore, acceleration techniques that are presented in [23] are implemented to further increase the efficiency and accuracy of the summation and integration. Once the acceleration techniques are performed, the Fourier integral over k_z is taken using discrete complex image method (DCIM) with the help of the generalized pencil of function (GPOF) method [32]. Note that some modifications are preformed during the implementation of the GPOF method (compared to ones presented in [17], [18], [25], [27]) and it is critical in order to obtain accurate results in particular along the axial line of the cylinder and the self term evaluation of the MoM impedance matrix. Thus, the region

of field points (with respect to the source point), where the novel CFGF representations proposed in this study remain accurate, is significantly wider than that of the previously available CFGF representations (including [27]). Briefly, in addition to cases where source and observation points are located at different radial distances from the axis of the cylinder, the proposed CFGF expressions are valid for almost all possible source and field points that lie on the same radial distance (such as the air-dielectric, dielectric-dielectric interfaces). The latter region includes the situation where both the source and field points are located on the axial line ($\rho = \rho'$ and $\phi = \phi'$) of the cylinder that exhibits a logarithmic singularity due to the argument of the Hankel function, and the source region where two current modes can partially or fully overlap with each other that exhibits a singularity during the MoM analysis. It should be emphasized that the final CFGF representations presented in this dissertation are slightly different than the ones presented in [27] in order to handle these singularities, and to avoid the necessity of an alternative representation in the MoM analysis of microstrip antennas/arrays on cylindrically stratified media.

Because the microstrip antennas are assumed to be fed via a probe in the radial direction, the probe-fed excitation is modeled by implementing an attachment mode that is consistent with the PWS current modes that are used to expand the induced current on the patches. In the course of modeling the probe-fed excitation, the probe-related components of CFGF representations ($G_{z\rho}$, $G_{\rho z}$, $G_{\phi\rho}$, $G_{\rho\phi}$) are also derived for the first time in the literature. Numerical results in the form of the input impedance of various microstrip antennas in the presence of several layers as well as the mutual coupling between two microstrip antennas are presented by comparing the results with the available results in the literature as well as the results obtained from the CST Microwave Studio which is an available commercial computer-aided design (CAD) tool.

The organization of this dissertation is as follows: In Chapter 2, the spectral domain Green's function representations due to electric sources are derived for the tangential and probe-related components. When $\rho = \rho'$ large n values are needed in the evaluation of the summation for the cylindrical eigenmodes in the spectral domain Green's function representations. Therefore, in order to overcome

possible numerical problems in the evaluation of Hankel and Bessel functions for large n values, starting with the reflection and transmission matrices, the spectral domain Green's function representations are rewritten in such a form that all the Hankel (Bessel) functions are in the form of ratios with another Hankel (Bessel) function. Then, Debye representations are defined for the ratio terms using the Debye expressions of the Hankel and Bessel functions given in the literature and used when necessary. Chapter 3 deals with the spectral domain Green's function representations in detail and they are written in a more compact form. In this part, to accelerate the summation, an envelope extraction with respect to n is applied using the series expansion of the zeroth-order Hankel function. Besides, in order to have a decaying spectral expression, an envelope extraction with respect to k_z is also applied. In this chapter, the Green's function representations for both the tangential and probe-related components are written in the most efficient form which can be used for all possible ρ and ρ' values. The formulation (valid when $\rho = \rho'$) for the probe-related terms is first given in this dissertation. In Chapter 4, the integration path is defined in order to obtain space domain Green's function representations from the spectral domain counterparts. The implementation of the GPOF method, which is used to obtain closed-form expressions in the space domain, is also given in this chapter. Mutual impedance calculations for both the tangential and probe-related components are given in Chapter 5. In the mutual impedance calculations, the derivatives on the Green's function representations are transferred onto the current modes in order to work with less singular terms. The spectral domain singularity which is due to the argument of the zeroth-order Hankel function is solved using the small argument approximation of the Hankel function. Similarly, the space domain singularity which occurs when the source and field points are on top each other is solved analytically for the mutual impedance calculations. Since probe-fed antennas are analyzed in this dissertation, the MoM formulation is given with an attachment mode definition used to model the continuity of the current form probe to the patch antenna in Chapter 6. The mutual impedance formulation related with the attachment mode is given in this chapter including the solutions for all singular terms. Evaluation of the input impedance of a probe-fed patch antenna and the mutual coupling between two probe-fed patch antennas in the presence of the attachment mode for

cylindrically stratified media are explained and numerical results in the form of the input impedance of several microstrip patch antennas and the mutual coupling between two antennas are presented in Chapter 7 which show the accuracy of both the CFGF representations and the hybrid MoM/Green's function technique with the attachment mode. Concluding remarks are given in Chapter 8. Finally, six Appendices are provided. In Appendix A, Debye representations of the ratio terms obtained using the Debye expressions available in the literature are given. In Appendix B, a fairly detailed explanation about the GPOF method, which is used to obtain closed-form Green's function representation from the spectral domain samples, is given. The details of the mutual impedance calculations related with zz, $z\phi$ and $\phi\phi$ cases are given in Appendices C, D and E, respectively. The two-fold mutual impedance formulations obtained from four-fold integrals are given with the special solutions of the most singular mutual impedance terms (self and overlapping) for the tangential components. In Appendix F, the even and odd properties of Green's functions and mutual impedance expressions are given since these even and odd properties are important in the efficient evaluation of the closed-form Green's function representations and in filling the impedance matrix and voltage vector in the MoM analysis of antennas. Furthermore, throughout this dissertation, G is used for the space domain Green's function, whereas $\tilde{G}$ denotes its spectral domain counterpart. The time dependence of $e^{j\omega t}$ is used, where $\omega = 2\pi f$ and f is the operating frequency. Also in this dissertation, all the Green's functions are due to an electric source.

Chapter 2

Spectral Domain Green's Function Representations

In the first two sections of this chapter, the spectral domain Green's function expressions given in [14], [17] and [18] for $\rho \neq \rho'$ are briefly summarized because the same expressions are used in the mutual impedance calculations for $\rho = \rho'$ case after they are modified in the third section of this chapter. The details of the formulation given in the first two sections of this chapter can be found in [14] and [17]-[18].

The general geometry of a cylindrically stratified media is illustrated in Fig. 2.1 where the geometry is assumed to be infinite in the z direction. The point source is located at (ρ', ϕ', z') in the source layer $i = j$ and the field point is located at (ρ, ϕ, z) in the field layer $i = m$ where m can be any layer. As shown in Fig. 2.1, layers may vary in their electric and magnetic properties (ϵ_i,μ_i) as well as their thicknesses. Moreover, a perfect electric conductor (PEC) or a perfect magnetic conductor (PMC) can be considered as the innermost or the outermost layer.

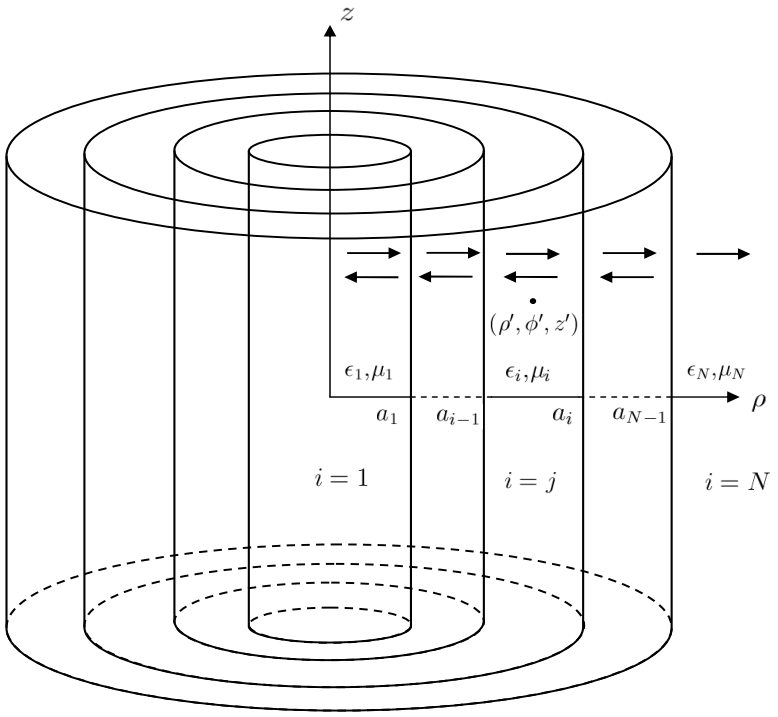

Figure 2.1: General geometry of a cylindrically stratified media and propagation of waves due to a point source in it

2.1 Spectral Domain Field Expressions Due to an Electric Source

The current of a dipole can be written in the spectral domain as [18]

$$\underline{J}(k_z) = I\ell\hat{\alpha}e^{jk_z z'}\frac{\delta(\rho-\rho')}{\rho}\delta(\phi-\phi') \tag{2.1}$$

where $I\ell$ is the current moment, $\hat{\alpha}$ is the unit direction which shows the direction of the current and z' is the location of the dipole along the z-axis. The field expression in the field point is the sum of the incoming and outgoing waves formed by the multiple reflections from the inner and outer boundaries as shown in Fig. 2.1. The incoming and outgoing waves can be expressed as the sum of standing and outgoing waves which are represented by the first-kind Bessel and second-kind Hankel functions, respectively. The z component of the fields in the

field point are given in [14] and [17]-[18] as

$$\begin{bmatrix} \tilde{E}_z \\ \tilde{H}_z \end{bmatrix} = -\frac{I\ell e^{jk_z z'}}{4w} \sum_{n=-\infty}^{\infty} e^{jn(\phi-\phi')} \underline{\underline{F_n}} \underline{S}_{n_j}. \tag{2.2}$$

For an electric source, $\underline{S}_{n_j}$ used in (2.2), is a 2×1 matrix operator given by

$$\underline{S}_{n_j} = \begin{bmatrix} \frac{1}{\epsilon_j}(k_j^2 \hat{a}_z + jk_z \nabla')\hat{\alpha} \\ -jw\hat{\alpha}(\hat{a}_z \times \nabla') \end{bmatrix} \tag{2.3}$$

and acts to its left-hand side. In (2.3) ∇' is defined to be

$$\nabla' = \hat{a}_\rho \frac{\partial}{\partial \rho'} - \hat{a}_\phi \frac{jn}{\rho'} + \hat{a}_z jk_z. \tag{2.4}$$

In (2.2) $\underline{\underline{F_n}}$ is a 2×2 matrix, when the field and source layers are the same ($m = j$) $\underline{\underline{F_n}}$ is defined as

$$\begin{aligned} \underline{\underline{F_n}} &= [J_n(k_{\rho_j}\rho)\underline{\underline{I}} + H_n^{(2)}(k_{\rho_j}\rho)\underline{\underline{\tilde{R}}}_{j,j-1}]\underline{\underline{\tilde{M}}}_{j-}[H_n^{(2)}(k_{\rho_j}\rho')\underline{\underline{I}} + J_n(k_{\rho_j}\rho')\underline{\underline{\tilde{R}}}_{j,j+1}] \\ &\qquad \text{for } \rho < \rho' \\ \underline{\underline{F_n}} &= [H_n^{(2)}(k_{\rho_j}\rho)\underline{\underline{I}} + J_n(k_{\rho_j}\rho)\underline{\underline{\tilde{R}}}_{j,j+1}]\underline{\underline{\tilde{M}}}_{j+}[J_n(k_{\rho_j}\rho')\underline{\underline{I}} + H_n^{(2)}(k_{\rho_j}\rho')\underline{\underline{\tilde{R}}}_{j,j-1}] \\ &\qquad \text{for } \rho > \rho' \end{aligned} \tag{2.5}$$

and when the field and source layers are different ($m \neq j$) $\underline{\underline{F_n}}$ becomes

$$\begin{aligned} \underline{\underline{F_n}} &= [J_n(k_{\rho_m}\rho)\underline{\underline{I}} + H_n^{(2)}(k_{\rho_m}\rho)\underline{\underline{\tilde{R}}}_{m,m-1}]\underline{\underline{\tilde{T}}}_{j,m}\underline{\underline{\tilde{M}}}_{j-}[H_n^{(2)}(k_{\rho_j}\rho')\underline{\underline{I}} + J_n(k_{\rho_j}\rho')\underline{\underline{\tilde{R}}}_{j,j+1}] \\ &\qquad \text{for } m < j \\ \underline{\underline{F_n}} &= [H_n^{(2)}(k_{\rho_m}\rho)\underline{\underline{I}} + J_n(k_{\rho_m}\rho)\underline{\underline{\tilde{R}}}_{m,m+1}]\underline{\underline{\tilde{T}}}_{j,m}\underline{\underline{\tilde{M}}}_{j+}[J_n(k_{\rho_j}\rho')\underline{\underline{I}} + H_n^{(2)}(k_{\rho_j}\rho')\underline{\underline{\tilde{R}}}_{j,j-1}] \\ &\qquad \text{for } m > j. \end{aligned} \tag{2.6}$$

In (2.5) and (2.6) $\underline{\underline{\tilde{M}}}_{j\pm}$ is defined as

$$\underline{\underline{\tilde{M}}}_{j\pm} = (\underline{\underline{I}} - \underline{\underline{\tilde{R}}}_{j,j\mp1}\underline{\underline{\tilde{R}}}_{j,j\pm1})^{-1} \tag{2.7}$$

where, $\underline{\underline{I}}$ is the unity matrix and $\underline{\underline{\tilde{R}}}_{j,j\mp1}$ is the generalized reflection matrix. The generalized reflection matrix $\underline{\underline{\tilde{R}}}_{j,j-1}$ contains multiple reflections from the inner

layers with respect to j, while $\underline{\underline{\tilde{R}}}_{j,j+1}$ contains multiple reflections from the outer layers. The subscript j denotes that $\underline{\underline{\tilde{R}}}_{j,j\mp1}$ is the generalized reflection matrix for layer j. The generalized reflection matrix can be defined as

$$\underline{\underline{\tilde{R}}}_{i,i\pm1} = \underline{\underline{R}}_{i,i\pm1} + \underline{\underline{T}}_{i\pm1,i}\underline{\underline{\tilde{R}}}_{i\pm1,i\pm2}\underline{\underline{\tilde{T}}}_{i,i\pm1} \tag{2.8}$$

where i denotes an arbitrary layer between 1 and N. Similar to $\underline{\underline{\tilde{R}}}$, $\underline{\underline{\tilde{T}}}$ is the generalized transmission matrix, which is defined as

$$\underline{\underline{\tilde{T}}}_{i,i\pm1} = (\underline{\underline{I}} - \underline{\underline{R}}_{i\pm1,i}\underline{\underline{\tilde{R}}}_{i\pm1,i\pm2})^{-1}\underline{\underline{T}}_{i,i\pm1}. \tag{2.9}$$

In (2.8) and (2.9), $\underline{\underline{R}}$ and $\underline{\underline{T}}$ denote the local reflection and transmission matrices, respectively. They contain the interactions between only the two layers which are given in their subscripts. Consequently, the local reflection and transmission matrices $\underline{\underline{R}}$ and $\underline{\underline{T}}$, respectively, are given by

$$\underline{\underline{R}}_{i,i+1} = \underline{\underline{D}}_i^{-1}[H_n^{(2)}(k_{\rho_i}a_i)\underline{\underline{H_n}}^{(2)}(k_{\rho_{i+1}}a_i) - H_n^{(2)}(k_{\rho_{i+1}}a_i)\underline{\underline{H_n}}^{(2)}(k_{\rho_i}a_i)] \tag{2.10}$$

$$\underline{\underline{T}}_{i,i+1} = \frac{2\omega}{\pi k_{\rho_i}^2 a_i}\underline{\underline{D}}_i^{-1}\begin{bmatrix} \epsilon_i & 0 \\ 0 & -\mu_i \end{bmatrix} \tag{2.11}$$

$$\underline{\underline{R}}_{i+1,i} = \underline{\underline{D}}_i^{-1}[J_n(k_{\rho_i}a_i)\underline{\underline{J_n}}(k_{\rho_{i+1}}a_i) - J_n(k_{\rho_{i+1}}a_i)\underline{\underline{J_n}}(k_{\rho_i}a_i)] \tag{2.12}$$

$$\underline{\underline{T}}_{i+1,i} = \frac{2\omega}{\pi k_{\rho_{i+1}}^2 a_i}\underline{\underline{D}}_i^{-1}\begin{bmatrix} \epsilon_{i+1} & 0 \\ 0 & -\mu_{i+1} \end{bmatrix} \tag{2.13}$$

with

$$\underline{\underline{D}}_i = H_n^{(2)}(k_{\rho_{i+1}}a_i)\underline{\underline{J_n}}(k_{\rho_i}a_i) - J_n(k_{\rho_i}a_i)\underline{\underline{H_n}}^{(2)}(k_{\rho_{i+1}}a_i). \tag{2.14}$$

Note that all the reflection and transmission matrices are 2×2 matrices, since the TE and TM modes are coupled in cylindrically stratified media. In the aforementioned equations, (2.10)-(2.14), we used $H_n^{(2)}(x)$, $\underline{\underline{H_n}}^{(2)}(x)$, $J_n(x)$ and $\underline{\underline{J_n}}(x)$. To write the expressions in a more compact form we will use $B_n(x)$ and $\underline{\underline{B_n}}(x)$ such that

$$\underline{\underline{B_n}}(k_{\rho_i}a_i) = \frac{1}{k_{\rho_i}^2 a_i}\begin{bmatrix} -j\omega\epsilon_i k_{\rho_i}a_i B_n'(k_{\rho_i}a_i) & nk_z B_n(k_{\rho_i}a_i) \\ nk_z B_n(k_{\rho_i}a_i) & j\omega\mu_i k_{\rho_i}a_i B_n'(k_{\rho_i}a_i) \end{bmatrix} \tag{2.15}$$

where $\underline{\underline{B_n}}(x)$ can be $\underline{\underline{J_n}}(x)$ or $\underline{\underline{H_n}}^{(2)}(x)$ and hence, the corresponding $B_n(x)$ will be $J_n(x)$ or $H_n^{(2)}(x)$, respectively. Finally, in all the previous equations $'$ is used for

the derivative with respect to $k_{\rho_i}a_i$ product such that $\frac{\partial}{\partial(k_{\rho_i}a_i)}$ with $k_{\rho_i} = \sqrt{k_i^2 - k_z^2}$ being the transverse propagation constant of the i^{th} layer and $k_i = \omega\sqrt{\epsilon_i\mu_i}$ being the wave number of i^{th} layer. In these formulations, layer $(i+1)$ is the outer layer and layer $(i-1)$ is the inner layer with respect to layer i. Besides, the reflection matrix $\underline{\underline{R}}_{i,i-1}$ can be obtained from (2.12) by writing $(i-1)$ instead of i. Similarly, $\underline{\underline{R}}_{i-1,i}$ term is obtained from (2.10) by writing $(i-1)$ instead of i.

The innermost or outermost layers in Fig. 2.1 can be a perfect electric conductor (PEC) or a perfect magnetic conductor (PMC) layer. The local reflection matrices from these layers are also given in [14] and [17]-[18]. However, PEC is mostly used as the innermost layer for many cylindrical structures. Therefore, the reflection matrix for an innermost PEC layer is given by

$$\underline{\underline{R}}_{2,1} = \begin{bmatrix} -\frac{J_n(k_{\rho_2}a_1)}{H_n^{(2)}(k_{\rho_2}a_1)} & 0 \\ 0 & -\frac{J_n^{'}(k_{\rho_2}a_1)}{H_n^{'(2)}(k_{\rho_2}a_1)} \end{bmatrix} \tag{2.16}$$

where a_1 is the radius of the PEC layer, which is denoted by i=1 in Fig. 2.1.

2.2 Spectral Domain Green's Function Representations

In the absence of charges and current sources, electric and magnetic fields satisfy the following Maxwell's equations in a homogeneous, isotropic and source-free medium;

$$\nabla \times \underline{\tilde{E}} = -j\omega\mu\underline{\tilde{H}} \tag{2.17}$$

$$\nabla \times \underline{\tilde{H}} = j\omega\epsilon\underline{\tilde{E}}. \tag{2.18}$$

The vector fields given in (2.17) and (2.18) can be decomposed into transverse (ϕ and ρ) components and z components. After the decomposition is completed, the transverse components in the field layer m are obtained as

$$\begin{bmatrix} \tilde{H}_\phi \\ \tilde{E}_\phi \end{bmatrix} = \begin{bmatrix} -\frac{jw\epsilon_m}{k_{\rho_m}}\frac{\partial}{\partial(k_{\rho_m}\rho)} & \frac{nk_z}{k_{\rho m}^2\rho} \\ \frac{nk_z}{k_{\rho m}^2\rho} & \frac{jw\mu_m}{k_{\rho_m}}\frac{\partial}{\partial(k_{\rho_m}\rho)} \end{bmatrix} \begin{bmatrix} \tilde{E}_z \\ \tilde{H}_z \end{bmatrix} \tag{2.19}$$

$$\begin{bmatrix} \tilde{H}_\rho \\ \tilde{E}_\rho \end{bmatrix} = \begin{bmatrix} -\frac{n\omega\epsilon_m}{k_{\rho m}^2\rho} & -\frac{jk_z}{k_{\rho m}}\frac{\partial}{\partial(k_{\rho m}\rho)} \\ -\frac{jk_z}{k_{\rho m}}\frac{\partial}{\partial(k_{\rho m}\rho)} & \frac{n\omega\mu_m}{k_{\rho m}^2\rho} \end{bmatrix} \begin{bmatrix} \tilde{E}_z \\ \tilde{H}_z \end{bmatrix} \tag{2.20}$$

where the z components are found from (2.2) using (2.3) for different directed electric sources. The spectral domain Green's functions, which relate the $\hat{z}$, $\hat{\phi}$ and $\hat{\rho}$ directed electric fields with the $\hat{z}$, $\hat{\phi}$ and $\hat{\rho}$ directed electric sources, are defined as

$$\begin{bmatrix} \tilde{E}_z \\ \tilde{E}_\phi \\ \tilde{E}_\rho \end{bmatrix} = \begin{bmatrix} \tilde{G}_{zz} & \tilde{G}_{z\phi} & \tilde{G}_{z\rho} \\ \tilde{G}_{\phi z} & \tilde{G}_{\phi\phi} & \tilde{G}_{\phi\rho} \\ \tilde{G}_{\rho z} & \tilde{G}_{\rho\phi} & \tilde{G}_{\rho\rho} \end{bmatrix} \begin{bmatrix} \tilde{J}_z \\ \tilde{J}_\phi \\ \tilde{J}_\rho \end{bmatrix}. \tag{2.21}$$

Using the current term given by (2.1), the spectral domain Green's functions are obtained as

$$\tilde{G}_{zz} = -\frac{1}{2\omega\epsilon_j}\sum_{n=0}^{\infty}\kappa_n\cos[n(\phi-\phi')]\,k_{\rho_j}^2 f_n^{11} \tag{2.22}$$

$$\frac{\tilde{G}_{\phi z}}{k_z} = -\frac{j}{2\omega\epsilon_j}\sum_{n=1}^{\infty}\sin[n(\phi-\phi')]k_{\rho_j}^2\left[\frac{n}{k_{\rho_m}^2\rho}f_n^{11} + \frac{j\omega\mu_m}{k_{\rho_m}k_z}\,\frac{\partial f_n^{21}}{\partial(k_{\rho_m}\rho)}\right] \tag{2.23}$$

$$\frac{\tilde{G}_{z\phi}}{k_z} = -\frac{j}{2\omega\epsilon_j}\sum_{n=1}^{\infty}\sin[n(\phi-\phi')]\left[\frac{n}{\rho'}f_n^{11} - \frac{j\omega\epsilon_j k_{\rho_j}}{k_z}\,\frac{\partial f_n^{12}}{\partial(k_{\rho_j}\rho')}\right] \tag{2.24}$$

$$\begin{aligned}\tilde{G}_{\phi\phi} = -\frac{1}{2\omega\epsilon_j}\sum_{n=0}^{\infty}\kappa_n\cos[n(\phi-\phi')]\Bigg[&\frac{nk_z}{k_{\rho_m}^2\rho}\Big(\frac{nk_z}{\rho'}f_n^{11} - j\omega\epsilon_j k_{\rho_j}\,\frac{\partial f_n^{12}}{\partial(k_{\rho_j}\rho')}\Big) \\ &+\frac{j\omega\mu_m}{k_{\rho_m}}\frac{\partial}{\partial(k_{\rho_m}\rho)}\,\Big(\frac{nk_z}{\rho'}f_n^{21} - j\omega\epsilon_j k_{\rho_j}\frac{\partial f_n^{22}}{\partial(k_{\rho_j}\rho')}\Big)\Bigg]\end{aligned} \tag{2.25}$$

where $\kappa_n = 0.5$ for $n = 0$ and 1, otherwise. Similarly, the probe-related components which are used for applications involving an excitation via a probe are derived as (also given in [20] and [24])

$$\frac{\tilde{G}_{\rho z}}{k_z} = -\frac{1}{2\omega\epsilon_j}\sum_{n=0}^{\infty}\kappa_n\cos[n(\phi-\phi')]k_{\rho_j}^2\left[-\frac{j}{k_{\rho_m}}\frac{\partial f_n^{11}}{\partial(k_{\rho_m}\rho)}+\frac{n\omega\mu_m}{k_z k_{\rho_m}^2\rho}f_n^{21}\right] \quad (2.26)$$

$$\begin{aligned}\tilde{G}_{\rho\phi} = & -\frac{j}{2\omega\epsilon_j}\sum_{n=1}^{\infty}\sin[n(\phi-\phi')]\left[-\frac{jk_z}{k_{\rho_m}}\frac{\partial}{\partial(k_{\rho_m}\rho)}(\frac{nk_z}{\rho'}f_n^{11}-j\omega\epsilon_j k_{\rho_j}\frac{\partial f_n^{12}}{\partial(k_{\rho_j}\rho')})\right.\\ & \left.+\frac{n\omega\mu_m}{k_{\rho_m}^2\rho}(\frac{nk_z}{\rho'}f_n^{21}-j\omega\epsilon_j k_{\rho_j}\frac{\partial f_n^{22}}{\partial(k_{\rho_j}\rho')})\right] \quad (2.27)\end{aligned}$$

$$\frac{\tilde{G}_{z\rho}}{k_z} = \frac{1}{2\omega\epsilon_j}\sum_{n=0}^{\infty}\kappa_n\cos[n(\phi-\phi')](jk_{\rho_j}\frac{\partial f_n^{11}}{\partial(k_{\rho_j}\rho')}+\frac{n\omega\epsilon_j}{k_z\rho'}f_n^{12}) \quad (2.28)$$

$$\begin{aligned}\tilde{G}_{\phi\rho} = & -\frac{j}{2\omega\epsilon_j}\sum_{n=1}^{\infty}\sin[n(\phi-\phi')]\left[\frac{nk_z}{k_{\rho_m}^2\rho}(jk_zk_{\rho_j}\frac{\partial f_n^{11}}{\partial(k_{\rho_j}\rho')}+\frac{n\omega\epsilon_j}{\rho'}f_n^{12})\right.\\ & \left.+\frac{j\omega\mu_m}{k_{\rho_m}}\frac{\partial}{\partial(k_{\rho_m}\rho)}(jk_zk_{\rho_j}\frac{\partial f_n^{21}}{\partial(k_{\rho_j}\rho')}+\frac{n\omega\epsilon_j}{\rho'}f_n^{22})\right]. \quad (2.29)\end{aligned}$$

In (2.22)-(2.29), f_n^{11}, f_n^{12}, f_n^{21} and f_n^{22} are the entries of $\underline{\underline{F_n}}$ (superscripts indicate the entries). In the Green's function expressions, the subscript j denotes the layer where the source point is located and m is used for the layer where the field point is located.

In (2.22)-(2.29), to increase the efficiency in the computation of the Green's function components, the odd and even properties of these components are used. For instance, using the odd and even properties with respect to cylindrical eigenmodes n, the summations that range from $-\infty$ to ∞ are folded over all n to range from 0 to ∞. Similarly, to speed up the integration with respect to k_z, if the Green's function component is an even function of k_z, the k_z integral is converted to a 0 to ∞ integral. However, if the Green's function component is an odd function of k_z, it is divided by k_z so the integrand becomes an even function of k_z. Then, the resultant integral is converted to a $0 \rightarrow \infty$ integral.

2.3 Spectral Domain Green's Function Representations when $(\rho = \rho')$

The Green's function representations given by (2.22)-(2.29) are accurate when ρ is far away from ρ' as it is illustrated in Fig. 2.2, and can not be used for $\rho = \rho'$ case which is essential in performing an analysis in cylindrically stratified media. In Fig. 2.2, the source and field points where $\rho = \rho' = a_1$ depicts a typical antenna analysis problem where the antenna is located at the dielectric-air interface. To obtain accurate Green's function representations at $\rho = \rho'$ and to compute them efficiently and accurately, the spectral domain Green's function expressions given by (2.22)-(2.29) are modified as explained, in [26]. In this dissertation these modified expressions are given once more with the appropriate changes that will help us to handle singularity problems when they are transformed to space domain.

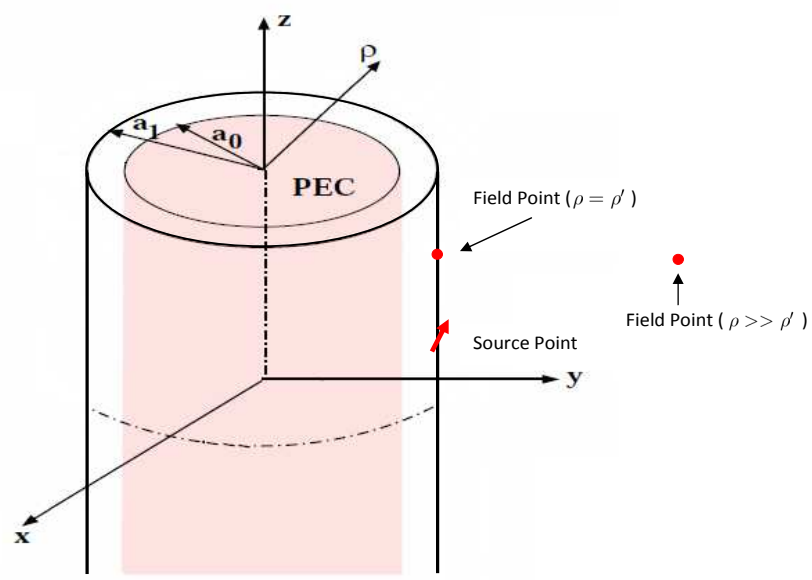

Figure 2.2: $\rho = \rho'$ and $\rho >> \rho'$ situations on a multilayered cylindrical geometry

When $\rho = \rho'$ the first problem is the slowly convergent behaviour of infinite summations used in (2.22)-(2.29). Since these summations are slowly convergent, computation of the Hankel and Bessel functions for large n values becomes

mandatory. However, for large n values, evaluation of the Hankel (Bessel) functions shows overflow/underflow problems. Therefore, instead of evaluating each Hankel (Bessel) function one at a time, they are written in the form of ratios (i.e., each Hankel (Bessel) function is written in ratio form with another Hankel (Bessel) function) and these ratios are directly evaluated. Note that in this dissertation, an expression in the form of ratios means that all the Hankel (Bessel) functions in that expression are written in ratio form with another Hankel (Bessel) function.

2.3.1 Spectral Domain Expressions In The Form of Ratios

Although the case of $\rho = \rho'$ is being analyzed, ρ is not written instead of ρ' or vice versa, in order not to create any confusion in the Green's function expressions. This way, the developed expressions can be easily extended to multilayer geometries. Besides, there are derivatives with respect ρ and ρ' that should be distinguished. Therefore, only at the final expressions when a simplification is required, ρ is equated to ρ'.

In order to write the spectral domain Green's function representations in the form of ratios, we start with $\underline{\underline{B_n}}(k_{\rho_i}a_i)$ term given by (2.15), and rewrite it as

$$\underline{\underline{B_n}}(k_{\rho_i}a_i) = \frac{B_n(k_{\rho_i}a_i)}{k_{\rho_i}^2 a_i} \begin{bmatrix} -j\omega\epsilon_i k_{\rho_i} a_i \frac{B_n'(k_{\rho_i}a_i)}{B_n(k_{\rho_i}a_i)} & nk_z \\ nk_z & j\omega\mu_i k_{\rho_i} a_i \frac{B_n'(k_{\rho_i}a_i)}{B_n(k_{\rho_i}a_i)} \end{bmatrix}. \tag{2.30}$$

Then, the $\underline{\underline{D}}_i$ expression in (2.14) is rewritten as

$$\underline{\underline{D}}_i = H_n^{(2)}(k_{\rho_{i+1}}a_i) J_n(k_{\rho_i}a_i) \left(\frac{\underline{\underline{J_n}}(k_{\rho_i}a_i)}{J_n(k_{\rho_i}a_i)} - \frac{\underline{\underline{H_n}}^{(2)}(k_{\rho_{i+1}}a_i)}{H_n^{(2)}(k_{\rho_{i+1}}a_i)} \right). \tag{2.31}$$

If we define

$$\underline{\underline{D}}_i = H_n^{(2)}(k_{\rho_{i+1}}a_i) J_n(k_{\rho_i}a_i) \underline{\underline{D}}_{in} \tag{2.32}$$

we obtain

$$\underline{\underline{D}}_{in} = \frac{\underline{\underline{J_n}}(k_{\rho_i}a_i)}{J_n(k_{\rho_i}a_i)} - \frac{\underline{\underline{H_n}}^{(2)}(k_{\rho_{i+1}}a_i)}{H_n^{(2)}(k_{\rho_{i+1}}a_i)} \tag{2.33}$$

and substituting (2.30) into (2.33), it is seen that (2.33) is obtained in the form of ratios. In a similar manner the local reflection matrix given by (2.10) can be written as

$$\underline{\underline{R}}_{i,i+1} = \underline{\underline{D}}_{i}^{-1}[H_n^{(2)}(k_{\rho_i}a_i)H_n^{(2)}(k_{\rho_{i+1}}a_i)]\left(\frac{\underline{\underline{H_n}}^{(2)}(k_{\rho_{i+1}}a_i)}{H_n^{(2)}(k_{\rho_{i+1}}a_i)} - \frac{\underline{\underline{H_n}}^{(2)}(k_{\rho_i}a_i)}{H_n^{(2)}(k_{\rho_i}a_i)}\right) \quad (2.34)$$

or in terms of $\underline{\underline{D}}_{in}$, (2.34) is rewritten as

$$\underline{\underline{R}}_{i,i+1} = \underline{\underline{D}}_{in}^{-1}\left[\frac{H_n^{(2)}(k_{\rho_i}a_i)}{J_n(k_{\rho_i}a_i)}\frac{H_n^{(2)}(k_{\rho_{i+1}}a_i)}{H_n^{(2)}(k_{\rho_{i+1}}a_i)}\right]\left(\frac{\underline{\underline{H_n}}^{(2)}(k_{\rho_{i+1}}a_i)}{H_n^{(2)}(k_{\rho_{i+1}}a_i)} - \frac{\underline{\underline{H_n}}^{(2)}(k_{\rho_i}a_i)}{H_n^{(2)}(k_{\rho_i}a_i)}\right). \quad (2.35)$$

When the certain simplifications are performed, $\underline{\underline{R}}_{i,i+1}$ is given by

$$\underline{\underline{R}}_{i,i+1} = \frac{H_n^{(2)}(k_{\rho_i}a_i)}{J_n(k_{\rho_i}a_i)}\underline{\underline{D}}_{in}^{-1}\left(\frac{\underline{\underline{H_n}}^{(2)}(k_{\rho_{i+1}}a_i)}{H_n^{(2)}(k_{\rho_{i+1}}a_i)} - \frac{\underline{\underline{H_n}}^{(2)}(k_{\rho_i}a_i)}{H_n^{(2)}(k_{\rho_i}a_i)}\right). \quad (2.36)$$

The Debye approximations for the ratio terms of the Hankel and Bessel functions are given in Appendix A. From (A.1) and (A.4), it is seen that

$$\lim_{n\to\infty}\frac{B_n^{'}(x)}{nB_n(x)} = C(k_z) \quad (2.37)$$

where $B_n = J_n$ or $B_n = H_n^{(2)}$ as mentioned before, and $C(k_z)$ is a constant with respect to n. Using this information, it can be seen that $\underline{\underline{D}}_{in}^{-1}$ decays with $1/n$ for large n values where the $(\frac{\underline{\underline{H_n}}^{(2)}(k_{\rho_{i+1}}a_i)}{H_n^{(2)}(k_{\rho_{i+1}}a_i)} - \frac{\underline{\underline{H_n}}^{(2)}(k_{\rho_i}a_i)}{H_n^{(2)}(k_{\rho_i}a_i)})$ term grows with n. Therefore, if we define

$$\underline{\underline{R}}n_{i,i+1} = \underline{\underline{D}}_{in}^{-1}\left(\frac{\underline{\underline{H_n}}^{(2)}(k_{\rho_{i+1}}a_i)}{H_n^{(2)}(k_{\rho_{i+1}}a_i)} - \frac{\underline{\underline{H_n}}^{(2)}(k_{\rho_i}a_i)}{H_n^{(2)}(k_{\rho_i}a_i)}\right) \quad (2.38)$$

we obtain

$$\underline{\underline{R}}_{i,i+1} = \frac{H_n^{(2)}(k_{\rho_i}a_i)}{J_n(k_{\rho_i}a_i)}\underline{\underline{R}}n_{i,i+1} \quad (2.39)$$

where $\underline{\underline{R}}n_{i,i+1}$ term becomes constant with respect to n for large n values.

Similar to $\underline{\underline{R}}_{i,i+1}$, the $\underline{\underline{R}}_{i+1,i}$ term given by (2.12) can be written as

$$\underline{\underline{R}}_{i+1,i} = \underline{\underline{D}}_{i}^{-1}[J_n(k_{\rho_i}a_i)J_n(k_{\rho_{i+1}}a_i)]\left(\frac{\underline{\underline{J_n}}(k_{\rho_{i+1}}a_i)}{J_n(k_{\rho_{i+1}}a_i)} - \frac{\underline{\underline{J_n}}(k_{\rho_i}a_i)}{J_n(k_{\rho_i}a_i)}\right), \quad (2.40)$$

which can be expressed as

$$\underline{\underline{R}}_{i+1,i} = \frac{J_n(k_{\rho_{i+1}}a_i)}{H_n^{(2)}(k_{\rho_{i+1}}a_i)}\underline{\underline{R}}n_{i+1,i} \tag{2.41}$$

where

$$\underline{\underline{R}}n_{i+1,i} = \underline{\underline{D}}_{in}^{-1}\left(\frac{\underline{\underline{J_n}}(k_{\rho_{i+1}}a_i)}{J_n(k_{\rho_{i+1}}a_i)} - \frac{\underline{\underline{J_n}}(k_{\rho_i}a_i)}{J_n(k_{\rho_i}a_i)}\right) \tag{2.42}$$

and $\underline{\underline{R}}n_{i+1,i}$ is also constant with respect to n for large n values.

In [14] and [17]-[18], the simplified expressions given by (2.11) and (2.13) are used for the local transmission matrices $\underline{\underline{T}}_{i,i+1}$ and $\underline{\underline{T}}_{i+1,i}$, respectively. However, when they are used in the $\underline{\underline{F_n}}$ expression given by (2.5), $\underline{\underline{F_n}}$ can not be expressed in the form of ratios. Therefore, the actual transmission matrix definitions, which are not simplified, are used in this dissertation. These actual transmission matrix definitions are

$$\underline{\underline{T}}_{i,i+1} = \underline{\underline{D}}_i^{-1}[H_n^{(2)}(k_{\rho_i}a_i)\underline{\underline{J_n}}(k_{\rho_i}a_i) - J_n(k_{\rho_i}a_i)\underline{\underline{H_n}}^{(2)}(k_{\rho_i}a_i)] \tag{2.43}$$

$$\underline{\underline{T}}_{i+1,i} = \underline{\underline{D}}_i^{-1}[H_n^{(2)}(k_{\rho_{i+1}}a_i)\underline{\underline{J_n}}(k_{\rho_{i+1}}a_i) - J_n(k_{\rho_{i+1}}a_i)\underline{\underline{H_n}}^{(2)}(k_{\rho_{i+1}}a_i)]. \tag{2.44}$$

Hence, similar to the reflection matrices, the transmission matrix $\underline{\underline{T}}_{i,i+1}$ is expressed as

$$\underline{\underline{T}}_{i,i+1} = \underline{\underline{D}}_i^{-1}\left[H_n^{(2)}(k_{\rho_i}a_i)J_n(k_{\rho_i}a_i)\right]\left(\frac{\underline{\underline{J_n}}(k_{\rho_i}a_i)}{J_n(k_{\rho_i}a_i)} - \frac{\underline{\underline{H_n}}^{(2)}(k_{\rho_i}a_i)}{H_n^{(2)}(k_{\rho_i}a_i)}\right) \tag{2.45}$$

or

$$\underline{\underline{T}}_{i,i+1} = \frac{H_n^{(2)}(k_{\rho_i}a_i)}{H_n^{(2)}(k_{\rho_{i+1}}a_i)}\underline{\underline{D}}_{in}^{-1}\left(\frac{\underline{\underline{J_n}}(k_{\rho_i}a_i)}{J_n(k_{\rho_i}a_i)} - \frac{\underline{\underline{H_n}}^{(2)}(k_{\rho_i}a_i)}{H_n^{(2)}(k_{\rho_i}a_i)}\right). \tag{2.46}$$

At this point the $\underline{\underline{T}}_{i,i+1}$ term, as expressed in (2.46), is in the form of ratios and constant with respect to n for large n values.

Similarly, $\underline{\underline{T}}_{i+1,i}$ is written as

$$\underline{\underline{T}}_{i+1,i} = \underline{\underline{D}}_i^{-1}[H_n^{(2)}(k_{\rho_{i+1}}a_i)J_n(k_{\rho_{i+1}}a_i)]\left(\frac{\underline{\underline{J_n}}(k_{\rho_{i+1}}a_i)}{J_n(k_{\rho_{i+1}}a_i)} - \frac{\underline{\underline{H_n}}^{(2)}(k_{\rho_{i+1}}a_i)}{H_n^{(2)}(k_{\rho_{i+1}}a_i)}\right) \tag{2.47}$$

or

$$\underline{\underline{T}}_{i+1,i} = \frac{J_n(k_{\rho_{i+1}}a_i)}{J_n(k_{\rho_i}a_i)}\underline{\underline{D}}_{in}^{-1}\left(\frac{\underline{\underline{J_n}}(k_{\rho_{i+1}}a_i)}{J_n(k_{\rho_{i+1}}a_i)} - \frac{\underline{\underline{H_n}}^{(2)}(k_{\rho_{i+1}}a_i)}{H_n^{(2)}(k_{\rho_{i+1}}a_i)}\right). \tag{2.48}$$

Similar to $\underline{\underline{T}}_{i,i+1}$ expression, $\underline{\underline{T}}_{i+1,i}$ term is now in the form of ratios and again constant with respect to n for large n values.

So far, the local reflection and transmission matrices are rewritten in the form of ratios. As the next step, these matrices are substituted into the generalized reflection and transmission matrices and expressed in the form of ratios. The $\underline{\underline{\tilde{R}}}_{i,i+1}$ term is given by

$$\underline{\underline{\tilde{R}}}_{i,i+1} = \underline{\underline{R}}_{i,i+1} + \underline{\underline{T}}_{i+1,i}\underline{\underline{\tilde{R}}}_{i+1,i+2}\underline{\underline{\tilde{T}}}_{i,i+1}. \tag{2.49}$$

In an N-layered cylindrical geometry, the first nonzero generalized reflection matrix for the outermost layers is $\underline{\underline{\tilde{R}}}_{N-1,N}$. $\underline{\underline{\tilde{R}}}_{N-1,N}$ term is in fact a local reflection matrix and is equal to $\underline{\underline{R}}_{N-1,N}$, since we have only N layer and $\underline{\underline{\tilde{R}}}_{N,N+1}$ is zero in (2.49). Thus, it is possible to write a general expression for $\underline{\underline{\tilde{R}}}_{i+1,i+2}$ using $\underline{\underline{R}}_{i,i+1}$ given by (2.39)

$$\underline{\underline{\tilde{R}}}_{i+1,i+2} = \frac{H_n^{(2)}(k_{\rho_{i+1}}a_{i+1})}{J_n(k_{\rho_{i+1}}a_{i+1})}\underline{\underline{\tilde{R}}}n_{i+1,i+2} \tag{2.50}$$

where again $\underline{\underline{\tilde{R}}}n_{i+1,i+2}$ term is in the from of ratios and constant with respect to n for large n values.

Since $\underline{\underline{\tilde{T}}}_{i,i+1}$ term is given by

$$\underline{\underline{\tilde{T}}}_{i,i+1} = (\underline{\underline{I}} - \underline{\underline{R}}_{i+1,i}\underline{\underline{\tilde{R}}}_{i+1,i+2})^{-1}\underline{\underline{T}}_{i,i+1} \tag{2.51}$$

using (2.41) and (2.50) it can be written as

$$\underline{\underline{\tilde{T}}}_{i,i+1} = \left(\underline{\underline{I}} - \frac{H_n^{(2)}(k_{\rho_{i+1}}a_{i+1})}{H_n^{(2)}(k_{\rho_{i+1}}a_i)}\frac{J_n(k_{\rho_{i+1}}a_i)}{J_n(k_{\rho_{i+1}}a_{i+1})}\underline{\underline{R}}n_{i+1,i}\underline{\underline{\tilde{R}}}n_{i+1,i+2}\right)^{-1}\underline{\underline{T}}_{i,i+1}. \tag{2.52}$$

Since all the functions in $\underline{\underline{\tilde{T}}}_{i,i+1}$ are in the form of ratios, $\underline{\underline{\tilde{T}}}_{i,i+1}$ is constant with respect to n for large n values. Substituting all the terms which are in the form of ratios into (2.49), the generalized reflection matrix $\underline{\underline{\tilde{R}}}_{i,i+1}$ becomes

$$\underline{\underline{\tilde{R}}}_{i,i+1} = \frac{H_n^{(2)}(k_{\rho_i}a_i)}{J_n(k_{\rho_i}a_i)}\underline{\underline{\tilde{R}}}n_{i,i+1}. \tag{2.53}$$

where

$$\underline{\underline{\tilde{R}}}n_{i,i+1} = \underline{\underline{R}}n_{i,i+1} + \underline{\underline{T}}_{i+1,i}\frac{H_n^{(2)}(k_{\rho_{i+1}}a_{i+1})}{H_n^{(2)}(k_{\rho_i}a_i)}\frac{J_n(k_{\rho_i}a_i)}{J_n(k_{\rho_{i+1}}a_{i+1})}\underline{\underline{\tilde{R}}}n_{i+1,i+2}\underline{\underline{\tilde{T}}}_{i,i+1}, \quad (2.54)$$

and it is clear that $\underline{\underline{\tilde{R}}}n_{i,i+1}$ term is in the form of ratios and constant with respect to n for large n values.

Equation (2.53) is the desired representation for $\underline{\underline{\tilde{R}}}_{i,i+1}$. However in a similar fashion, we must define the $\underline{\underline{\tilde{R}}}_{i,i-1}$ term which is given by

$$\underline{\underline{\tilde{R}}}_{i,i-1} = \underline{\underline{R}}_{i,i-1} + \underline{\underline{T}}_{i-1,i}\underline{\underline{\tilde{R}}}_{i-1,i-2}\underline{\underline{\tilde{T}}}_{i,i-1}. \quad (2.55)$$

Similar to $\underline{\underline{\tilde{R}}}_{i+1,i+2}$, $\underline{\underline{\tilde{R}}}_{i-1,i-2}$ is zero for the innermost layer, so the first nonzero $\underline{\underline{\tilde{R}}}_{i-1,i-2}$ term behaves in the same manner as $\underline{\underline{R}}_{i,i-1}$. Hence, it is written as

$$\underline{\underline{\tilde{R}}}_{i-1,i-2} = \frac{J_n(k_{\rho_{i-1}}a_{i-2})}{H_n^{(2)}(k_{\rho_{i-1}}a_{i-2})}\underline{\underline{\tilde{R}}}n_{i-1,i-2} \quad (2.56)$$

where $\underline{\underline{\tilde{R}}}n_{i-1,i-2}$ is in the form of ratios and constant with respect to n for large n values. The $\underline{\underline{\tilde{T}}}_{i,i-1}$ term is

$$\underline{\underline{\tilde{T}}}_{i,i-1} = (\underline{\underline{I}} - \underline{\underline{R}}_{i-1,i}\underline{\underline{\tilde{R}}}_{i-1,i-2})^{-1}\underline{\underline{T}}_{i,i-1} \quad (2.57)$$

where the $\underline{\underline{R}}_{i-1,i}$ term is obtained as

$$\underline{\underline{R}}_{i-1,i} = \frac{H_n^{(2)}(k_{\rho_{i-1}}a_{i-1})}{J_n(k_{\rho_{i-1}}a_{i-1})}\underline{\underline{R}}n_{i-1,i} \quad (2.58)$$

by writing $i-1$ instead of i in (2.39), and where $\underline{\underline{R}}n_{i-1,i}$ term is in the form of ratios. The $\underline{\underline{\tilde{T}}}_{i,i-1}$ term is then expressed as

$$\underline{\underline{\tilde{T}}}_{i,i-1} = \left(\underline{\underline{I}} - \frac{H_n^{(2)}(k_{\rho_{i-1}}a_{i-1})}{H_n^{(2)}(k_{\rho_{i-1}}a_{i-2})}\frac{J_n(k_{\rho_{i-1}}a_{i-2})}{J_n(k_{\rho_{i-1}}a_{i-1})}\underline{\underline{R}}n_{i-1,i}\underline{\underline{\tilde{R}}}n_{i-1,i-2}\right)^{-1}\underline{\underline{T}}_{i,i-1} \quad (2.59)$$

where $\underline{\underline{\tilde{T}}}_{i,i-1}$ is in the form of ratios.

The $\underline{\underline{R}}_{i,i-1}$ term is obtained from (2.41) as

$$\underline{\underline{R}}_{i,i-1} = \frac{J_n(k_{\rho_i}a_{i-1})}{H_n^{(2)}(k_{\rho_i}a_{i-1})}\underline{\underline{R}}n_{i,i-1} \quad (2.60)$$

by writing $i-1$ instead of i. Finally, substituting all terms which are in the form of ratios into (2.55), $\underline{\underline{\tilde{R}}}_{i,i-1}$ expression is obtained as

$$\underline{\underline{\tilde{R}}}_{i,i-1} = \frac{J_n(k_{\rho_i}a_{i-1})}{H_n^{(2)}(k_{\rho_i}a_{i-1})}\underline{\underline{\tilde{R}}}n_{i,i-1} \tag{2.61}$$

where

$$\underline{\underline{\tilde{R}}}n_{i,i-1} = \underline{\underline{R}}n_{i,i-1} + \underline{\underline{T}}_{i-1,i}\frac{H_n^{(2)}(k_{\rho_i}a_{i-1})}{H_n^{(2)}(k_{\rho_{i-1}}a_{i-2})}\frac{J_n(k_{\rho_{i-1}}a_{i-2})}{J_n(k_{\rho_i}a_{i-1})}\underline{\underline{\tilde{R}}}n_{i-1,i-2}\underline{\underline{\tilde{T}}}_{i,i-1} \tag{2.62}$$

and $\underline{\underline{\tilde{R}}}n_{i,i-1}$ is constant with respect to n for large n values.

When $\rho = \rho'$, the source and field layers are the same. Denoting this layer by the index j, the expression in (2.5) must be used for the $\underline{\underline{F_n}}$ term. Note that the two expressions for $\rho > \rho'$ and $\rho < \rho'$ become equal to each other when $\rho = \rho'$. For the rest of this chapter, the $\rho > \rho'$ expression given by

$$\underline{\underline{F_n}} = [H_n^{(2)}(k_{\rho_j}\rho)\underline{\underline{I}} + J_n(k_{\rho_j}\rho)\underline{\underline{\tilde{R}}}_{j,j+1}]\underline{\underline{\tilde{M}}}_{j+}[J_n(k_{\rho_j}\rho')\underline{\underline{I}} + H_n^{(2)}(k_{\rho_j}\rho')\underline{\underline{\tilde{R}}}_{j,j-1}] \tag{2.63}$$

will be considered. Regarding the $\underline{\underline{F_n}}$ in (2.63), the expressions for the tangential components of the Green's function representations given by (2.22)-(2.29) contain derivatives of $\underline{\underline{F_n}}$ with respect to $k_{\rho_j}\rho$ and $k_{\rho_j}\rho'$. Since $\underline{\underline{I}}$, $\underline{\underline{\tilde{R}}}_{j,j-1}$, $\underline{\underline{\tilde{M}}}_{j+}$ and $\underline{\underline{\tilde{R}}}_{j,j+1}$ do not contain any ρ or ρ', these derivatives are given by

$$\frac{\partial \underline{\underline{F_n}}}{\partial(k_{\rho_j}\rho)} = [H_n^{'(2)}(k_{\rho_j}\rho)\underline{\underline{I}} + J_n^{'}(k_{\rho_j}\rho)\underline{\underline{\tilde{R}}}_{j,j+1}]\underline{\underline{\tilde{M}}}_{j+}[J_n(k_{\rho_j}\rho')\underline{\underline{I}} + H_n^{(2)}(k_{\rho_j}\rho')\underline{\underline{\tilde{R}}}_{j,j-1}] \tag{2.64}$$

$$\frac{\partial \underline{\underline{F_n}}}{\partial(k_{\rho_j}\rho')} = [H_n^{(2)}(k_{\rho_j}\rho)\underline{\underline{I}} + J_n(k_{\rho_j}\rho)\underline{\underline{\tilde{R}}}_{j,j+1}]\underline{\underline{\tilde{M}}}_{j+}[J_n^{'}(k_{\rho_j}\rho')\underline{\underline{I}} + H_n^{'(2)}(k_{\rho_j}\rho')\underline{\underline{\tilde{R}}}_{j,j-1}] \tag{2.65}$$

$$\begin{aligned}\frac{\partial^2 \underline{\underline{F_n}}}{\partial(k_{\rho_j}\rho')\partial(k_{\rho_j}\rho)} = {} & [H_n^{'(2)}(k_{\rho_j}\rho)\underline{\underline{I}} + J_n^{'}(k_{\rho_j}\rho)\underline{\underline{\tilde{R}}}_{j,j+1}]\underline{\underline{\tilde{M}}}_{j+} \\ & .[J_n^{'}(k_{\rho_j}\rho')\underline{\underline{I}} + H_n^{'(2)}(k_{\rho_j}\rho')\underline{\underline{\tilde{R}}}_{j,j-1}].\end{aligned} \tag{2.66}$$

The $\underline{\underline{\tilde{M}}}_{j+}$ expression appearing in (2.63)-(2.66) is expressed as

$$\underline{\underline{\tilde{M}}}_{j+} = (\underline{\underline{I}} - \underline{\underline{\tilde{R}}}_{j,j-1}\underline{\underline{\tilde{R}}}_{j,j+1})^{-1} \tag{2.67}$$

where $\underline{\underline{\tilde{R}}}_{j,j-1}$ is obtained putting j instead of i in (2.61) such that

$$\underline{\underline{\tilde{R}}}_{j,j-1} = \frac{J_n(k_{\rho_j}a_{j-1})}{H_n^{(2)}(k_{\rho_j}a_{j-1})}\underline{\underline{\tilde{R}}}n_{j,j-1} \tag{2.68}$$

and similarly, $\underline{\underline{\tilde{R}}}_{j,j+1}$ is written using (2.53) as

$$\underline{\underline{\tilde{R}}}_{j,j+1} = \frac{H_n^{(2)}(k_{\rho_j}a_j)}{J_n(k_{\rho_j}a_j)}\underline{\underline{\tilde{R}}}n_{j,j+1}. \tag{2.69}$$

Substituting the $\underline{\underline{\tilde{R}}}_{j,j+1}$ and $\underline{\underline{\tilde{R}}}_{j,j-1}$ terms into the $\underline{\underline{\tilde{M}}}_j+$ expression given by (2.67), we obtain

$$\underline{\underline{\tilde{M}}}_j+ = \left(\underline{\underline{I}} - \frac{H_n^{(2)}(k_{\rho_j}a_j)}{H_n^{(2)}(k_{\rho_j}a_{j-1})}\frac{J_n(k_{\rho_j}a_{j-1})}{J_n(k_{\rho_j}a_j)}\underline{\underline{\tilde{R}}}n_{j,j-1}\underline{\underline{\tilde{R}}}n_{j,j+1}\right)^{-1}. \tag{2.70}$$

It is seen that $\underline{\underline{\tilde{M}}}_j+$ term in (2.70) is in the form of ratios and constant with respect to n for large n values.

Finally, we can write the $\underline{\underline{F_n}}$ expression in (2.63) as

$$\underline{\underline{F_n}} = H_n^{(2)}(k_{\rho_j}\rho)J_n(k_{\rho_j}\rho')\underline{\underline{F}}n_n \tag{2.71}$$

where

$$\begin{aligned}\underline{\underline{F}}n_n \;=\; & \left(\left[\underline{\underline{I}} + \frac{H_n^{(2)}(k_{\rho_j}a_j)}{H_n^{(2)}(k_{\rho_j}\rho)}\frac{J_n(k_{\rho_j}\rho)}{J_n(k_{\rho_j}a_j)}\underline{\underline{\tilde{R}}}n_{j,j+1}\right]\underline{\underline{\tilde{M}}}_{j+}\right. \\ & \left.\cdot\left[\underline{\underline{I}} + \frac{H_n^{(2)}(k_{\rho_j}\rho')}{H_n^{(2)}(k_{\rho_j}a_{j-1})}\frac{J_n(k_{\rho_j}a_{j-1})}{J_n(k_{\rho_j}\rho')}\underline{\underline{\tilde{R}}}n_{j,j-1}\right]\right)\end{aligned} \tag{2.72}$$

which is constant with respect to n for large n values.

Similarly, (2.64) can be written as

$$\frac{\partial\underline{\underline{F_n}}}{\partial(k_{\rho_j}\rho)} = nH_n^{(2)}(k_{\rho_j}\rho)J_n(k_{\rho_j}\rho')\underline{\underline{F}}n_{nd\rho} \tag{2.73}$$

where

$$\underline{\underline{F}}n_{nd\rho} = \frac{H_n^{'(2)}(k_{\rho_j}\rho)}{nH_n^{(2)}(k_{\rho_j}\rho)}\left(\left[\underline{\underline{I}} + \frac{H_n^{(2)}(k_{\rho_j}a_j)}{H_n^{'(2)}(k_{\rho_j}\rho)}\frac{J_n^{'}(k_{\rho_j}\rho)}{J_n(k_{\rho_j}a_j)}\underline{\underline{\tilde{R}}}n_{j,j+1}\right]\underline{\underline{\tilde{M}}}_{j+} \cdot \left[\underline{\underline{I}} + \frac{H_n^{(2)}(k_{\rho_j}\rho')}{H_n^{(2)}(k_{\rho_j}a_{j-1})}\frac{J_n(k_{\rho_j}a_{j-1})}{J_n(k_{\rho_j}\rho')}\underline{\underline{\tilde{R}}}n_{j,j-1}\right]\right), \tag{2.74}$$

which is in the form of ratios and constant with respect to n for large n values.

The same methodology is also valid for (2.65) such that it is written as

$$\frac{\partial \underline{\underline{F_n}}}{\partial(k_{\rho_j}\rho')} = nH_n^{(2)}(k_{\rho_j}\rho)J_n(k_{\rho_j}\rho')\underline{\underline{F}}n_{nd\rho'} \tag{2.75}$$

where

$$\underline{\underline{F}}n_{nd\rho'} = \frac{J_n^{'}(k_{\rho_j}\rho')}{nJ_n(k_{\rho_j}\rho')}\left(\left[\underline{\underline{I}} + \frac{H_n^{(2)}(k_{\rho_j}a_j)}{H_n^{(2)}(k_{\rho_j}\rho)}\frac{J_n(k_{\rho_j}\rho)}{J_n(k_{\rho_j}a_j)}\underline{\underline{\tilde{R}}}n_{j,j+1}\right]\underline{\underline{\tilde{M}}}_{j+} \cdot \left[\underline{\underline{I}} + \frac{H_n^{'(2)}(k_{\rho_j}\rho')}{H_n^{(2)}(k_{\rho_j}a_{j-1})}\frac{J_n(k_{\rho_j}a_{j-1})}{J_n^{'}(k_{\rho_j}\rho')}\underline{\underline{\tilde{R}}}n_{j,j-1}\right]\right), \tag{2.76}$$

and is the constant term with respect to n for large n values.

Finally, (2.66) can be written as

$$\frac{\partial^2 \underline{\underline{F_n}}}{\partial(k_{\rho_j}\rho')\partial(k_{\rho_j}\rho)} = n^2H_n^{(2)}(k_{\rho_j}\rho)J_n(k_{\rho_j}\rho')\underline{\underline{F}}n_{nd\rho d\rho'} \tag{2.77}$$

where the constant term with respect to n for large n values is

$$\underline{\underline{F}}n_{nd\rho d\rho'} = \frac{H_n^{'(2)}(k_{\rho_j}\rho)}{nH_n^{(2)}(k_{\rho_j}\rho)}\frac{J_n^{'}(k_{\rho_j}\rho')}{nJ_n(k_{\rho_j}\rho')}\left(\left[\underline{\underline{I}} + \frac{H_n^{(2)}(k_{\rho_j}a_j)}{H_n^{'(2)}(k_{\rho_j}\rho)}\frac{J_n^{'}(k_{\rho_j}\rho)}{J_n(k_{\rho_j}a_j)}\underline{\underline{\tilde{R}}}n_{j,j+1}\right]\underline{\underline{\tilde{M}}}_{j+} \cdot \left[\underline{\underline{I}} + \frac{J_n(k_{\rho_j}a_{j-1})}{J_n^{'}(k_{\rho_j}\rho')}\frac{H_n^{'(2)}(k_{\rho_j}\rho')}{H_n^{(2)}(k_{\rho_j}a_{j-1})}\underline{\underline{\tilde{R}}}n_{j,j-1}\right]\right). \tag{2.78}$$

Consequently, $\underline{\underline{F_n}}$, $\frac{\partial \underline{\underline{F_n}}}{\partial(k_{\rho_j}\rho)}$, $\frac{\partial \underline{\underline{F_n}}}{\partial(k_{\rho_j}\rho')}$ and $\frac{\partial^2 \underline{\underline{F_n}}}{\partial(k_{\rho_j}\rho')\partial(k_{\rho_j}\rho)}$ terms are obtained in the form of ratios. Furthermore, it is shown that they are constant with respect to n for large n values. The terms which can not be written in the form of ratios are also given as a multiplicant in the final expressions (2.71), (2.73), (2.75) and (2.77).

The main reasons to write the spectral domain Green's function components in such a form are (i) to improve the efficiency of the summation over the cylindrical eigenmodes n, which becomes important especially when $\rho = \rho'$; and (ii) to treat the computation problems around the source ($\rho = \rho'$, $\phi = \phi'$ and $z = z'$), which will be addressed in the next chapter.

The Bessel and Hankel functions, which are written in the form of ratios, are evaluated using Matlab in the following way: For small n values, each function is evaluated separately. For large n values, where these functions can be replaced by their Debye representations, the Debye representations given in Appendix A are used in the ratio terms and instead of evaluating each function separately, the ratios are evaluated directly.

Chapter 3

Integral Form of Space Domain Green's Function Representations

3.1 Space Domain Green's Function Representations For Tangential Components

The spectral domain Green's function representations given by (2.22)-(2.25) yield accurate results only when the source and field points are far away from each other in terms of the radial distance. In this section using (2.71), (2.73), (2.75) and (2.77), we modify the spectral domain Green's function representations so that accurate space domain Green's function representations can be obtained for all possible source and field points including $\rho = \rho'$. Although ρ is equal to ρ' as shown in Fig. 3.1, in the provided expressions ρ and ρ' are kept distinct to avoid possible confusions in explaining the methodology, in particular when handling the derivatives with respect to ρ and ρ', separately.

Fig. 3.1 illustrates the geometry of current modes on a multilayer cylindrical structure together with the cross-sectional view from the top. Similar to Fig. 2.1 the structure is assumed to be infinite in the $z-$ direction. A PEC cylindrical ground, denoted by the subscript $j = 0$, forms the innermost region with a radius

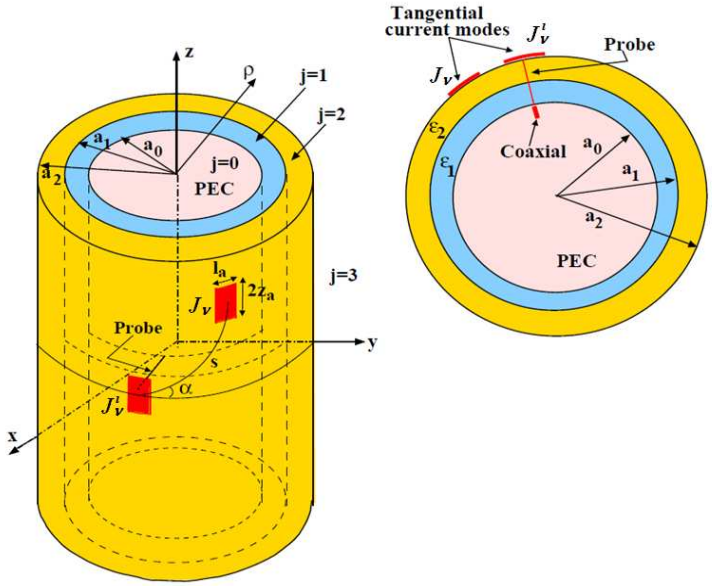

Figure 3.1: Tangential current modes and a probe on cylindrically layered media

a_0, and material layers, denoted by the subscript $j = 1, 2, ...$ surround the PEC region coaxially, as shown in Fig. 3.1 (subscript $j = 1$ denotes the substrate layer; subscript $j = 2$ denotes the superstrate layer, and subscript $j = 3$ denotes the air layer in Fig. 3.1). Each layer has a permittivity, permeability, and radius denoted by ϵ_j, μ_j and a_j, respectively. Furthermore, current modes, denoted by $J'_v(\rho', \phi', z')$ and $J_v(\rho, \phi, z)$ are depicted in Fig. 3.1 where $v = \phi$ or z. A $z-$ or $\phi-$ directed tangential current source, defined at air-dielectric or dielectric-dielectric interface has a dimension of $2z_a \times l_a$ (with $l_a = a_j\phi_a$) along the $z-$ and $\phi-$ directions or $2l_a \times z_a$ along the $\phi-$ and $z-$ directions, respectively. On the other hand, if the current mode is normal to an interface (excitation via a probe), it is usually located inside a layer, assumed to be infinitesimally thin in terms of $\phi-$ and $z-$ coordinates, and has a certain length along the radial direction. Finally, in Fig. 3.1, s denotes the geodesic distance between the two current modes (or between the source and observation points for the CFGF expressions) and α is the angle between the geodesic path and the $\phi-$ axis.

The spectral domain Green's function components, $\tilde{G}_{uv}$ ($u = z$ or ϕ, $v = z$ or

ϕ), given by (2.22)-(2.25) are rewritten in the following form:

$$\frac{\tilde{G}_{uv}}{k_z^l} = -\frac{1}{4\omega\epsilon_j}\sum_{n=-\infty}^{\infty}(k_{\rho_j}^2)^q n^p H_n^{(2)}(k_{\rho_j}\rho)J_n(k_{\rho_j}\rho')f_{uv}(n,k_z)e^{jn(\Delta\phi)} \quad (3.1)$$

where $\Delta\phi = \phi - \phi'$, and for $uv = zz:\ p=0, q=1, l=0$, for $uv=\phi z:$ $p=1, q=0, l=1$, for $uv = z\phi:\ p=1, q=0, l=1$ and finally for $uv=\phi\phi:\ p=2, q=0, l=0$. The key term in (3.1) is $f_{uv}(n,k_z)$ explicitly given by

$$f_{zz}(n,k_z) = f_{r1}^{11} \quad (3.2)$$

$$f_{\phi z}(n,k_z) = k_{\rho_j}^2\left[\frac{1}{k_{\rho_m}^2\rho}f_{r1}^{11} + \frac{j\omega\mu_m}{k_{\rho_m}k_z}\ f_{r2}^{21}\right] \quad (3.3)$$

$$f_{z\phi}(n,k_z) = \frac{1}{\rho'}f_{r1}^{11} - \frac{j\omega\epsilon_j k_{\rho_j}}{k_z}\ f_{r3}^{12} \quad (3.4)$$

$$f_{\phi\phi}(n,k_z) = \frac{k_z}{k_{\rho_m}^2\rho}\left[\frac{k_z}{\rho'}f_{r1}^{11} - j\omega\epsilon_j k_{\rho_j}f_{r3}^{12}\right] + \frac{j\omega\mu_i}{k_{\rho_m}}\left[\frac{k_z}{\rho'}f_{r2}^{21} - j\omega\epsilon_j k_{\rho_j}f_{r4}^{22}\right] \quad (3.5)$$

where f_{r1}^{11}, f_{r2}^{21}, f_{r2}^{12}, f_{r3}^{12}, f_{r4}^{22} are the corresponding entries (each superscript indicates the corresponding entry) of $\underline{\underline{F_{r1}}}$,$\underline{\underline{F_{r2}}}$, $\underline{\underline{F_{r3}}}$, $\underline{\underline{F_{r4}}}$ linked to $\underline{\underline{F_n}}$ as

$$\underline{\underline{F_{r1}}} = \underline{\underline{I}}n_n = \frac{1}{H_n^{(2)}(k_{\rho_j}\rho)J_n(k_{\rho_j}\rho')}\underline{\underline{F_n}} \quad (3.6)$$

$$\underline{\underline{F_{r2}}} = \underline{\underline{I}}n_{nd\rho} = \frac{1}{nH_n^{(2)}(k_{\rho_j}\rho)J_n(k_{\rho_j}\rho')}\frac{\partial\underline{\underline{F_n}}}{\partial(k_{\rho_m}\rho)} \quad (3.7)$$

$$\underline{\underline{F_{r3}}} = \underline{\underline{I}}n_{nd\rho'} = \frac{1}{nH_n^{(2)}(k_{\rho_j}\rho)J_n(k_{\rho_j}\rho')}\frac{\partial\underline{\underline{F_n}}}{\partial(k_{\rho_j}\rho')} \quad (3.8)$$

$$\underline{\underline{F_{r4}}} = \underline{\underline{I}}n_{nd\rho d\rho'} = \frac{1}{n^2H_n^{(2)}(k_{\rho_j}\rho)J_n(k_{\rho_j}\rho')}\frac{\partial^2\underline{\underline{F_n}}}{\partial(k_{\rho_j}\rho')\partial(k_{\rho_m}\rho)}\,. \quad (3.9)$$

In (3.1) [together with (3.6)-(3.9)], all special cylindrical functions (Hankel and Bessel functions) are in the form of ratios except the $H_n^{(2)}(k_{\rho_j}\rho)J_n(k_{\rho_j}\rho')$ product as explained in Chapter 2. Consequently, the accuracy of the summation over n is improved since possible numerical problems for large n values are avoided by using the Debye approximations for the ratio terms as explained in Appendix A.

To further improve the accuracy and efficiency of the summation over n, an envelope extraction method with respect to n is applied to (3.1). Briefly, the

limiting value of $f_{uv}(n,k_z)$ for very large n values is numerically determined as

$$\lim_{n\to\infty} f_{uv}(n,k_z) \approx C_{uv}(k_z) \tag{3.10}$$

which is actually constant with respect to n. In the numerical evaluation of $f_{uv}(n,k_z)$, a couple of large n values around $n=10000$ can be used to determine $C_{uv}(k_z)$ .Then, recognizing the series expansion of $H_0^{(2)}(k_{\rho_j}|\bar{\rho}-\bar{\rho}'|)$, given by

$$\sum_{n=-\infty}^{\infty} H_n^{(2)}(k_{\rho_j}\rho)J_n(k_{\rho_j}\rho')e^{jn\Delta\phi} = H_0^2(k_{\rho_j}|\bar{\rho}-\bar{\rho}'|) = S_1\,, \tag{3.11}$$

$C_{uv}(k_z)$ is subtracted from (3.1) and added as a function of S_1 with the aid of (3.11). Hence, (3.1) becomes

$$\begin{aligned}\frac{\tilde{G}_{uv}}{k_z^l} &= -\frac{1}{4\omega\epsilon_j}\left\{\sum_{n=-\infty}^{\infty}(k_{\rho_j}^2)^q n^p H_n^{(2)}(k_{\rho_j}\rho)J_n(k_{\rho_j}\rho')\left[f_{uv}(n,k_z)-C_{uv}(k_z)\right]e^{jn\Delta\phi}\right.\\ &\left. + C_{uv}(k_z)(k_{\rho_j}^2)^q F_1^{uv}\left[S_1\right]\right\}\end{aligned} \tag{3.12}$$

where

$$F_1^{zz}[S_1] = S_1 \tag{3.13}$$

$$F_1^{z\phi}[S_1] = F_1^{\phi z}[S_1] = j\frac{\partial S_1}{\partial\phi'} = -j\frac{\partial S_1}{\partial\phi} \tag{3.14}$$

$$F_1^{\phi\phi}[S_1] = \frac{\partial^2 S_1}{\partial\phi\partial\phi'}\,. \tag{3.15}$$

Note that in the course of writing (3.13)-(3.15), the Fourier series (with respect to n) relation between the spectral domain and space domain Green's functions is recognized such that both the $(-j\frac{\partial}{\partial\phi})$ and $(j\frac{\partial}{\partial\phi'})$ terms in the space domain correspond to n in the spectral domain.

As a result of this step, the modified summation given in (3.12) converges very rapidly and hence, the limits of the infinite summation can be truncated at relatively small values, N_t (i.e., $\sum_{n=-\infty}^{\infty} \to \sum_{n=-N_t}^{N_t}$) even for relatively large cylinders. This is illustrated in Fig. 3.2, where the imaginary part of $\tilde{G}_{zz}$ versus N_t is plotted for $\Delta\phi = 0.0046$, $k_z = 0$ and $\rho = \rho' = a_1$ using (3.1) and (3.12) (real

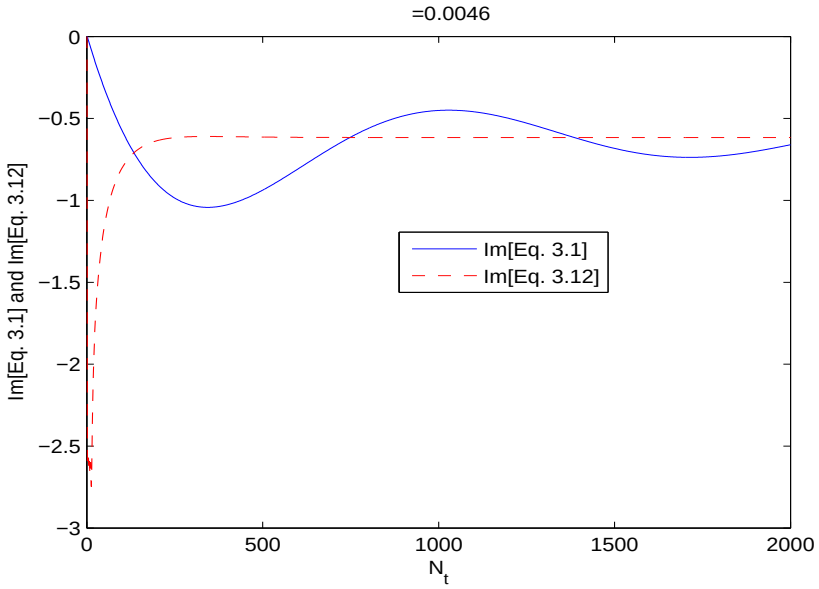

Figure 3.2: Imaginary parts of (3.1) (solid line) and (3.12) (dashed line) with respect to the number of summations for zz case when $\Delta\phi = 0.0046$. The cylinder parameters are: $a_0 = 20$ cm, $a_1 = 20.795$ cm, $\epsilon_r = 2.32$ and $f = 3.2$ GHz

parts of both summations converge rapidly) for a dielectric coated PEC cylinder with $a_0 = 20$ cm, $a_1 = 20.795$ cm, $\epsilon_r = 2.32$ and $f = 3.2$ GHz.

The space domain Green's function, G_{uv}, is related to the spectral domain Green's function, $\tilde{G}_{uv}$, by an inverse Fourier transform (IFT) over k_z, given by

$$G_{uv} = \frac{1}{2\pi} \int_{-\infty}^{\infty} \tilde{G}_{uv} e^{-jk_z(z-z')} dk_z \,. \tag{3.16}$$

However, when $\Delta\phi$ is very small, very large k_z values are required so that (3.16) can converge. Unfortunately, the imaginary part of (3.12) poses numerical problems (i.e., it does not decay) for large values of k_z. These numerical problems are illustrated in Fig. 3.3 where the imaginary parts of (3.12) for $\tilde{G}_{zz}$ are plotted versus real k_z for different $\Delta\phi$ values for the aforementioned cylinder (dielectric coated PEC cylinder with $a_0 = 20$ cm, $a_1 = 20.795$ cm, $\epsilon_r = 2.32$ and $f = 3.2$ GHz). As seen in Fig. 3.3, the imaginary parts have a problematic behaviour especially for $\Delta\phi = 0.0004$ (there is not any special meaning of $\Delta\phi = 0.0004$. It is only the smallest $\Delta\phi$ value obtained for this example).

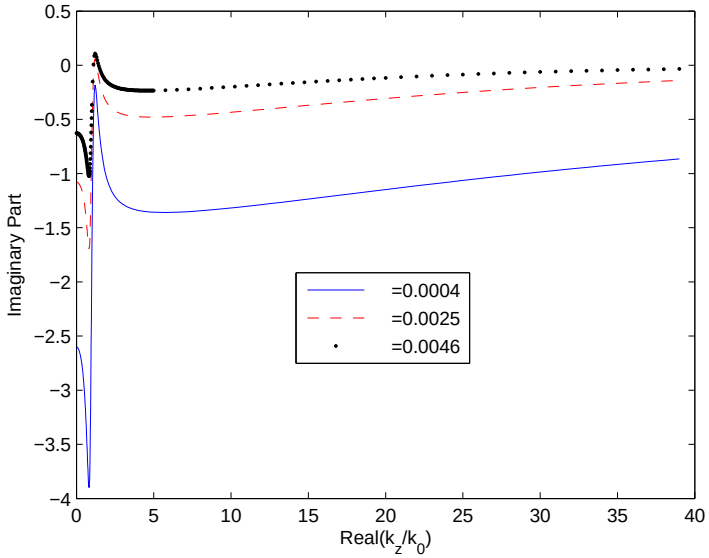

Figure 3.3: Imaginary part of $\tilde{G}_{zz}$ in (3.12) for different $\Delta\phi$ (in radian) values for the same cylinder parameters given in Fig. 3.2

The source of this problem is mainly the second term of (3.12) (i.e., $C_{uv}(k_z)(k_{\rho_j}^2)^q F_1^{uv}[S_1]$). The remedy for this problem is performing a second envelope extraction with respect to k_z. Briefly, for asymptotically large k_z value (i.e., $k_z \to \infty$ denoted as $k_{z\infty}$ and $k_{z\infty}$ can be chosen around $1000k_0$), the value of $C_{uv}(k_z)$, represented by $C_{uv}(k_{z\infty})$, is found numerically. Then, the product $-\frac{1}{4\omega\epsilon_j}C_{uv}(k_{z\infty})(k_{\rho_j}^2)^q F_1^{uv}[S_1]$ is subtracted in the spectral domain from (3.12) and its Fourier transform is added to the final space domain Green's function representation as a function of $\frac{e^{-jk_j\left|\bar{r}-\bar{r}'\right|}}{\left|\bar{r}-\bar{r}'\right|}$ using the relation

$$I_1 = \frac{e^{-jk_j\left|\bar{r}-\bar{r}'\right|}}{\left|\bar{r}-\bar{r}'\right|} = \frac{-j}{2}\int_{-\infty}^{\infty} H_0^2(k_{\rho_j}\left|\bar{\rho}-\bar{\rho}'\right|)e^{-jk_z(z-z')}dk_z. \tag{3.17}$$

Consequently, the resultant expression for the tangential components of the space domain Green's function representations becomes,

$$\begin{aligned} G_{uv} \;=\; & (\frac{j\partial}{\partial z})^l \left\{ \frac{1}{2\pi}\int_{-\infty}^{\infty} \left(\frac{\tilde{G}_{uv}}{k_z^l} + \frac{1}{4\omega\epsilon_j} C_{uv}(k_{z\infty})(k_{\rho_j}^2)^q F_1^{uv}[S_1] \right) e^{-jk_z(z-z')}dk_z \right. \\ & \left. -\frac{j}{4\pi\omega\epsilon_j} C_{uv}(k_{z\infty}) \left(k_j^2 - \frac{\partial^2}{\partial z \partial z'} \right)^q F_2^{uv}[I_1] \right\} \end{aligned} \tag{3.18}$$

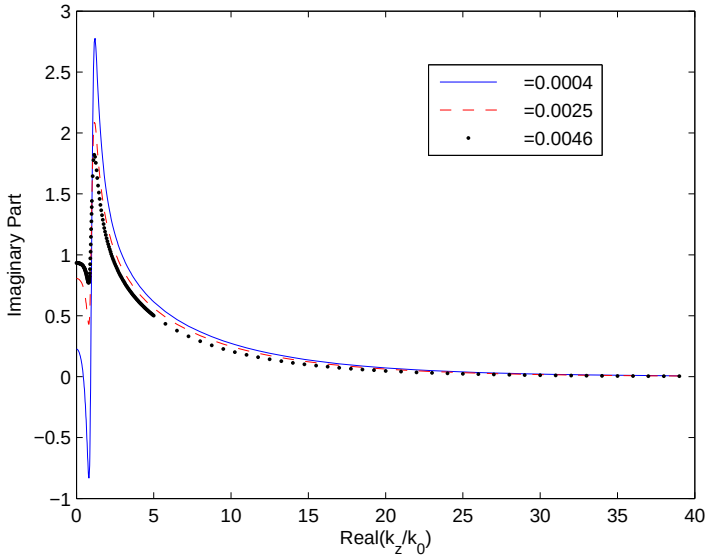

Figure 3.4: Imaginary part of $\tilde{G}_{zz}$ integrand in (3.18) for different $\Delta\phi$ (in radian) values for the same cylinder parameters given in Fig. 3.2

where

$$F_2^{zz}[I_1] = I_1 \tag{3.19}$$

$$F_2^{z\phi}[I_1] = F_2^{\phi z}[I_1] = j\frac{\partial I_1}{\partial \phi'} = -j\frac{\partial I_1}{\partial \phi} \tag{3.20}$$

$$F_2^{\phi\phi}[I_1] = \frac{\partial^2 I_1}{\partial \phi \partial \phi'}\,. \tag{3.21}$$

Note that similar to the $F_1^{uv}[.]$ case, the partial derivatives with respect to ϕ and ϕ' in the space domain closed-form part of (3.18) [i.e., (3.20) and (3.21)] are due to n in the spectral domain. Besides, as it is seen from (3.18), the $(k_{\rho_j}^2)$ term in spectral domain corresponds to the $(k_j^2 - \frac{\partial^2}{\partial z \partial z'})$ term in the space domain since both the $(j\frac{\partial}{\partial z})$ and $(-j\frac{\partial}{\partial z'})$ terms in the space domain correspond to k_z in the spectral domain (note that $k_{\rho_j}^2 = k_j^2 - k_z^2$).

Although the space domain Green's function representation given by (3.18) is not in closed-form, the integrand in (3.18) is now fast decaying even for very small $\Delta\phi$ values. The imaginary part of the integrand of (3.18) for $u = z$, $v = z$ is plotted in Fig. 3.4 for different $\Delta\phi$ values for the aforementioned cylinder. As

it is seen in Fig. 3.4, the integrand of (3.18) for $u = z$, $v = z$ is now well-behaved and converges to zero as desired. Note that the real parts of both (3.12) and the integrand of (3.18) do not pose any difficulty. Also note that because the first term of (3.18) has an integral (Fourier transform integral), the present form of the tangential components of the Green's function representations is not in closed-form. Therefore, the inverse Fourier transform which is the first term of (3.18) is evaluated in closed-form with the aid of GPOF method as explained in Chapter 4. Finally, the even and odd properties of the Green's functions that are given in Appendix F are used in this dissertation and as seen from Appendix F, $G_{\phi z}$ is not computed but determined using the $G_{z\phi}$ results.

3.2 Space Domain Green's Function Representations For The Probe-Related Components ($G_{z\rho}$, $G_{\phi\rho}$, $G_{\rho z}$, $G_{\rho\phi}$)

Similar to the tangential components, the spectral domain Green's function representations for the probe-related components can be written as

$$\frac{\tilde{G}_{v\rho}}{k_z^l} = -\frac{1}{4\omega\epsilon_j}\left\{\sum_{n=-\infty}^{\infty} n^p H_n^{(2)}(k_{\rho_j}\rho)J_n(k_{\rho_j}\rho')f_{v\rho}(n,k_z)e^{jn\Delta\phi}\right\} \quad (3.22)$$

where $l = 1$, $p = 1$ for $v = z$, and $l = 0$, $p = 2$ for $v = \phi$. In this dissertation, $G_{\rho z}$ and $G_{\rho\phi}$ components are not computed and these components are determined using the $G_{z\rho}$ and $G_{\phi\rho}$ terms, respectively, using the even and odd properties of the related Green's function components given in Appendix F. The key term in (3.22) is $f_{v\rho}$ and it is explicitly given by

$$f_{z\rho} = -jk_{\rho_j}f_{\rho 3}^{11} - \frac{\omega\epsilon_j}{k_z\rho'}f_{\rho 1}^{12} \quad (3.23)$$

$$f_{\phi\rho} = \frac{k_z}{k_{\rho_m}^2\rho}\left[jk_zk_{\rho_j}f_{\rho 3}^{11} + \frac{\omega\epsilon_j}{\rho'}f_{\rho 1}^{12}\right] + \frac{j\omega\mu_m}{k_{\rho_m}}\left[jk_zk_{\rho_j}f_{\rho 4}^{21} + \frac{\omega\epsilon_j}{\rho'}f_{\rho 2}^{22}\right] \quad (3.24)$$

where $f_{\rho 3}^{11}$, $f_{\rho 1}^{12}$, $f_{\rho 4}^{21}$, $f_{\rho 2}^{22}$ are the corresponding entries (each superscript indicates the corresponding entry) of $\underline{\underline{F_{\rho 1}}}$,$\underline{\underline{F_{\rho 2}}}$, $\underline{\underline{F_{\rho 3}}}$, $\underline{\underline{F_{\rho 4}}}$ linked to $\underline{\underline{F_n}}$ as

$$\underline{\underline{F_{\rho 1}}} = \frac{1}{H_n^{(2)}(k_{\rho_j}\rho)J_n(k_{\rho_j}\rho')}\,\underline{\underline{F_n}} \tag{3.25}$$

$$\underline{\underline{F_{\rho 2}}} = \frac{1}{nH_n^{(2)}(k_{\rho_j}\rho)J_n(k_{\rho_j}\rho')}\,\frac{\partial \underline{\underline{F_n}}}{\partial(k_{\rho_m}\rho)} \tag{3.26}$$

$$\underline{\underline{F_{\rho 3}}} = \frac{1}{nH_n^{(2)}(k_{\rho_j}\rho)J_n(k_{\rho_j}\rho')}\,\frac{\partial \underline{\underline{F_n}}}{\partial(k_{\rho_j}\rho')} \tag{3.27}$$

$$\underline{\underline{F_{\rho 4}}} = \frac{1}{n^2H_n^{(2)}(k_{\rho_j}\rho)J_n(k_{\rho_j}\rho')}\,\frac{\partial^2 \underline{\underline{F_n}}}{\partial(k_{\rho_j}\rho')\partial(k_{\rho_m}\rho)}\,. \tag{3.28}$$

In (3.22) the $f_{v\rho}$ term is odd with respect to n. Therefore, in order to apply the envelope extraction with respect to n, the result of the following summation is to be obtained:

$$\sum_{n=1}^{\infty} H_n^{(2)}(k_{\rho_j}\rho)J_n(k_{\rho_j}\rho')\sin(n\Delta\phi). \tag{3.29}$$

Unfortunately, there is not any closed-form expression for the summation given in (3.29). Moreover, it is not possible to obtain this summation using any expression such as (3.11). Therefore, in order to evaluate (3.22) the spectral domain $\tilde{G}_{z\rho}$ and $\tilde{G}_{\phi\rho}$ components are modified as follows:

$$\frac{\tilde{G}_{v\rho}}{k_z^l} = -\frac{1}{4\omega\epsilon_j}\left\{\sum_{n=-\infty}^{\infty} k_{\rho_j} n^p H_n^{(2)}(k_{\rho_j}\rho)J_n'(k_{\rho_j}\rho')\Big[\frac{nJ_n(k_{\rho_j}\rho')}{k_{\rho_j}J_n'(k_{\rho_j}\rho')}f_{v\rho}(n,k_z)\Big]e^{jn\Delta\phi}\right\}. \tag{3.30}$$

In (3.30), $[\frac{nJ_n(k_{\rho_j}\rho')}{k_{\rho_j}J_n'(k_{\rho_j}\rho')}f_{v\rho}(n,k_z)]$ term is now even with respect to n and it converges to a constant value as n gets large using the Debye approximations given in Appendix A. k_{ρ_j} term is also added as a multiplicant to use the ρ' derivative of (3.11) in the rest of the probe-related components of Green's function representations. Note that in this new formulation, $p = 0$, $l = 1$ for $v = z$, and $p = 1$, $l = 0$ for $v = \phi$. Defining

$$\tilde{f}_{v\rho}(n,k_z,\rho') = \frac{nJ_n(k_{\rho_j}\rho')}{k_{\rho_j}J_n'(k_{\rho_j}\rho')}f_{v\rho}(n,k_z), \tag{3.31}$$

the spectral domain $\tilde{G}_{v\rho}$ components can be expressed as

$$\frac{\tilde{G}_{v\rho}}{k_z^l} = -\frac{1}{4\omega\epsilon_j}\left\{\sum_{n=-\infty}^{\infty} k_{\rho_j} n^p H_n^{(2)}(k_{\rho_j}\rho) J_n'(k_{\rho_j}\rho') \tilde{f}_{v\rho}(n, k_z, \rho') e^{jn\Delta\phi}\right\} \quad (3.32)$$

where $\tilde{f}_{v\rho}(n, k_z, \rho')$ is now ρ' dependent. Similar to the tangential components, an envelope extraction with respect to n is performed and the $\tilde{G}_{v\rho}$ components are written as

$$\begin{aligned}\frac{\tilde{G}_{v\rho}}{k_z^l} = & -\frac{1}{4\omega\epsilon_j}\left\{\sum_{n=-\infty}^{\infty} k_{\rho_j} n^p H_n^{(2)}(k_{\rho_j}\rho) J_n'(k_{\rho_j}\rho') e^{jn\Delta\phi}\Big[\tilde{f}_{v\rho}(n, k_z, \rho') - \tilde{C}_{v\rho}(k_z, \rho')\Big]\right. \\ & + \Big[\tilde{C}_{v\rho}(k_z, \rho') - \tilde{C}_{v\rho}(k_z, \rho' = \rho)\Big] F_1^{v\rho}[S_1] \\ & \left. + \Big[\tilde{C}_{v\rho}(k_z, \rho' = \rho)\Big] F_1^{v\rho}[S_1]\right\} \end{aligned} \quad (3.33)$$

where S_1 is given by (3.11) and

$$F_1^{z\rho}[S_1] = \frac{\partial S_1}{\partial \rho'} \quad (3.34)$$

$$F_1^{\phi\rho}[S_1] = -j\frac{\partial^2 S_1}{\partial\phi\partial\rho'}. \quad (3.35)$$

Notice that in (3.33), $\tilde{C}_{v\rho}(k_z, \rho' = \rho) F_1^{v\rho}[S_1]$ term is also subtracted from second term and added as a new term. The reason of this operation can be explained as follows: The ρ' dependence in the third term of (3.33) exists only in $F_1^{v\rho}[S_1]$ as it can be seen from (3.34)-(3.35). Thus, the ρ' integration for this term is simplified to

$$\int_{\rho'=p_s}^{\rho'=p_e} \frac{\partial S_1}{\partial \rho'} d\rho' = S_1(p_e) - S_1(p_s). \quad (3.36)$$

where p_s and p_e denote the start and end points of the probe, respectively. For the first and second terms of (3.33), ρ' integration is performed in the spectral domain from the efficiency point of view.

Finally, similar to the tangential components, the product $-\frac{1}{4\omega\epsilon_j}\tilde{C}_{v\rho}(k_{z\infty}, \rho' = \rho) F_1^{v\rho}[S_1]$ is subtracted in the spectral domain from (3.33) and its Fourier transform is added to the final space domain Green's function representation as a function of I_1 so that possible numerical problems for very large k_z values are

avoided. Consequently, the resultant expression for the $G_{v\rho}$ components of the space domain Green's function representations becomes

$$G_{v\rho} = (\frac{j\partial}{\partial z})^l \left\{ \frac{1}{2\pi} \int_{-\infty}^{\infty} \left(\frac{\tilde{G}_{v\rho}}{k_z^l} + \frac{1}{4\omega\epsilon_j} C_{v\rho}(k_{z\infty}, \rho' = \rho)\, F_1^{v\rho}\,[S_1] \right) e^{-jk_z(z-z')} dk_z \right.$$
$$\left. - \frac{j}{4\pi\omega\epsilon_j} C_{v\rho}(k_{z\infty}, \rho' = \rho) F_2^{v\rho}[I_1] \right\} \tag{3.37}$$

where

$$F_2^{z\rho}[I_1] = \frac{\partial I_1}{\partial \rho'} \tag{3.38}$$

$$F_2^{\phi\rho}[I_1] = -j\frac{\partial^2 I_1}{\partial\phi\partial\rho'}. \tag{3.39}$$

and I_1 is defined in (3.17).

Note that because the first term of (3.37) has an integral (Fourier transform integral), its present form is not in closed-form. Therefore, its inverse Fourier transform is evaluated in closed-form with the aid of the GPOF method as explained in Chapter 4.

Chapter 4

Closed-Form Evaluation of Space Domain Green's Function Representations

The spectral domain Green's function representations which have a Fourier integral with respect to k_z are transformed into the space domain by the inverse Fourier transformation given by

$$G_{uv} = \frac{1}{2\pi} \int_{-\infty}^{\infty} dk_z e^{-jk_z(z-z')} \tilde{G}_{uv} \tag{4.1}$$

where G_{uv} is the space domain Green's function representation. This formula is a time consuming numerical integration of spectral domain Green's function representation such that it ranges from $-\infty$ to ∞ along the real axis of the complex k_z plane. Therefore, the final form of the spectral domain Green's function representations (integral parts of (3.18) and (3.37) for tangential and probe-related components, respectively) are written as even functions of k_z. Then, the original Fourier k_z integral is folded to a 0 to ∞ integral by writing (4.1) as

$$G_{uv} = \frac{1}{\pi} (\frac{j\partial}{\partial z})^l \Big\{ \int_0^{\infty} dk_z \cos[k_z(z-z')] \frac{\tilde{G}_{uv}}{k_z^l} \Big\}. \tag{4.2}$$

In this dissertation, the discrete complex image method (DCIM) is proposed in the calculation of the space domain Green's function representations as a sum

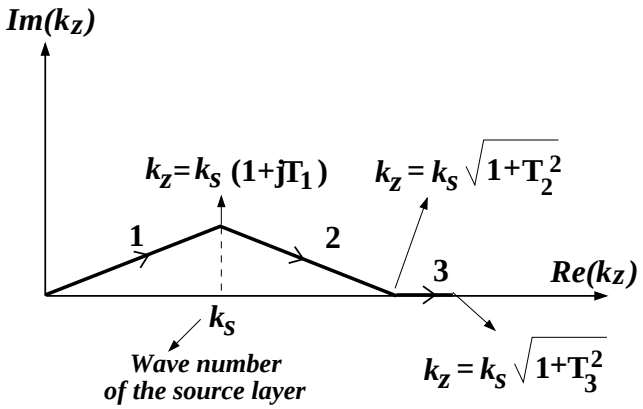

Figure 4.1: Deformed integration path used for radiation/scattering problems

of complex images by approximating the spectral domain Green's function representations (the integrand of (4.2)) in terms of complex exponentials. The numerical method which is used to find the exponential approximations of the spectral domain Green's function representations is the generalized pencil of function (GPOF) method. Therefore, in this dissertation we provide approximate closed-form expressions in terms of a couple of complex images for the space domain Green's function representations using DCIM with the aid of GPOF method. In [18], for $\rho >> \rho'$ case (radiation/scattering problem), the spectral domain Green's function representations which are again even functions of k_z are evaluated on the integration path given in Fig. 4.1 to overcome the effects of the pole and branchpoint singularities.

In order to obtain the desired accuracy when $\rho = \rho'$, the deformed integration path given in Fig 4.2 is used in this dissertation. It should be noted that the deformed integration path is an approximation of the original one (integration on the real k_z axis). Around k_s (the wave number of the source layer) the integration path given in Fig 4.2 is broken into small pieces in order to work with less number of spectral samples and complex exponentials. Instead of a single path before k_s as illustrated in Fig 4.1, two paths Γ' and Γ_1 are defined in Fig 4.2 where T' can be chosen between 0.5 and 0.8. The value of T_1 ($0.1 < T_1 < 0.5$) should be kept small to minimize the deviation from the original path. Moreover, T_2 should be large enough so that the value of k_z is larger than those of the wave

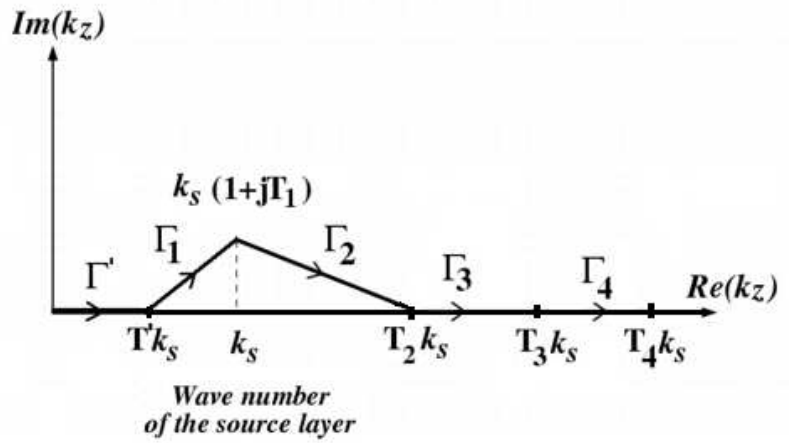

Figure 4.2: Deformed integration path

numbers of all layers ensuring that none of the singularities lies on the deformed path. T_2 can be between 4 and 6 where the other parameters can be chosen as $20 < T_3 < 30$ and $30 < T_4 < 40$, respectively. Up to $T_3 k_s$ four paths are defined instead of two (when the path given in Fig 4.2 is compared with the one given in Fig 4.1), in order to work with less number of samples since large number of samples are needed around k_s. In other words, with the integration path given in Fig 4.2 non-uniform sampling is achieved (large number of samples around k_s and less samples in other paths). On Γ_4, the spectral domain Green's function representations have smooth decaying behaviour for all possible $\Delta\phi$ values. To reach this path, Γ_3 is used as a transition path to be far away from k_s.

The parameters that define the deformed integration path are as follows:

$$\Gamma' : \quad k_z = k' \frac{t'}{T'}, \quad 0 \leq t' < T' \tag{4.3}$$

$$\Gamma_1 : \quad k_z = \left[k' + (k_1 - k') \frac{t_1}{T' - T_1} \right], \quad 0 \leq t_1 < T' - T_1 \tag{4.4}$$

$$\Gamma_2 : \quad k_z = \left[k_1 + (k_2 - k_1) \frac{t_2}{T_2 - T_1} \right], \quad 0 \leq t_2 < T_2 - T_1 \tag{4.5}$$

$$\Gamma_3 : \quad k_z = \left[k_2 + (k_3 - k_2) \frac{t_3}{T_3 - T_2} \right], \quad 0 \leq t_3 < T_3 - T_2 \tag{4.6}$$

$$\Gamma_4 : \quad k_z = \left[k_3 + (k_4 - k_3) \frac{t_4}{T_4 - T_3} \right], \quad 0 \leq t_4 < T_4 - T_3 \tag{4.7}$$

where k_s is the wave number of the source layer and $k' = T'k_s$, $k_1 = k_s + jk_sT_1$, $k_2 = T_2k_s$, $k_3 = T_3k_s$ and $k_4 = T_4k_s$.

To obtain space domain counterparts, the spectral domain Green's function representations are sampled on paths Γ', Γ_1, Γ_2, Γ_3 and Γ_4 by taking N', N_1, N_2, N_3 and N_4 samples, respectively. Using GPOF (the details of GPOF is discussed in Appendix B), the samples are expressed in terms of M', M_1, M_2, M_3 and M_4 complex exponentials of k_z on each part of the integration path. Let the approximated spectral domain Green's function representation (or the outputs of the GPOF on each path) be

$$\tilde{G}'_{GPOF_{uv}} \cong \sum_{m=1}^{M'} b_{m_t} e^{s_{m_t} t'} \tag{4.8}$$

$$\tilde{G}^1_{GPOF_{uv}} \cong \sum_{n=1}^{M_1} b_{n_t} e^{s_{n_t} t_1} \tag{4.9}$$

$$\tilde{G}^2_{GPOF_{uv}} \cong \sum_{l=1}^{M_2} b_{l_t} e^{s_{l_t} t_2} \tag{4.10}$$

$$\tilde{G}^3_{GPOF_{uv}} \cong \sum_{s=1}^{M_3} b_{s_t} e^{s_{s_t} t_3} \tag{4.11}$$

$$\tilde{G}^4_{GPOF_{uv}} \cong \sum_{p=1}^{M_4} b_{p_t} e^{s_{p_t} t_4} \tag{4.12}$$

where the spectral domain Green's function representation is approximated as

$$\tilde{G}_{GPOF_{uv}} \cong \tilde{G}'_{GPOF_{uv}} + \tilde{G}^1_{GPOF_{uv}} + \tilde{G}^2_{GPOF_{uv}} + \tilde{G}^3_{GPOF_{uv}} + \tilde{G}^4_{GPOF_{uv}}. \tag{4.13}$$

These outputs of GPOF are then transformed to complex exponentials of k_z as follows:

$$\tilde{G}'_{GPOF_{uv}} \cong \sum_{m=1}^{M'} b_{m_t} e^{s_{m_t} t'} = \sum_{m=1}^{M'} b_{m_k} e^{k_z s_{m_k}} \tag{4.14}$$

$$\tilde{G}^1_{GPOF_{uv}} \cong \sum_{n=1}^{M_1} b_{n_t} e^{s_{n_t} t_1} = \sum_{n=1}^{M_1} b_{n_k} e^{k_z s_{n_k}} \tag{4.15}$$

$$\tilde{G}^2_{GPOF_{uv}} \cong \sum_{l=1}^{M_2} b_{l_t} e^{s_{l_t} t_2} = \sum_{l=1}^{M_2} b_{l_k} e^{k_z s_{l_k}} \tag{4.16}$$

$$\tilde{G}^3_{GPOF_{uv}} \cong \sum_{s=1}^{M_3} b_{s_t} e^{s_{s_t} t_3} = \sum_{s=1}^{M_3} b_{s_k} e^{k_z s_{s_k}} \tag{4.17}$$

$$\tilde{G}^4_{GPOF_{uv}} \cong \sum_{p=1}^{M_4} b_{p_t} e^{s_{p_t} t_4} = \sum_{p=1}^{M_4} b_{p_k} e^{k_z s_{p_k}} \tag{4.18}$$

such that

$$b_{m_k} = b_{m_t} \tag{4.19}$$

$$s_{m_k} = s_{m_t} \frac{T'}{k'} \tag{4.20}$$

$$b_{n_k} = b_{n_t} e^{-s_{n_t} k' \frac{(T'-T_1)}{(k_1-k')}} \tag{4.21}$$

$$s_{n_k} = s_{n_t} \frac{(T'-T_1)}{(k_1-k')} \tag{4.22}$$

$$b_{l_k} = b_{l_t} e^{-s_{l_t} k_1 \frac{(T_2-T_1)}{(k_2-k_1)}} \tag{4.23}$$

$$s_{l_k} = s_{l_t} \frac{(T_2-T_1)}{(k_2-k_1)} \tag{4.24}$$

$$b_{s_k} = b_{s_t} e^{-s_{s_t} k_2 \frac{(T_3-T_2)}{(k_3-k_2)}} \tag{4.25}$$

$$s_{s_k} = s_{s_t} \frac{(T_3-T_2)}{(k_3-k_2)} \tag{4.26}$$

$$b_{p_k} = b_{p_t} e^{-s_{p_t} k_3 \frac{(T_4-T_3)}{(k_4-k_3)}} \tag{4.27}$$

$$s_{p_k} = s_{p_t} \frac{(T_4-T_3)}{(k_4-k_3)}. \tag{4.28}$$

Note that, as explained in Appendix B, inputs of the GPOF method are the spectral domain samples, the number of samples N, the number of complex exponentials M and the sampling interval δt. In GPOF implementation, the sampling interval δt is chosen to be $\delta t = T'/N'$, $\delta t = (T'-T_1)/N_1$, $\delta t = (T_2-T_1)/N_2$, $\delta t = (T_3-T_2)/N_3$ and $\delta t = (T_4-T_3)/N_4$ on paths Γ', Γ_1, Γ_2, Γ_3 and Γ_4, respectively. As a result of the GPOF implementation, the spectral domain Green's function representations are obtained in the form of complex exponentials of k_z and the integral given by

$$G_{GPOF_{uv}}(z-z') = \frac{1}{\pi} \int_{\Gamma'+\Gamma_1+\Gamma_2+\Gamma_3+\Gamma_4} dk_z cos[k_z(z-z')] \tilde{G}_{GPOF_{uv}} \tag{4.29}$$

is evaluated analytically. Consequently, the following expressions are obtained for the space domain Green's function representations:

$$G^{'}_{GPOF_{uv}}(z-z') \approx \frac{1}{2\pi}\sum_{m=1}^{M'} b_{m_k}\left(\frac{e^{k'[s_{m_k}+j(z-z')]}-1}{s_{m_k}+j(z-z')} + \frac{e^{k'[s_{m_k}-j(z-z')]}-1}{s_{m_k}-j(z-z')}\right), \tag{4.30}$$

$$G^{1}_{GPOF_{uv}}(z-z') \approx \frac{1}{2\pi}\sum_{n=1}^{M_1} b_{n_k}\left(\frac{e^{k_1[s_{n_k}+j(z-z')]}-e^{k'[s_{n_k}+j(z-z')]}}{s_{n_k}+j(z-z')} + \frac{e^{k_1[s_{n_k}-j(z-z')]}-e^{k'[s_{n_k}-j(z-z')]}}{s_{n_k}-j(z-z')}\right), \tag{4.31}$$

$$G^{2}_{GPOF_{uv}}(z-z') \approx \frac{1}{2\pi}\sum_{l=1}^{M_2} b_{l_k}\left(\frac{e^{k_2[s_{l_k}+j(z-z')]}-e^{k_1[s_{l_k}+j(z-z')]}}{s_{l_k}+j(z-z')} + \frac{e^{k_2[s_{l_k}-j(z-z')]}-e^{k_1[s_{l_k}-j(z-z')]}}{s_{l_k}-j(z-z')}\right), \tag{4.32}$$

$$G^{3}_{GPOF_{uv}}(z-z') \approx \frac{1}{2\pi}\sum_{s=1}^{M_3} b_{s_k}\left(\frac{e^{k_3[s_{s_k}+j(z-z')]}-e^{k_2[s_{s_k}+j(z-z')]}}{s_{s_k}+j(z-z')} + \frac{e^{k_3[s_{s_k}-j(z-z')]}-e^{k_2[s_{s_k}-j(z-z')]}}{s_{s_k}-j(z-z')}\right), \tag{4.33}$$

$$G^{4}_{GPOF_{uv}}(z-z') \approx \frac{1}{2\pi}\sum_{p=1}^{M_4} b_{p_k}\left(\frac{e^{k_4[s_{p_k}+j(z-z')]}-e^{k_3[s_{p_k}+j(z-z')]}}{s_{p_k}+j(z-z')} + \frac{e^{k_4[s_{p_k}-j(z-z')]}-e^{k_3[s_{p_k}-j(z-z')]}}{s_{p_k}-j(z-z')}\right) \tag{4.34}$$

where the final space domain representation is obtained as

$$G_{GPOF_{uv}} = G^{'}_{GPOF_{uv}} + G^{1}_{GPOF_{uv}} + G^{2}_{GPOF_{uv}} + G^{3}_{GPOF_{uv}} + G^{4}_{GPOF_{uv}}. \tag{4.35}$$

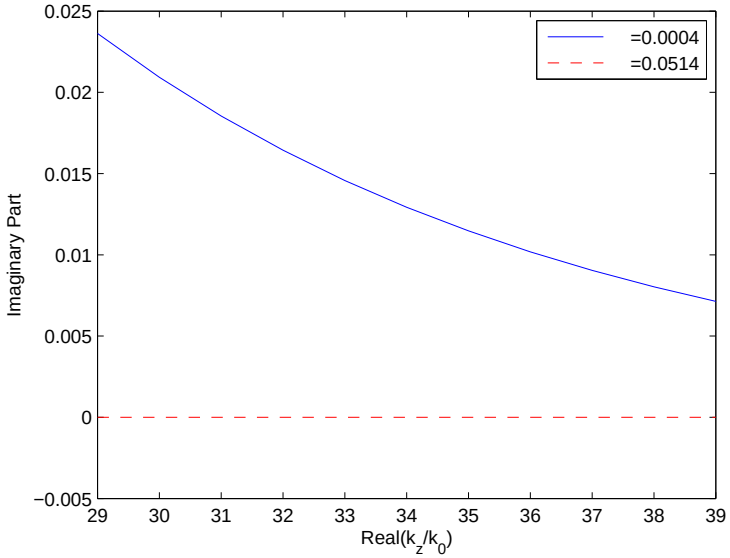

Figure 4.3: Imaginary part of $\tilde{G}_{zz}$ integrand on Γ_4 in (3.18) for different $\Delta\phi$ (in radian) values for the same cylinder parameters given in Fig. 3.2

Note that in this dissertation, the two-level GPOF implementation given in [18] is not used due to the envelope extraction with respect to k_z that we performed as explained in Chapter 3. Recall that when implementing the envelope extraction with respect to k_z, the value of the spectral domain Green's function representation for large k_z (for k_z values much larger than k_4) is subtracted in the spectral domain and its Fourier transform is added to the final space domain Green's function representation analytically (i.e., in closed-form). Therefore, contributions coming from large k_z values are automatically included in closed-form. As a result of this step, when the integral (i.e., the first) terms of (3.18) for tangential components and (3.37) for probe-related components are considered for GPOF implementation, the magnitudes of these terms show a variation (due to their imaginary parts) on Γ_4 for different $\Delta\phi$ values as shown in Fig. 4.3. When $\Delta\phi$ is small, the magnitude is relatively large (in the order of 10^{-1}, 10^{-2}, etc.). When $\Delta\phi$ is large, the magnitude is very small (in the order of 10^{-7}, 10^{-8}) and may be noisy (see Fig. 4.4 when $\Delta\phi = 0.0514$). However, when the magnitude is very small and noisy for large k_z values (i.e., on Γ_4, see Fig. 4.4) numerical issues may occur in the implementation of GPOF leading to

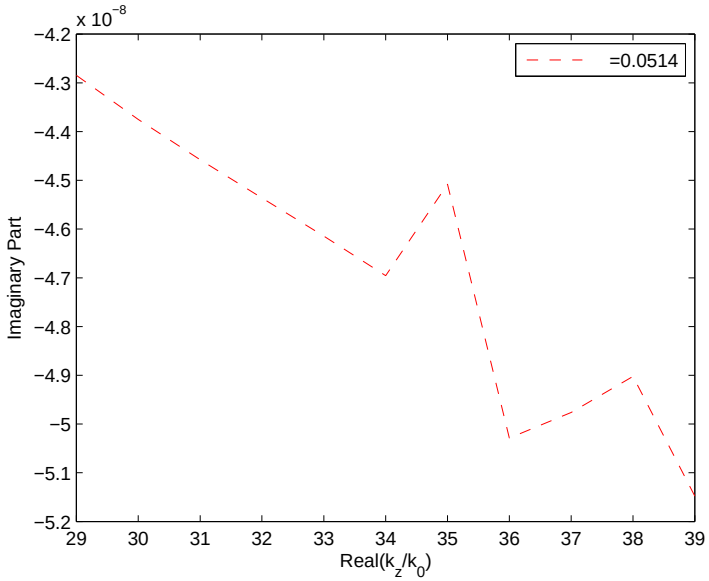

Figure 4.4: Imaginary part of $\tilde{G}_{zz}$ integrand on Γ_4 in (3.18) for $\Delta\phi = 0.0514$ (in radian) for the same cylinder parameters given in Fig. 3.2

a resultant complex exponential that may have an exponent (i.e., s_{p_k}) with real part greater than zero.

Consequently, in this dissertation, contributions coming from the k_z values larger than k_4 are not included because they are usually very small even for relatively small k_z values (because of the envelope extraction). Furthermore, when $\Delta\phi$ is small (the threshold value for small $\Delta\phi$ is set by the user) and especially for the source region where the source and observation points are very close to each other, k_4 can be set to a large value (sometimes $1000k_0$, only in the numerical evaluation of (4.34), without taking any spectral sample beyond k_4) to make sure that contributions coming from large k_z values are properly included. One final note that we initialize all GPOF parameters (i.e., T', T_1, T_2, T_3, T_4, N', N_1, N_2, N_3, N_4, M', M_1, M_2, M_3, M_4, δ_t, etc) before we attempt to solve a microstrip antenna/array problem. Therefore, these parameters should be kept the same regardless of the $\Delta\phi$ value.

Chapter 5

Mutual Impedance Calculations and The Treatment of Singularities

To be able to safely use the developed CFGF representations in a MoM solution procedure, the CFGF representations should be valid for almost all possible source and field points that lie on the same radial distance from the axis of the cylinder. However, there are two types of singularities that should be treated carefully. One of them is so called the spectral domain singularity and occurs along the axial line ($\rho = \rho'$, $\phi = \phi'$). The other one is so called the space domain singularity and occurs when the source and observation points overlap with each other ($\rho = \rho'$, $\phi = \phi'$, $z = z'$). These two singularities are fortunately integrable singularities, and are treated analytically during the mutual impedance calculations in a Galerkin type MoM procedure by performing the integrals over the surface areas of basis and testing current modes as explained in a detailed way in this chapter and in Appendices C, D and E for zz, $z\phi = \phi z$ and $\phi\phi$ couplings, respectively.

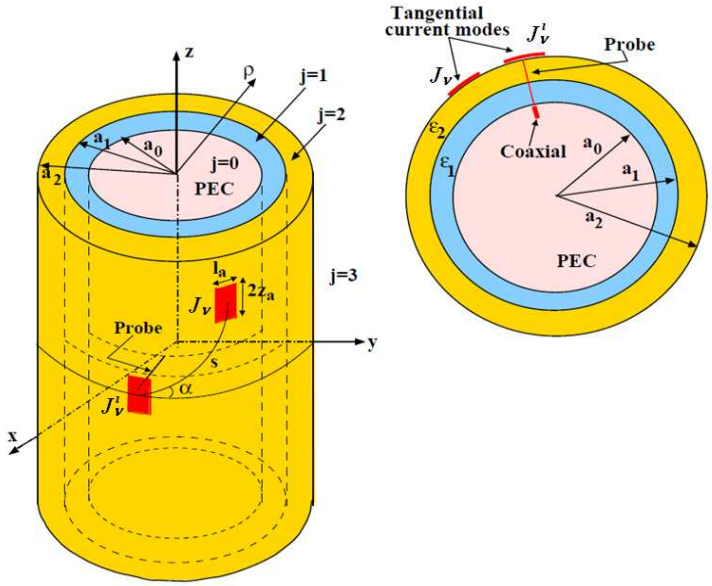

Figure 5.1: Geometry of the problem. Current modes on a multilayer cylindrical structure together with its cross-sectional view from the top

5.1 Geometry and Current Mode Definitions

Fig. 3.1 is redrawn as Fig. 5.1 and the descriptions of the geometry is repeated to be able to explain the mutual impedance calculations clearly. As mentioned in Chapter 3, the geometry of current modes on a multilayer cylindrically stratified media is illustrated in Fig. 5.1 together with a cross-sectional view from the top. The structure is assumed to be infinite in the z direction. A PEC cylindrical ground, denoted by the subscript $j = 0$, forms the innermost region with a radius a_0, and material layers, denoted by the subscript $j = 1, 2, ...$ surround the PEC region coaxially, as shown in Fig. 5.1 (subscript $j = 1$ denotes the substrate layer; subscript $j = 2$ denotes the superstrate layer, and subscript $j = 3$ denotes the air layer in Fig. 5.1). Each layer has a permittivity, permeability, and radius denoted by ϵ_j, μ_j and a_j, respectively. Furthermore, current modes, denoted by $J'_v(\rho', \phi', z')$ and $J_v(\rho, \phi, z)$ are depicted in Fig. 5.1 where $v = \phi$ or z. A $z-$ or $\phi-$ directed tangential current source, defined at air-dielectric or dielectric-dielectric interface has a dimension of $2z_a \times l_a$ (with $l_a = a_j\phi_a$) along the $z-$ and $\phi-$ directions or $2l_a \times z_a$ along the $\phi-$ and $z-$ directions, respectively. On the other

hand, if the current mode is normal to an interface (excitation via a probe), it is usually located inside a layer, assumed to be infinitesimally thin in terms of $\phi-$ and $z-$ coordinates, and has a certain length along the radial direction. Finally, in Fig. 5.1 s denotes the geodesic distance between the two current modes (or between the source and observation points for the CFGF expressions) and α is the angle between the geodesic path and the $\phi-$ axis. Note that during the mutual impedance calculations for tangential components ρ is equal to ρ'. However, when the probe-related components are involved ρ is very close to ρ' but usually $\rho \neq \rho'$.

The mutual impedance, $Z_{12_{uv}}$, between two current modes (J_{1_u}, J_{2_v}) is simply given by

$$Z_{12_{uv}} = \int_{s_2} E_{1_u} J_{2_v}\, ds \tag{5.1}$$

where E_{1_u} is the field due to the current mode J_{1_u} and s_2 is the area occupied by the current mode J_{2_v}. In this dissertation, the tangential current modes are selected to be piecewise sinusoidal (PWS) current modes. As an example, the expression for a piecewise sinusoid $z-$ directed current mode, J_z, located at $\rho = a_1$ in Fig. 5.1 is given in the space domain as

$$J_z(\phi, z) = \text{rect}(\frac{a_1\phi}{l_a/2})\frac{1}{l_a}\text{PWS}(k_a, z_a, z) \tag{5.2}$$

where l_a is the dimension along the $\phi-$ direction and $2z_a$ is the dimension along the $z-$ direction and

$$\text{rect}(\frac{x}{a}) = \begin{cases} 1, & |x| < a \\ 0, & \text{otherwise} \end{cases} \tag{5.3}$$

$$\text{PWS}(k_a, z_a, z) = \begin{cases} \frac{\sin[k_a(z_a - |z|)]}{\sin(k_a z_a)}, & |z| < z_a \\ 0, & \text{otherwise} \end{cases}. \tag{5.4}$$

Similarly, the expression for a piecewise sinusoid $\phi-$ directed current mode, J_ϕ, located at $\rho = a_1$ in Fig. 5.1 is expressed in the space domain as

$$J_\phi(\phi, z) = \text{rect}(\frac{z}{z_a/2})\frac{1}{z_a}\text{PWS}(k_a, l_a, a_1\phi). \tag{5.5}$$

In (5.2) and (5.5) k_a is defined either as

$$k_a = k_0\sqrt{\frac{\text{Re}(\epsilon_{r_i}) + 1}{2} + \frac{\text{Re}(\epsilon_{r_i}) - 1}{2}(1 + 10\frac{t_{hi}}{\min(W, L)})^{-0.5}} \tag{5.6}$$

or as

$$k_a = k_0\sqrt{\frac{\mathrm{Re}(\epsilon_{r_i}) + \mathrm{Re}(\epsilon_{r_{i+1}})}{2}}. \tag{5.7}$$

where ϵ_{r_i} is the permittivity of the i^{th} dielectric region, t_{hi} is the thickness of the i^{th} dielectric region, W and L are the width and length of the microstrip antenna, respectively and Re(.) denotes the real part of the permittivity since the dielectric region can be lossy. When the microstrip antenna is located at the air-dielectric interface, the definition given by (5.6) is used for k_a. On the other hand, if the antenna is located at the dielectric-dielectric interface (substrate-superstrate situation), (5.7) is used for k_a.

5.2 Mutual Impedance Calculations For Tangential Components

Defining E_{1_u} in (5.1) as $E_{1_u} = \int_{s_1} G_{uv} J_{1_u}$ with s_1 being the area occupied by the current mode J_{1_u}, the mutual impedance formulation can be expressed as

$$Z_{12uv} = \int\int\int\int J_{1_u} J_{2_v} G_{uv} dz dz' d\beta d\beta' \tag{5.8}$$

where $\beta = \rho\phi$, $\beta' = \rho'\phi'$ and $d\beta = \rho d\phi$ (and $d\beta' = \rho' d\phi'$). In (5.8) $dz'd\beta' = ds_1$ and $dzd\beta = ds_2$.

To find the mutual impedance results for tangential components for all problematic cases (that exhibit singularity), (5.8) will be rewritten and analyzed in detail. Starting with the space domain Green's function representation, G_{uv}, given by (3.18) for tangential components, G_{uv} is expressed as

$$G_{uv} = (k_j^2 - \frac{\partial^2}{\partial z \partial z'})^q (j\frac{\partial}{\partial z})^{r_1} (-j\frac{\partial}{\partial \phi})^{t_1} (j\frac{\partial}{\partial \phi'})^{t_2} G_{uv2} \tag{5.9}$$

where for $uv = zz$ case $q = 1, r_1 = 0, t_1 = 0, t_2 = 0$; for $uv = z\phi = \phi z$ case $q = 0, r_1 = 1, t_1 = 0, t_2 = 1$; and for $uv = \phi\phi$ case $q = 0, r_1 = 0, t_1 = 1, t_2 = 1$. As seen in (5.9) G_{uv} and G_{uv2} are related to each other by the derivatives with respect to ϕ, ϕ', z and z'. Note that (5.9) is obtained from (3.18) by recognizing

the Fourier series (with respect to n) and Fourier Transform (with respect to k_z) relations between the spectral domain and space domain Green's functions. Briefly, the term $(k_j^2 - \frac{\partial^2}{\partial z \partial z'})$ in the space domain corresponds to $k_{\rho_j}^2$ in the spectral domain. Similarly, the $(j\frac{\partial}{\partial z})$ term in the space domain corresponds to k_z in the spectral domain. Finally, both the $(-j\frac{\partial}{\partial \phi})$ and $(j\frac{\partial}{\partial \phi'})$ terms in the space domain correspond to n in the spectral domain. On the other hand, the advantages of rewriting G_{uv} as (5.9) are as follows: (i) For the zz component, the spectral domain counterpart of G_{uv2} decays faster than that of G_{uv} with respect to k_z. (ii) For the $\phi\phi$ component, the spectral domain counterpart of G_{uv2} decays faster than that of G_{uv} with respect to n. (iii) Most importantly, these derivatives are transferred onto current modes using integration by parts. Thereby, the aforementioned two different types of singularities are kept as integrable singularities. Consequently, for the rest of this chapter G_{uv2} is the part of the Green's function that appears in the mutual impedance calculations.

After transferring the derivatives acting on G_{uv} onto the PWS current modes (which are differentiable) using integration by parts, the following mutual impedance expressions are obtained for tangential components.

$$Z_{12zz} = \int\int\int\int \Big(k_0^2 J_z J_{z'} G_{zz2} - \frac{\partial J_z}{\partial z}\frac{\partial J_{z'}}{\partial z'} G_{zz2}\Big) dz dz' d\beta d\beta' \tag{5.10}$$

$$Z_{12z\phi} = \int\int\int\int (-j)\frac{\partial J_z}{\partial z}(-j)\frac{\partial J_{\phi'}}{\partial \phi'} G_{z\phi 2} dz dz' d\beta d\beta' \tag{5.11}$$

$$Z_{12\phi\phi} = \int\int\int\int \frac{\partial J_\phi}{\partial \phi}\frac{\partial J_{\phi'}}{\partial \phi'} G_{\phi\phi 2} dz dz' d\beta d\beta'. \tag{5.12}$$

The details about the expressions (5.10), (5.11), (5.12) are given in Appendix (C.1), Appendix (D.1), Appendix (E.1), respectively.

In order to discuss the mutual impedance calculations for tangential components let G_{uv2} be defined in the form of inverse Fourier transform (IFT) as

$$G_{uv2} = \mathcal{F}^{-1}\Big\{ -\frac{1}{4\omega\epsilon_j} \sum_{n=-\infty}^{\infty} H_n^{(2)}(k_{\rho_j}\rho) J_n(k_{\rho_j}\rho') f_{uv}(n,k_z) e^{jn(\Delta\phi)} \Big\}. \tag{5.13}$$

where $\mathcal{F}^{-1}\{.\}$ denotes the IFT operation. Note that the IFT is performed using the DCIM with the aid of the GPOF method. After performing the envelope extraction with respect to n, (5.13) is written as

$$\begin{aligned} G_{uv2} &= \mathcal{F}^{-1}\Big\{ -\frac{1}{4\omega\epsilon_j} \sum_{n=-\infty}^{\infty} H_n^{(2)}(k_{\rho_j}\rho) J_n(k_{\rho_j}\rho') [f_{uv}(n,k_z) - C_{uv}(k_z)] e^{jn(\Delta\phi)} \Big\} \\ &\quad + \mathcal{F}^{-1}\Big\{ -\frac{1}{4\omega\epsilon_j} C_{uv}(k_z) H_0^{(2)}(k_{\rho_j} |\bar{\rho} - \bar{\rho}'|) \Big\}. \end{aligned} \tag{5.14}$$

Similarly, after performing the envelope extraction with respect to k_z, the following expression is obtained

$$\begin{aligned} G_{uv2} &= \mathcal{F}^{-1}\Big\{ -\frac{1}{4\omega\epsilon_j} \sum_{n=-\infty}^{\infty} H_n^{(2)}(k_{\rho_j}\rho) J_n(k_{\rho_j}\rho') [f_{uv}(n,k_z) - C_{uv}(k_z)] e^{jn(\Delta\phi)} \Big\} \\ &\quad + \mathcal{F}^{-1}\Big\{ -\frac{1}{4\omega\epsilon_j} [C_{uv}(k_z) - C_{uv}(k_{z\infty})] H_0^{(2)}(k_{\rho_j} |\bar{\rho} - \bar{\rho}'|) \Big\} \\ &\quad + \mathcal{F}^{-1}\Big\{ -\frac{1}{4\omega\epsilon_j} C_{uv}(k_{z\infty}) H_0^{(2)}(k_{\rho_j} |\bar{\rho} - \bar{\rho}'|) \Big\}. \end{aligned} \tag{5.15}$$

The IFT of the last term of (5.15) is available in closed-form. Therefore, (5.15) is written as

$$\begin{aligned} G_{uv2} &= \mathcal{F}^{-1}\Big\{ -\frac{1}{4\omega\epsilon_j} \sum_{n=-\infty}^{\infty} H_n^{(2)}(k_{\rho_j}\rho) J_n(k_{\rho_j}\rho') [f_{uv}(n,k_z) - C_{uv}(k_z)] e^{jn(\Delta\phi)} \Big\} \\ &\quad + \mathcal{F}^{-1}\Big\{ -\frac{1}{4\omega\epsilon_j} \left[C_{uv}(k_z) - C_{uv}(k_{z\infty})\right] H_0^{(2)}(k_{\rho_j} |\bar{\rho} - \bar{\rho}'|) \Big\} \\ &\quad - \frac{j}{4\pi\omega\epsilon_j} C_{uv}(k_{z\infty}) \frac{e^{-jk_j\left|\bar{r}-\bar{r}'\right|}}{|\bar{r} - \bar{r}'|}. \end{aligned} \tag{5.16}$$

The representation given by (5.16) is used in the mutual impedance calculations given by (5.10)-(5.12) when there is no singularity. The treatment for the singularities are given next.

5.2.1 Spectral Domain Singularity ($\rho = \rho'$, $\phi = \phi'$)

The spectral domain singularity occurs along the axial line (when $\rho = \rho'$ and $\phi = \phi'$) because the argument of the Hankel function $H_0^2(k_{\rho_j}\,|\bar{\rho} - \bar{\rho}'|)$ becomes zero as given by

$$|\bar{\rho} - \bar{\rho}'| = \sqrt{\rho^2 + \rho'^2 - 2\rho\rho'\cos(\Delta\phi)}. \tag{5.17}$$

The remedy for this problem is to use the small argument approximation of the Hankel function given by

$$H_0^2(k_{\rho_j}\,|\bar{\rho} - \bar{\rho}'|) \approx 1 - j\frac{2}{\pi}\log\left(\frac{\gamma k_{\rho_j}}{2}\right) - j\frac{2}{\pi}\log\left(|\bar{\rho} - \bar{\rho}'|\right) \tag{5.18}$$

where $\gamma = 1.781$. As seen in (5.18), the last term $-j\frac{2}{\pi}\log(|\bar{\rho} - \bar{\rho}'|)$ exhibits a logarithmic singularity when $\rho = \rho'$ and $\phi = \phi'$ and yields numerical problems for small $\Delta\phi$ values ($\rho = \rho'$). Therefore, for the tangential components, when $\Delta\phi$ is small, approximating $\cos(\Delta\phi)$ term as $1 - \frac{\Delta\phi^2}{2}$, $|\bar{\rho} - \bar{\rho}'|$ can be simplified to

$$|\bar{\rho} - \bar{\rho}'| \approx \rho|\phi - \phi'| = |\beta - \beta'| \tag{5.19}$$

where $\beta = \rho\phi$ and $\beta' = \rho'\phi'$ and $\rho = \rho'$.

As the next step, the term $-j\frac{2}{\pi}\log(|\bar{\rho} - \bar{\rho}'|)$ is replaced with $-j\frac{2}{\pi}\log(|\beta - \beta'|)$. Then it is subtracted from $H_0^2(k_{\rho_j}\,|\bar{\rho} - \bar{\rho}'|)$ and added as a new term to the Green's function representations. Consequently, (5.16) becomes

$$\begin{aligned} G_{uv2} \;=\; & \mathcal{F}^{-1}\Big\{ -\frac{1}{4\omega\epsilon_j}\sum_{n=-\infty}^{\infty} H_n^{(2)}(k_{\rho_j}\rho)J_n(k_{\rho_j}\rho')[f_{uv}(n,k_z) - C_{uv}(k_z)]e^{jn(\Delta\phi)}\Big\} \\ & + \mathcal{F}^{-1}\Big\{ -\frac{1}{4\omega\epsilon_j}\left[C_{uv}(k_z) - C_{uv}(k_{z\infty})\right]\left(H_0^{(2)}(k_{\rho_j}\,|\bar{\rho} - \bar{\rho}'|) - \Big[-j\frac{2}{\pi}\log\left(|\beta - \beta'|\right)\Big]\right)\Big\} \\ & - j\frac{2}{\pi}\log\left(|\beta - \beta'|\right)\mathcal{F}^{-1}\Big\{ -\frac{1}{4\omega\epsilon_j}\left[C_{uv}(k_z) - C_{uv}(k_{z\infty})\right]\Big\} \\ & - \frac{j}{4\pi\omega\epsilon_j}C_{uv}(k_{z\infty})\frac{e^{-jk_j\left|\bar{r} - \bar{r}'\right|}}{|\bar{r} - \bar{r}'|}. \end{aligned} \tag{5.20}$$

In order to handle the singularity in the numerical evaluation of the second term of (5.20), the $\left[1 - j\frac{2}{\pi}\log\left(\frac{\gamma k_{\rho_j}}{2}\right)\right]$ term is used for the $\left(H_0^{(2)}(k_{\rho_j}\,|\bar{\rho} - \bar{\rho}'|) - \Big[- j\frac{2}{\pi}\log\left(|\beta - \beta'|\right)\Big]\right)$ term when β is exactly equal to β'. In this dissertation, the

terms like the $\Big(H_0^{(2)}(k_{\rho_j}\,|\bar{\rho}-\bar{\rho}'|) - \Big[-j\frac{2}{\pi}\log\left(|\beta-\beta'|\right)\Big]\Big)$ term is called non-singular or regular although they are numerically singular at the specific point (i.e., $\beta = \beta'$). The third term of (5.20) is evaluated analytically as defined in Appendix C.4, Appendix D.3 and Appendix E.4 for zz, $z\phi$ and $\phi\phi$ cases, respectively.

5.2.2 Space Domain Singularity ($\rho = \rho'$, $\phi = \phi'$, $z = z'$)

The space domain singularity occurs when the source and observation points overlap with each other (i.e., $\bar{r} = \bar{r}'$ which means $\rho = \rho'$, $\phi = \phi'$ and $z = z'$). When $\bar{r} = \bar{r}'$ the denominator of the last term of (3.18) for the G_{uv} expression (or the last term of 5.20 [or (5.16)]) that involves $I_1 = \frac{e^{-jk_j\left|\bar{r}-\bar{r}'\right|}}{\left|\bar{r}-\bar{r}'\right|}$ exhibits the singularity problem. To treat this singularity analytically, first recognizing that

$$\left|\bar{r}-\bar{r}'\right| = \sqrt{|\bar{\rho}-\bar{\rho}'|^2 + |z-z'|^2}. \tag{5.21}$$

and making use of (5.19), I_1 is approximated as

$$I_1 \approx I_1' = \frac{1}{\sqrt{(\beta-\beta')^2+(z-z')^2}}. \tag{5.22}$$

Then, I_1' is subtracted from I_1 in (5.20) and the subtracted term is added as a new term. As a result G_{uv2} is expressed as

$$\begin{aligned}
G_{uv2} \;=\; & \mathcal{F}^{-1}\Big\{ -\frac{1}{4\omega\epsilon_j}\sum_{n=-\infty}^{\infty} H_n^{(2)}(k_{\rho_j}\rho)J_n(k_{\rho_j}\rho')[f_{uv}(n,k_z)-C_{uv}(k_z)]e^{jn(\Delta\phi)}\Big\} \\
& \mathcal{F}^{-1}\Big\{ -\frac{1}{4\omega\epsilon_j}\left[C_{uv}(k_z)-C_{uv}(k_{z\infty})\right]\Big(H_0^{(2)}(k_{\rho_j}\,|\bar{\rho}-\bar{\rho}'|) - \Big[-j\frac{2}{\pi}\log\left(|\beta-\beta'|\right)\Big]\Big)\Big\} \\
& -j\frac{2}{\pi}\log\left(|\beta-\beta'|\right)\mathcal{F}^{-1}\Big\{ -\frac{1}{4\omega\epsilon_j}\left[C_{uv}(k_z)-C_{uv}(k_{z\infty})\right]\Big\} \\
& -\frac{j}{4\pi\omega\epsilon_j}C_{uv}(k_{z\infty})\Big(\frac{e^{-jk_j\left|\bar{r}-\bar{r}'\right|}}{|\bar{r}-\bar{r}'|} - \frac{1}{\sqrt{(\beta-\beta')^2+(z-z')^2}}\Big) \\
& -\frac{j}{4\pi\omega\epsilon_j}C_{uv}(k_{z\infty})\frac{1}{\sqrt{(\beta-\beta')^2+(z-z')^2}}.
\end{aligned} \tag{5.23}$$

Similar to the spectral domain singularity, in the numerical evaluation of the $\Big(\frac{e^{-jk_j\left|\bar{r}-\bar{r}'\right|}}{\left|\bar{r}-\bar{r}'\right|} - \frac{1}{\sqrt{(\beta-\beta')^2+(z-z')^2}}\Big)$ term, the $-jk_j$ term is used when $\rho = \rho'$, $\phi = \phi'$

and $z = z'$ in order to solve the numerical singularity. The $-jk_j$ term comes from the Taylor series expansion of the exponential function. The last term of (5.23) is singular when the source and field points overlap with each other. Hence, it must be evaluated analytically. During the mutual impedance calculations, overlapping of source and field points occur / may occur when the two current modes (i.e., basis and testing functions) are on the top of each other (self term) and partially overlapping with each other (overlapping terms). Details of the analytic evaluation of the last term of (5.23) for these situations are in Appendix C.2-C.3, Appendix D.2 and Appendix E.2-E.3 for zz, $z\phi = \phi z$ and $\phi\phi$ cases, respectively.

5.3 Mutual Impedance Calculations For Probe-Related Components

In this study, the microstrip antennas are fed via an ideal probe with an infinitesimally thin thickness. Hence, the probe is modeled as

$$J_\rho = \frac{I_0 \delta(\rho\phi - r l_f)\delta(z - z_f)}{\rho} \tag{5.24}$$

where $I_0 = 1$ is the magnitude of the excitation current and $\delta(.)$ is the Dirac delta function. Therefore, the mutual impedance expression for probe-related components for $v = \phi$ or $v = z$ is defined as a three-fold integral given by

$$V_{v\rho} = -\int\int J_v \int G_{v\rho} d\rho' dz d\beta. \tag{5.25}$$

It should be noted that instead of $Z_{12v\rho}$ we prefer to use $V_{v\rho}$ for the mutual impedance expressions of probe-related terms. The main reason for this notation is that they form the entries of the voltage vector $\underline{V}$ in the MoM calculations. Also note that the minus sign in front of the integrals in (5.25) is due to the fact that the electric field direction and the integration path direction for the ρ' integral are opposite. Similar to the tangential components, recognizing that $(j\frac{\partial}{\partial z})$ and $(-j\frac{\partial}{\partial \phi})$ terms in the space domain correspond to k_z and n in the spectral domain,

respectively, the inner ρ' integral is rewritten as

$$\int G_{v\rho} d\rho' = (-j\frac{\partial}{\partial \phi})^p (j\frac{\partial}{\partial z})^l \int G_{v\rho 2} d\rho' \tag{5.26}$$

where $p = 0$, $l = 1$ for $z\rho$ case and $p = 1$, $l = 0$ for $\phi\rho$ case. After transferring the derivatives acting on $G_{v\rho}$ onto the PWS current modes (which are differentiable) using integration by parts, the following mutual impedance expressions are obtained for the probe-related components:

$$V_{z\rho} = -\int\int (-j)\frac{\partial J_z}{\partial z} \int G_{z\rho 2} d\rho' d\beta dz, \tag{5.27}$$

$$V_{\phi\rho} = -\int\int (j)\frac{\partial J_\phi}{\partial \phi} \int G_{\phi\rho 2} d\rho' d\beta dz. \tag{5.28}$$

When there is no singularity in the probe-related components, the ρ' integral is performed first to increase the efficiency. Therefore, making use of the IFT of (3.32), the mutual impedance calculations for the probe-related components start with the ρ' integral of (5.26). Hence the ρ' integral of (5.26) is written as

$$\int G_{v\rho 2} d\rho' = \int \mathcal{F}^{-1}\left\{ -\frac{1}{4\omega\epsilon_j} \sum_{n=-\infty}^{\infty} k_{\rho_j} H_n^{(2)}(k_{\rho_j}\rho) J_n'(k_{\rho_j}\rho') \tilde{f}_{v\rho}(n, k_z, \rho') e^{jn\Delta\phi} \right\} d\rho'. \tag{5.29}$$

After the envelope extraction with respect to n as explained in Section 3.2, the following expression is obtained:

$$\begin{aligned} &\int G_{v\rho 2} d\rho' = \\ &\int \mathcal{F}^{-1}\left\{ -\frac{1}{4\omega\epsilon_j} \sum_{n=-\infty}^{\infty} k_{\rho_j} H_n^{(2)}(k_{\rho_j}\rho) J_n'(k_{\rho_j}\rho') [\tilde{f}_{v\rho}(n, k_z, \rho') - \tilde{C}_{v\rho}(k_z, \rho')] e^{jn\Delta\phi} \right\} d\rho' \\ &+ \int \mathcal{F}^{-1}\left\{ -\frac{1}{4\omega\epsilon_j} \tilde{C}_{v\rho}(k_z, \rho') F_3^{v\rho}[S_1] \right\} d\rho' \end{aligned} \tag{5.30}$$

where

$$F_3^{v\rho}[S_1] = \frac{\partial H_0^2(k_{\rho_j} |\bar{\rho} - \bar{\rho}'|))}{\partial \rho'}. \tag{5.31}$$

As the next step, the term $\tilde{C}_{v\rho}(k_z, \rho' = \rho)F_3^{v\rho}[S_1]$ is subtracted from the second term of (5.30) and its contribution (after the integration with respect to ρ' is evaluated) is added analytically as given by

$$\begin{aligned}
&\int G_{v\rho 2} d\rho' = \\
&\int \mathcal{F}^{-1}\left\{ -\frac{1}{4\omega\epsilon_j} \sum_{n=-\infty}^{\infty} k_{\rho_j} H_n^{(2)}(k_{\rho_j}\rho) J_n'(k_{\rho_j}\rho')[\tilde{f}_{v\rho}(n, k_z, \rho') - \tilde{C}_{v\rho}(k_z, \rho')] e^{jn\Delta\phi} \right\} d\rho' \\
&+ \int \mathcal{F}^{-1}\left\{ -\frac{1}{4\omega\epsilon_j} [\tilde{C}_{v\rho}(k_z, \rho') - \tilde{C}_{v\rho}(k_z, \rho' = \rho)] F_3^{v\rho}[S_1] \right\} d\rho' \\
&+ \mathcal{F}^{-1}\left\{ -\frac{1}{4\omega\epsilon_j} \tilde{C}_{v\rho}(k_z, \rho' = \rho) H_0^2(k_{\rho_j} |\bar{\rho} - \bar{\rho}'|)\Big|_{\rho'=p_e} \right\} \\
&- \mathcal{F}^{-1}\left\{ -\frac{1}{4\omega\epsilon_j} \tilde{C}_{v\rho}(k_z, \rho' = \rho) H_0^2(k_{\rho_j} |\bar{\rho} - \bar{\rho}'|)\Big|_{\rho'=p_s} \right\}
\end{aligned} \tag{5.32}$$

Note that, as explained in Section 3.2, in the course of obtaining the last two terms of (5.32) (these are the analytically added parts), the following is used:

$$\int_{\rho'=p_s}^{\rho'=p_e} \frac{\partial S_1}{\partial \rho'} d\rho' = S_1(p_e) - S_1(p_s). \tag{5.33}$$

Also note that the ρ' integration for the first two terms of (5.32) is performed numerically using a simple numerical integration algorithm.

Finally, a second envelope extraction with respect to k_z is applied as explained in Section 3.2 and the final form of the ρ' integral of (5.26) is obtained as

$$\begin{aligned}
&\int G_{v\rho 2} d\rho' = \\
&\int \mathcal{F}^{-1}\left\{ -\frac{1}{4\omega\epsilon_j} \sum_{n=-\infty}^{\infty} k_{\rho_j} H_n^{(2)}(k_{\rho_j}\rho) J_n'(k_{\rho_j}\rho')[\tilde{f}_{v\rho}(n, k_z, \rho') - \tilde{C}_{v\rho}(k_z, \rho')] e^{jn\Delta\phi} \right\} d\rho' \\
&+ \int \mathcal{F}^{-1}\left\{ -\frac{1}{4\omega\epsilon_j} [\tilde{C}_{v\rho}(k_z, \rho') - \tilde{C}_{v\rho}(k_z, \rho' = \rho)] F_3^{v\rho}[S_1] \right\} d\rho' \\
&+ \mathcal{F}^{-1}\left\{ -\frac{1}{4\omega\epsilon_j} [\tilde{C}_{v\rho}(k_z, \rho' = \rho) - \tilde{C}_{v\rho}(k_{z\infty}, \rho' = \rho)] H_0^2(k_{\rho_j} |\bar{\rho} - \bar{\rho}'|)\Big|_{\rho'=p_e} \right\} \\
&- \mathcal{F}^{-1}\left\{ -\frac{1}{4\omega\epsilon_j} [\tilde{C}_{v\rho}(k_z, \rho' = \rho) - \tilde{C}_{v\rho}(k_{z\infty}, \rho' = \rho)] H_0^2(k_{\rho_j} |\bar{\rho} - \bar{\rho}'|)\Big|_{\rho'=p_s} \right\} \\
&- \frac{j}{4\pi\omega\epsilon_j} \tilde{C}_{v\rho}(k_{z\infty}, \rho' = \rho) \frac{e^{-jk_j\left|\bar{r} - \bar{r}'\right|}}{|\bar{r} - \bar{r}'|}\Bigg|_{\rho'=p_e}
\end{aligned}$$

$$+\frac{j}{4\pi\omega\epsilon_j}\tilde{C}_{v\rho}(k_{z\infty},\rho'=\rho)\frac{e^{-jk_j\left|\bar{r}-\bar{r}'\right|}}{\left|\bar{r}-\bar{r}'\right|}\Bigg|_{\rho'=p_s} \tag{5.34}$$

At this step, (5.34) can be used in (5.25) to calculate the probe-related mutual impedances except the cases where singularities exist. The treatment of the singularities are given next.

5.3.1 Spectral Domain Singularity ($\rho=\rho'$, $\phi=\phi'$)

Similar to the tangential components, the spectral domain singularity occurs along the axial line (when $\phi=\phi'$ and $\rho=\rho'$) because the argument of the Hankel function $H_0^2(k_{\rho_j}\left|\bar{\rho}-\bar{\rho}'\right|)$ becomes zero as given by

$$\left|\bar{\rho}-\bar{\rho}'\right|=\sqrt{\rho^2+\rho'^2-2\rho\rho'\cos(\Delta\phi)}. \tag{5.35}$$

Again using the small argument approximation of the Hankel function given by

$$H_0^2(k_{\rho_j}\left|\bar{\rho}-\bar{\rho}'\right|)\approx 1-j\frac{2}{\pi}\log\left(\frac{\gamma k_{\rho_j}}{2}\right)-j\frac{2}{\pi}\log\left(\left|\bar{\rho}-\bar{\rho}'\right|\right) \tag{5.36}$$

it can be seen that the last term $-j\frac{2}{\pi}\log\left(\left|\bar{\rho}-\bar{\rho}'\right|\right)$ exhibits a logarithmic singularity when $\rho=\rho'$ and $\phi=\phi'$. Therefore, similar to the tangential components, approximating $\cos(\Delta\phi)$ as $1-\frac{\Delta\phi^2}{2}$ for small $\Delta\phi$ values, $\left|\bar{\rho}-\bar{\rho}'\right|$ can be approximated as

$$\left|\bar{\rho}-\bar{\rho}'\right|\approx\sqrt{(\rho-\rho')^2+\frac{\rho'}{\rho}(\beta-\rho\phi')^2}. \tag{5.37}$$

It should be emphasized that (5.37) is different than (5.19) since there is a ρ' integration in (5.25) that will play a role during the treatment of this singularity.

Note that the problematic parts of (5.34) are the third and forth terms when $\rho=\rho'$. The second term does not pose any problem because the multiplication term $[\tilde{C}_{v\rho}(k_z,\rho')-\tilde{C}_{v\rho}(k_z,\rho'=\rho)]$ cancels this singularity (actually this product yields zero when $\left|\bar{\rho}-\bar{\rho}'\right|=0$ and hence, the contribution coming from this term vanishes). Using the approximated $\left|\bar{\rho}-\bar{\rho}'\right|$ [given by (5.37)] in $-j\frac{2}{\pi}\log\left(\left|\bar{\rho}-\bar{\rho}'\right|\right)$,

$-j\frac{2}{\pi}\log\left(\sqrt{(\rho-\rho')^2+\frac{\rho'}{\rho}(\beta-\rho\phi')^2}\right)$ is subtracted from $H_0^2(k_{\rho_j}|\bar{\rho}-\bar{\rho}'|)$ in the third and fourth terms of (5.34) and added as new terms. Hence, (5.34) becomes

$$
\begin{aligned}
&\int G_{v\rho 2}d\rho' = \\
&\int \mathcal{F}^{-1}\left\{-\frac{1}{4\omega\epsilon_j}\sum_{n=-\infty}^{\infty}k_{\rho_j}H_n^{(2)}(k_{\rho_j}\rho)J_n'(k_{\rho_j}\rho')[\tilde{f}_{v\rho}(n,k_z,\rho')-\tilde{C}_{v\rho}(k_z,\rho')]e^{jn\Delta\phi}\right\}d\rho' \\
&+\int \mathcal{F}^{-1}\left\{-\frac{1}{4\omega\epsilon_j}[\tilde{C}_{v\rho}(k_z,\rho')-\tilde{C}_{v\rho}(k_z,\rho'=\rho)]F_3^{v\rho}[S_1]\right\}d\rho' \\
&+\mathcal{F}^{-1}\left\{-\frac{1}{4\omega\epsilon_j}[\tilde{C}_{v\rho}(k_z,\rho'=\rho)-\tilde{C}_{v\rho}(k_{z\infty},\rho'=\rho)]\Big(H_0^2(k_{\rho_j}|\bar{\rho}-\bar{\rho}'|)\Big|_{\rho'=p_e}\right. \\
&\left.-\Big[-j\frac{2}{\pi}\log\left(\sqrt{(\rho-\rho')^2+\frac{\rho'}{\rho}(\beta-\rho\phi')^2}\right)\Big]\Big|_{\rho'=p_e}\right)\Bigg\} \\
&-\mathcal{F}^{-1}\left\{-\frac{1}{4\omega\epsilon_j}[\tilde{C}_{v\rho}(k_z,\rho'=\rho)-\tilde{C}_{v\rho}(k_{z\infty},\rho'=\rho)]\Big(H_0^2(k_{\rho_j}|\bar{\rho}-\bar{\rho}'|)\Big|_{\rho'=p_s}\right. \\
&\left.-\Big[-j\frac{2}{\pi}\log\left(\sqrt{(\rho-\rho')^2+\frac{\rho'}{\rho}(\beta-\rho\phi')^2}\right)\Big]\Big|_{\rho'=p_s}\right)\Bigg\} \\
&-\frac{j}{4\pi\omega\epsilon_j}\tilde{C}_{v\rho}(k_{z\infty},\rho'=\rho)\frac{e^{-jk_j\left|\bar{r}-\bar{r}'\right|}}{|\bar{r}-\bar{r}'|}\Bigg|_{\rho'=p_e} \\
&+\frac{j}{4\pi\omega\epsilon_j}\tilde{C}_{v\rho}(k_{z\infty},\rho'=\rho)\frac{e^{-jk_j\left|\bar{r}-\bar{r}'\right|}}{|\bar{r}-\bar{r}'|}\Bigg|_{\rho'=p_s} \\
&+\mathcal{F}^{-1}\left\{-\frac{1}{4\omega\epsilon_j}[\tilde{C}_{v\rho}(k_z,\rho'=\rho)-\tilde{C}_{v\rho}(k_{z\infty},\rho'=\rho)]\right. \\
&\left.\Big[-j\frac{2}{\pi}\log\left(\sqrt{(\rho-\rho')^2+\frac{\rho'}{\rho}(\beta-\rho\phi')^2}\right)\Big]\Big|_{\rho'=p_e}\right\} \\
&-\mathcal{F}^{-1}\left\{-\frac{1}{4\omega\epsilon_j}[\tilde{C}_{v\rho}(k_z,\rho'=\rho)-\tilde{C}_{v\rho}(k_{z\infty},\rho'=\rho)]\right. \\
&\left.\Big[-j\frac{2}{\pi}\log\left(\sqrt{(\rho-\rho')^2+\frac{\rho'}{\rho}(\beta-\rho\phi')^2}\right)\Big]\Big|_{\rho'=p_s}\right\} \qquad (5.38)
\end{aligned}
$$

Similar to the tangential components, in (5.38) when a numerical singularity occurs in $\left(H_0^2(k_{\rho_j}|\bar{\rho}-\bar{\rho}'|)\Big|_{\rho'=p_e,p_s}-\Big[-j\frac{2}{\pi}\log\left(\sqrt{(\rho-\rho')^2+\frac{\rho'}{\rho}(\beta-\rho\phi')^2}\right)\Big]\Big|_{\rho'=p_e,p_s}\right)$ term, the $\left[1-j\frac{2}{\pi}\log\left(\frac{\gamma k_{\rho_j}}{2}\right)\right]$ term is used. The last two terms of (5.38) are the newly added terms and must be evaluated analytically during the mutual

impedance calculations as follows: First, (5.38) is substituted into (5.25). As a result of this step we have a two-fold space domain integration (note that all ρ' integrals for the nonsingular terms given by (5.38) are numerically evaluated in a straight forward way). Then, integration by part is implemented and the derivatives are transferred to the testing functions. Finally, for the $z\rho$ case, the singular integral is evaluated analytically with respect to β as follows.

$$\int \log\Big(\sqrt{(\rho-\rho')^2+\frac{\rho'}{\rho}(\beta-\rho\phi')^2}\Big)d\beta = \frac{1}{2}\Big(\beta\log[\frac{\rho'(\beta-\rho\phi')^2}{\rho}+(\rho-\rho')^2]$$
$$-\rho\phi'\log[\rho\rho'^2+(\phi'^2-2)\rho^2\rho'-2\beta\phi'\rho\rho'+\beta^2\rho'+\rho^3]$$
$$-2\sqrt{\frac{\rho}{\rho'}}(\rho'-\rho)\tan^{-1}\Big(\frac{\beta\rho'-\phi'\rho\rho'}{(\rho'-\rho)\sqrt{\rho\rho'}}\Big)+2\beta\Big). \tag{5.39}$$

The remaining integral with respect to z can be numerically integrated easily using a simple Gaussian quadrature algorithm since no singularity is left.

Regarding the $\phi\rho$ case, a slightly different approach is followed since both J_ϕ and its derivative with respect to ϕ are functions of β. Therefore, the singular integral for the $\phi\rho$ case is

$$\int J_{\phi 2}(\phi)\Big[\log\Big(\sqrt{(\rho-\rho')^2+\frac{\rho'}{\rho}(\beta-\rho\phi')^2}\Big)\Big]d\beta \tag{5.40}$$

where

$$J_{\phi 2}(\phi) = (j)\frac{\partial J_\phi}{\partial \phi}. \tag{5.41}$$

To be able to use the result of (5.39) for the $\phi\rho$ case, the expression $J_{\phi 2}(\phi')$ is subtracted from $J_{\phi 2}(\phi)$ and added as follows

$$\int (J_{\phi 2}(\phi)-J_{\phi 2}(\phi'))\Big[\log\Big(\sqrt{(\rho-\rho')^2+\frac{\rho'}{\rho}(\beta-\rho\phi')^2}\Big)\Big]d\beta$$
$$+J_{\phi 2}(\phi')\int \log\Big(\sqrt{(\rho-\rho')^2+\frac{\rho'}{\rho}(\beta-\rho\phi')^2}\Big)d\beta. \tag{5.42}$$

As seen in (5.42), there are two terms that have to be integrated. The second integral is now in the same form as that of (5.39) and hence, evaluated analytically. On the other hand, there is no singularity in the first integral as $[J_{\phi 2}(\phi)-J_{\phi 2}(\phi')]$ is exactly zero when $\rho=\rho'$ and $\phi=\phi'$, which makes the first integral vanish along the axial line.

5.3.2 Space Domain Singularity ($\rho = \rho'$, $\phi = \phi'$, $z = z'$)

Finally, the space domain singularity for the probe-related components exists when $\bar{r} = \bar{r}'$ ($\rho = \rho'$, $\phi = \phi'$ and $z = z'$). However, note that $\bar{r} = \bar{r}'$ may not exactly occur. Instead, because the length of the probe is fairly short ρ may approach to ρ' ($\rho \approx \rho'$) and $\phi = \phi'$ and $z = z'$ may occur. Therefore, this singularity must be treated as if $\bar{r} = \bar{r}'$. Similar to the tangential components the terms that involve $I_1 = \frac{e^{-jk_j\left|\bar{r}-\bar{r}'\right|}}{\left|\bar{r}-\bar{r}'\right|}$ in (5.38) must be analytically treated when $\bar{r} \approx \bar{r}'$ during the mutual impedance calculations. Making use of (5.37) for $|\bar{\rho} - \bar{\rho}'|$, the term I_1 is approximated as I_1' given by

$$I_1' = \frac{1}{\sqrt{(\rho-\rho')^2 + \frac{\rho'}{\rho}(\beta - \rho\phi')^2 + (z-z')^2}}. \tag{5.43}$$

Then I_1' is subtracted from I_1 in (5.38) and added as two new terms (the last two terms).

Consequently (5.38) becomes

$$\begin{aligned}
&\int G_{v\rho 2} d\rho' = \\
&\int \mathcal{F}^{-1}\left\{-\frac{1}{4\omega\epsilon_j}\sum_{n=-\infty}^{\infty} k_{\rho_j} H_n^{(2)}(k_{\rho_j}\rho) J_n'(k_{\rho_j}\rho')[\tilde{f}_{v\rho 2}(n, k_z, \rho') - \tilde{C}_{v\rho 2}(k_z, \rho')] e^{jn\Delta\phi}\right\} d\rho' \\
&+ \int \mathcal{F}^{-1}\left\{-\frac{1}{4\omega\epsilon_j}[\tilde{C}_{v\rho 2}(k_z, \rho') - \tilde{C}_{v\rho 2}(k_z, \rho' = \rho)] F_3^{v\rho}[S_1]\right\} d\rho' \\
&+\mathcal{F}^{-1}\left\{-\frac{1}{4\omega\epsilon_j}[\tilde{C}_{v\rho 2}(k_z, \rho' = \rho) - \tilde{C}_{v\rho 2}(k_{z\infty}, \rho' = \rho)]\Big(H_0^2(k_{\rho_j}|\bar{\rho} - \bar{\rho}'|)\Big|_{\rho'=p_e}\right. \\
&\left.-\Big[-j\frac{2}{\pi}\log\Big(\sqrt{(\rho-\rho')^2 + \frac{\rho'}{\rho}(\beta-\rho\phi')^2}\Big)\Big]\Big|_{\rho'=p_e}\Big)\right\} \\
&-\mathcal{F}^{-1}\left\{-\frac{1}{4\omega\epsilon_j}[\tilde{C}_{v\rho 2}(k_z, \rho' = \rho) - \tilde{C}_{v\rho 2}(k_{z\infty}, \rho' = \rho)]\Big(H_0^2(k_{\rho_j}|\bar{\rho} - \bar{\rho}'|)\Big|_{\rho'=p_s}\right. \\
&\left.-\Big[-j\frac{2}{\pi}\log\Big(\sqrt{(\rho-\rho')^2 + \frac{\rho'}{\rho}(\beta-\rho\phi')^2}\Big)\Big]\Big|_{\rho'=p_s}\Big)\right\} \\
&-\frac{j}{4\pi\omega\epsilon_j}\tilde{C}_{v\rho 2}(k_{z\infty}, \rho' = \rho)\Big(\frac{e^{-jk_j\left|\bar{r}-\bar{r}'\right|}}{|\bar{r}-\bar{r}'|}\Big|_{\rho'=p_e} - \frac{1}{\sqrt{(\rho-\rho')^2 + \frac{\rho'}{\rho}(\beta-\rho\phi')^2 + (z-z')^2}}\Big|_{\rho'=p_e}\Big)
\end{aligned}$$

$$
\begin{aligned}
&+\frac{j}{4\pi\omega\epsilon_j}\tilde{C}_{v\rho 2}(k_{z\infty},\rho'=\rho)\Big(\frac{e^{-jk_j\left|\bar{r}-\bar{r}'\right|}}{\left|\bar{r}-\bar{r}'\right|}\Big|_{\rho'=p_s}-\frac{1}{\sqrt{(\rho-\rho')^2+\frac{\rho'}{\rho}(\beta-\rho\phi')^2+(z-z')^2}}\Big|_{\rho'=p_s}\Big)\\
&+\mathcal{F}^{-1}\Big\{-\frac{1}{4\omega\epsilon_j}[\tilde{C}_{v\rho 2}(k_z,\rho'=\rho)-\tilde{C}_{v\rho 2}(k_{z\infty},\rho'=\rho)]\\
&\Big[-j\frac{2}{\pi}\log\Big(\sqrt{(\rho-\rho')^2+\frac{\rho'}{\rho}(\beta-\rho\phi')^2}\Big)\Big]\Big|_{\rho'=p_e}\Big\}\\
&-\mathcal{F}^{-1}\Big\{-\frac{1}{4\omega\epsilon_j}[\tilde{C}_{v\rho 2}(k_z,\rho'=\rho)-\tilde{C}_{v\rho 2}(k_{z\infty},\rho'=\rho)]\\
&\Big[-j\frac{2}{\pi}\log\Big(\sqrt{(\rho-\rho')^2+\frac{\rho'}{\rho}(\beta-\rho\phi')^2}\Big)\Big]\Big|_{\rho'=p_s}\Big\}\\
&-\frac{j}{4\pi\omega\epsilon_j}\tilde{C}_{v\rho 2}(k_{z\infty},\rho'=\rho)\frac{1}{\sqrt{(\rho-\rho')^2+\frac{\rho'}{\rho}(\beta-\rho\phi')^2+(z-z')^2}}\Big|_{\rho'=p_e}\\
&+\frac{j}{4\pi\omega\epsilon_j}\tilde{C}_{v\rho 2}(k_{z\infty},\rho'=\rho)\frac{1}{\sqrt{(\rho-\rho')^2+\frac{\rho'}{\rho}(\beta-\rho\phi')^2+(z-z')^2}}\Big|_{\rho'=p_s}
\end{aligned}
\tag{5.44}
$$

In (5.44), when $\rho=\rho'$, $\phi=\phi'$ and $z=z'$, the $-jk_j$ term is used instead of the $\Big(\frac{e^{-jk_j\left|\bar{r}-\bar{r}'\right|}}{\left|\bar{r}-\bar{r}'\right|}\Big|_{\rho'=p_e,p_s}-\frac{1}{\sqrt{(\rho-\rho')^2+\frac{\rho'}{\rho}(\beta-\rho\phi')^2+(z-z')^2}}\Big|_{\rho'=p_e,p_s}\Big)$ term. As seen in (5.44), the last two terms of (5.44) are nearly the singular terms and are treated analytically during the mutual impedance calculations (during the integration through the area of the test current). For the $z\rho$ case as follows: when the last two terms of (5.44) are substituted into (5.27) the analytical result of

$$
\int\frac{1}{\sqrt{(\rho-\rho')^2+\frac{\rho'}{\rho}(\beta-\rho\phi')^2+(z-z')^2}}d\beta \tag{5.45}
$$

is needed. Its closed-form expression is given by

$$
\int\frac{1}{\sqrt{(\rho-\rho')^2+\frac{\rho'}{\rho}(\beta-\rho\phi')^2+(z-z')^2}}d\beta=\sqrt{\frac{\rho}{\rho'}}\sinh^{-1}\Big(\frac{\sqrt{\frac{\rho'}{\rho}}(\beta-\rho\phi')}{\sqrt{(z-z')^2+(\rho-\rho')^2}}\Big). \tag{5.46}
$$

Making use the result of (5.46) in the mutual impedance calculation, the remaining $z-$ integration is simply performed using a Gaussian quadrature algorithm numerically.

Regarding the $\phi\rho$ component a different approach is followed because $J_{\phi 2}(\phi)$ is a function of β. Moreover, the methodology followed in the treatment of the spectral domain singularity can not be used because a term similar to $[J_{\phi 2}(\phi) - J_{\phi 2}(\phi')]$ may not exactly cancel the space domain singularity when (5.44) is used. Therefore, the analytical evaluation of the space domain singularity for the $\phi\rho$ case uses (5.38) rather than (5.44). The terms that yield the space domain singularity in (5.38) can be written as $I_{v\rho 1}$ and $I_{v\rho 2}$ given by

$$I_{v\rho 1} = \left. \frac{e^{-jk_j\left|\bar{r}-\bar{r}'\right|}}{\left|\bar{r}-\bar{r}'\right|} \right|_{\rho'=p_e} \tag{5.47}$$

$$I_{v\rho 2} = \left. \frac{e^{-jk_j\left|\bar{r}-\bar{r}'\right|}}{\left|\bar{r}-\bar{r}'\right|} \right|_{\rho'=p_s} \tag{5.48}$$

Substituting (5.47) and (5.48) into (5.27), the singular integral that must be analytically evaluated during the mutual impedance formulation can be written as

$$\int J_{\phi 2}(\phi) I_{v\rho i} d\beta \qquad (i = 1, 2) \tag{5.49}$$

where $J_{\phi 2}(\phi)$ is given in (5.41). Then similar to the procedure related with the spectral domain singularity [see (5.42)], (5.49) is written as

$$\begin{aligned} &\int \left(J_{\phi 2}(\phi) I_{v\rho i} - \left. \frac{J_{\phi 2}(\phi')}{\sqrt{(\rho-\rho')^2 + \frac{\rho'}{\rho}(\beta-\rho\phi')^2 + (z-z')^2}} \right|_{\rho'=\rho'_i} \right) d\beta \\ &+ J_{\phi 2}(\phi') \int \left. \frac{1}{\sqrt{(\rho-\rho')^2 + \frac{\rho'}{\rho}(\beta-\rho\phi')^2 + (z-z')^2}} \right|_{\rho'=\rho'_i} d\beta, \qquad (i = 1, 2), \end{aligned} \tag{5.50}$$

where $\rho'_1 = p_e$ and $\rho'_2 = p_s$. In (5.50), the first term is not singular and it is possible to make the numerical evaluation with a simple Gaussian quadrature algorithm. However, in the numerical evaluation of the $\left(J_{\phi 2}(\phi) I_{v\rho i} - \left. \frac{J_{\phi 2}(\phi')}{\sqrt{(\rho-\rho')^2 + \frac{\rho'}{\rho}(\beta-\rho\phi')^2 + (z-z')^2}} \right|_{\rho'=\rho'_i} \right)$ term, the numerical singularity occurs when $\rho =$

ρ', $\phi = \phi'$ and $z = z'$. In this numerical singularity case, the $\Big[-jk_j J_{\phi 2}(\phi) \Big]$ term is used instead of the $\Big(J_{\phi 2}(\phi) I_{v\rho i} - \frac{J_{\phi 2}(\phi')}{\sqrt{(\rho-\rho')^2 + \frac{\rho'}{\rho}(\beta - \rho\phi')^2 + (z-z')^2}} \Big|_{\rho'=\rho_i'} \Big)$ term for only this specific point during the numerical integration. The second term can now be evaluated using (5.46) similar to the $z\rho$ case.

Chapter 6

Method of Moments Formulation

In this chapter, the details of the MoM procedure is given in the presence of an attachment mode with a special emphasis on the attachment mode that is used to model the probe-fed antennas more accurately by ensuring the current continuity from probe to the patch antennas. Then, the formulations for the input impedance of a microstrip antenna as well as the mutual coupling between two microstrip antennas are given.

6.1 Attachment Mode and Related Mutual Impedance Calculations

To model a probe-fed type antenna feeding accurately during the MoM procedure by ensuring the continuity of the current from the probe to the patch, an attachment mode is defined and used. A $z-$ directed attachment mode is defined as

$$J_{z_{att}} = \begin{cases} \frac{0.5\sin(k_a(z_{att}-|z|))}{l_{att}\sin[k_a z_{att}]}, z \geq z_{att} \\ \\ -\frac{0.5\sin(k_a(z_{att}-|z|))}{l_{att}\sin[k_a z_{att}]}, z < z_{att} \end{cases} \tag{6.1}$$

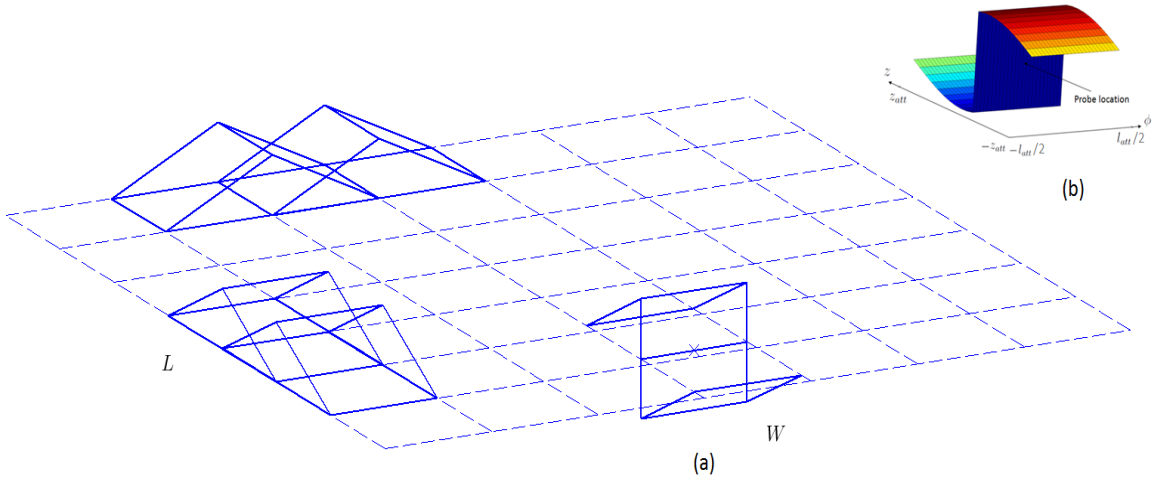

Figure 6.1: The $z-$ and $\phi-$ directed current modes and a $z-$ directed attachment mode defined on the microstrip antenna are given in (a). In (b), a colored 3−D picture of a $z-$ directed attachment mode (with different k_a, z_{att} and l_{att} parameters) is given. $\times$ denotes the exact location of the probe.

in the $2z_{att} \times l_{att}$ region where the probe is at the center of this region. Fig. 6.1 (a) illustrates a typical 3−D picture of the $z-$ and $\phi-$ directed PWS current modes used to capture $\underline{J}_s(\bar{r}')$ (the induced current on the patch antenna) and a $z-$ directed attachment mode which is consistent with the PWS current modes defined on the microstrip antenna. A $z-$ directed attachment mode is also given in Fig. 6.1 (b) with different k_a, z_{att} and l_{att} parameters. Note that the shape of the PWS current modes (also the shape of the attachment mode) changes with respect to k_a and u_a (or u_{att}) of a $u-$ directed current (or attachment) mode. When k_a is chosen as $\pi/(2u_a)$, the PWS becomes a half sinuous in the $u-$ direction. When k_a or u_a of a $u-$ directed current mode is decreased, the PWS current modes become triangular. A $\phi-$ directed attachment mode can be defined in a similar way by changing z by $\rho\phi$, z_{att} by l_{att}.

In the definition of an attachment mode, one critical issue is the selection of the size of the attachment mode, namely z_{att} and l_{att}. In this study, the size of the attachment mode is related with the size of the basis functions that are used to expand the induced current $\underline{J}_s(\bar{r}')$ on the conducting patches. Our

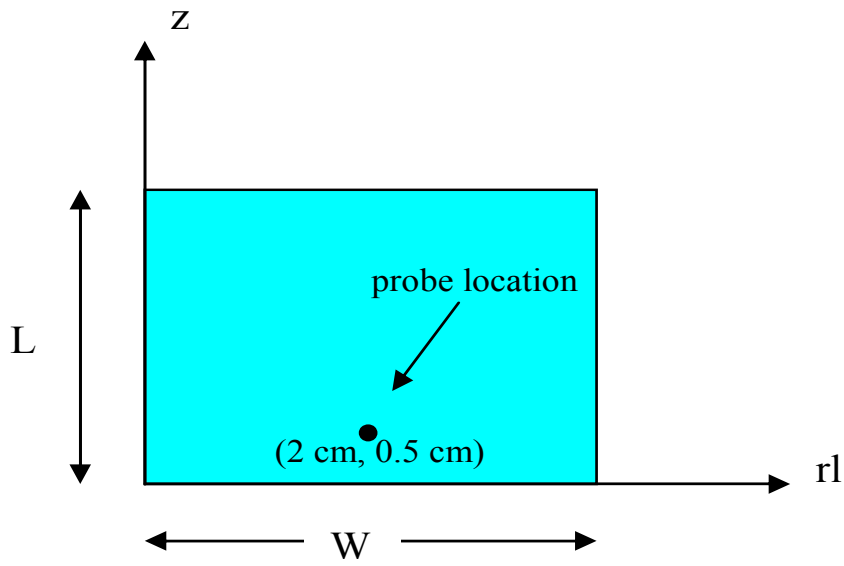

Figure 6.2: A microstrip patch antenna with W=4 cm, L=3 cm and fed via a probe at the location (rl_f, z_f)=(2 cm,0.5 cm) at f=3.2 GHz

rule of thumb for such a selection is that for a $u-$ directed attachment mode ($u = z$ or ϕ), $u_{att} \leq u_a$ where $u_a = z_a$ or l_a for a $z-$ or $\phi-$ directed PWS, respectively, and $v_{att} = v_a/2$ or $v_{att} = v_a$ [$v_{att} = l_{att}/2$ or $z_{att}/2$ (i.e., the other direction) and $v_a = l_a/2$ or $z_a/2$ (i.e., the other direction)] depending on the placement of the probe with respect to $u-$ directed basis functions along the $v-$ direction. Therefore, considering a $z-$ directed attachment mode given by (6.1) on a fixed-sized patch antenna, the following two examples are given to illustrate how the sizes of z_{att} and l_{att} are decided.

Consider a microstrip patch antenna with dimensions W=4 cm in the $rl-$ direction ($rl = \rho\phi$) and L=3 cm in the $z-$ direction. This antenna is fed via a probe at (rl_f, z_f)=$(u/2 = 2\,\text{cm}, 0.5\,\text{cm})$ as shown in Fig. 6.2 at $f = 3.2$ GHz. For the first example, the conducting patch on which $\underline{J}_s(\bar{r}')$ exists is divided into 4 subdomains along the $z-$ and $\phi-$ directions, respectively. Therefore, $P = K = 12$ and $N = 24$. Fig. 6.3 illustrates the magnitude, the shape and the location of $J_{z_{att}}$ with respect to the 3 $z-$ directed current modes along the $z-$ direction. In this example $z_{att} = 0.5\,\text{cm} < z_a$ is chosen. Fig. 6.4 shows

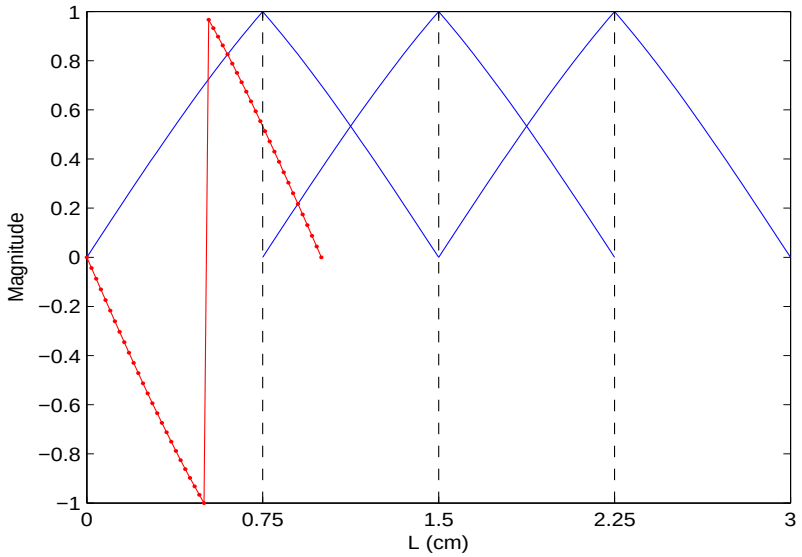

Figure 6.3: The magnitude, shape and location of a z-directed attachment mode with respect to 3 $z-$ directed PWS current modes along the $z-$ direction for an antenna whose parameters are given in Fig. 6.2

the placement of the attachment mode and the size of l_{att}. Because the exact location of the probe along the $rl-$ direction is exactly between the two $z-$ directed PWS basis functions, $l_{att} = l_a$ is chosen. For the second example, the same conducting patch on which $\underline{J}_s(\vec{r}')$ exists is divided into 7 subdomains along the $z-$ and $rl-$ directions, respectively. Hence, $P = K = 42$ and $N = 84$. Similar to Fig. 6.3, Fig. 6.5 illustrates the magnitude, the shape and the location of $J_{z_{att}}$ with respect to 6 $z-$ directed current modes along the $z-$ direction. In this example $z_{att} = z_a = 0.43\,\text{cm}$ is chosen. Similar to Fig. 6.4, Fig. 6.6 illustrates the placement of the attachment mode and the length of l_{att}. Because the exact location of the probe along the $rl-$ direction is the middle of a $z-$ directed current mode, $l_{att} = l_a/2$ is chosen. Note that because the size of the basis functions (or P, K and hence, N) can be preselected, one of the aforementioned placements of the probe with respect to expansion functions can always be satisfied.

The mutual impedance calculations related with the attachment mode requires the calculation of the following mutual impedance expressions: $Z_{12zz_{att}}$, $Z_{12\phi z_{att}}$, $Z_{12z_{att}\rho}$, $Z_{12\phi\phi_{att}}$, $Z_{12z\phi_{att}}$, $Z_{12\phi_{att}\rho}$. Although $Z_{12z_{att}z}$, $Z_{12z_{att}\phi}$, $Z_{12\phi_{att}\phi}$

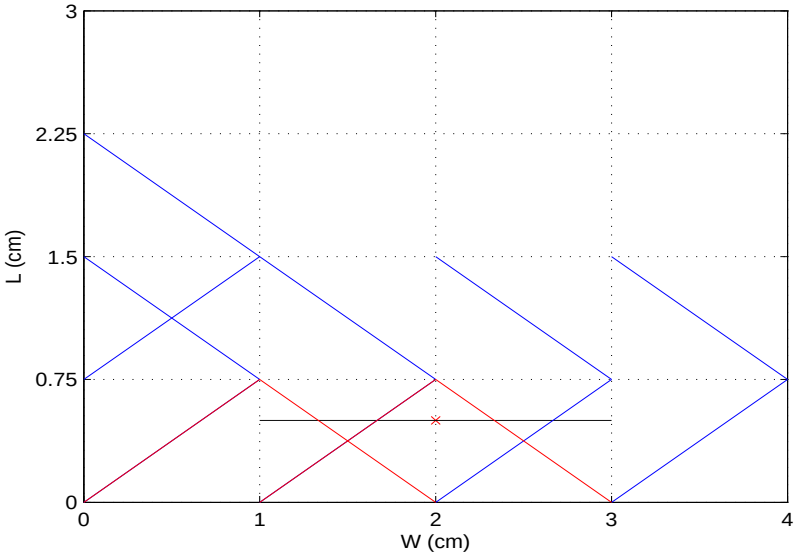

Figure 6.4: The placement of the $z-$ directed attachment mode on the same antenna, whose parameters are given in Fig. 6.2 together with some of the $z-$ and $\phi-$ directed PWS basis functions. $\times$ denotes the exact location of the probe.

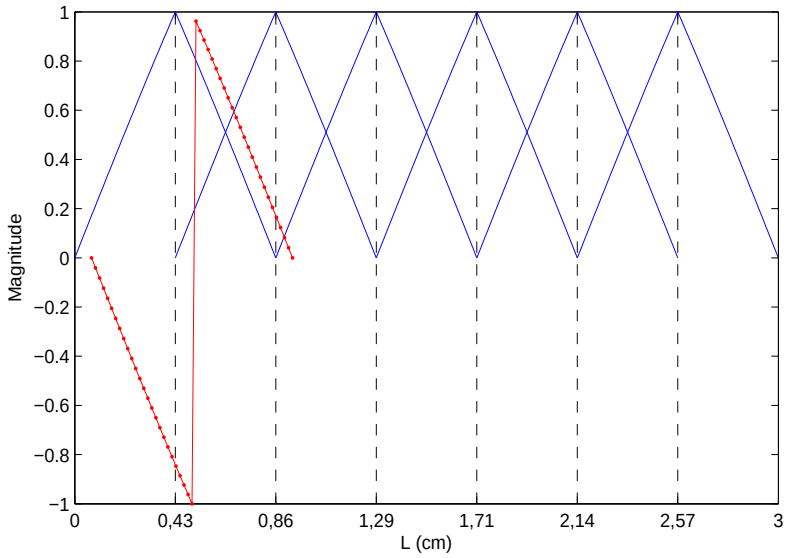

Figure 6.5: The magnitude, shape and location of a z-directed attachment mode with respect to 6 $z-$ directed PWS current modes along the $z-$ direction for an antenna whose parameters are given in Fig. 6.2

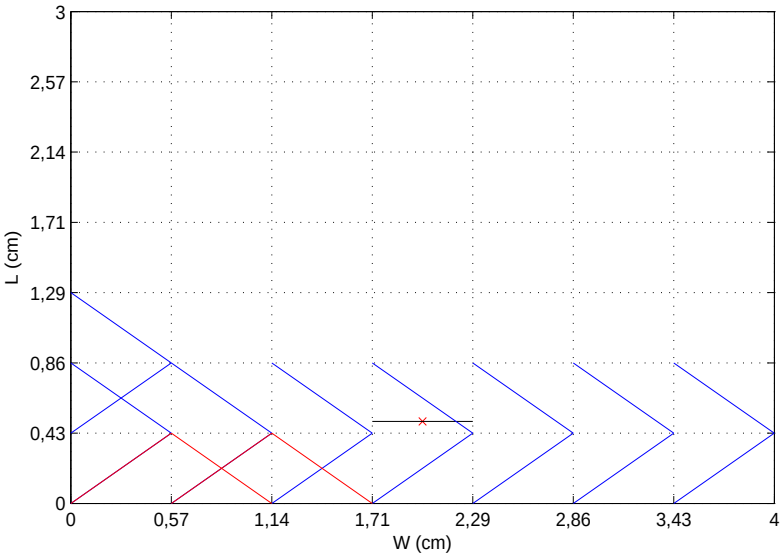

Figure 6.6: The placement of $z-$ directed attachment mode on the same antenna, whose parameters are given in Fig. 6.2 together with some of the $z-$ and $\phi-$ directed PWS basis functions. $\times$ denotes the exact location of the probe.

and $Z_{12\phi_{att}z}$ terms are included in the MoM analysis, there is no need to evaluate these terms, as will be explained in Section 6.4. Besides, as explained in Appendix F, $V_{\rho z_{att}} = V_{z_{att}\rho}$ and $V_{\rho\phi_{att}} = V_{\phi_{att}\rho}$.

Regarding the mutual impedance expression between a $z-$ directed current mode and J_{zatt} ($z-$ directed attachment mode), the related four-fold integral is given by

$$Z_{12zz_{att}} = \int\int\int\int J_z J_{z_{att}} G_{zz} dz dz' d\beta d\beta'. \tag{6.2}$$

Similar to the Z_{12zz} calculations, the $k_{\rho_j}^2$ expression in the spectral domain corresponds to $(k_j^2 - \frac{\partial^2}{\partial z \partial z'})$ in the space domain. Hence, G_{zz} is written as

$$G_{zz} \;=\; (k_j^2 - \frac{\partial^2}{\partial z \partial z'}) G_{zz2}. \tag{6.3}$$

where G_{zz2} is obtained from (5.20) for $uv = zz$ case. Using an integration by

parts twice the mutual impedance expression becomes

$$Z_{12zz_{att}} = \int\int\int\int \Big(k_0^2 J_z J_{z_{att}} G_{zz2} - \frac{\partial J_z}{\partial z}\frac{\partial J_{z_{att}}}{\partial z'} G_{zz2}\Big) dz dz' d\beta d\beta' - \int\int\int \frac{\partial J_z}{\partial z}\frac{1}{2l_{att}} G_{zz2} dz d\beta d\beta'. \quad (6.4)$$

Notice that the second term in (6.4) is due to the definition of an attachment mode as it appears to be discontinuous at the probe location [see (6.1)]. The value of the attachment mode is $+\alpha$ and $-\alpha$ ($\alpha \neq 0$) at the upper and lower halves of the attachment mode, respectively. Therefore, the end point contributions must be included when an integration by parts is used. Two contributions, coming from the upper half and lower half parts of the attachment mode, are added and the result forms the second term in (6.4).

The spectral domain singularity $\Big(\log(|\bar{\rho} - \bar{\rho}'|) \approx \log(|\beta - \beta'|)\Big)$ is treated in the same way as that of Z_{12zz} case. On the other hand, a slightly different approach is used for the space domain singularity. Briefly, substituting (5.20) into (6.4), the mutual impedance term related with the space domain singularity for the first term of (6.4) can be written as

$$\int\int J_{zz_{att}}(z, z') I_1 dz' d\beta \quad (6.5)$$

where $J_{zz_{att}}(z, z') = (k_0^2 J_z J_{z_{att}} - \frac{\partial J_z}{\partial z}\frac{\partial J_{z_{att}}}{\partial z'})$ and I_1 is given in (3.17). Then, using (5.22), the term $J_{zz_{att}}(z, z' = z) I_1'$ is subtracted and added to (6.5) resulting

$$\int\int \Big(J_{zz_{att}}(z, z') I_1 - J_{zz_{att}}(z, z' = z) I_1'\Big) dz' d\beta + \int\int J_{zz_{att}}(z, z' = z) I_1' dz' d\beta. \quad (6.6)$$

Rewriting the second term in (6.6) as

$$\int\int J_{zz_{att}}(z, z' = z) I_1' dz' d\beta = J_{zz_{att}}(z, z' = z) \int\int I_1' dz' d\beta, \quad (6.7)$$

the $\int\int I_1' dz' d\beta$ integrals can be evaluated analytically using (D.18) and (D.19). After the z' and β integrals are evaluated analytically, the remaining z and β' integrals are evaluated using a simple Gaussian quadrature algorithm. Note that the first integral in (6.6) is regular and the numerical singularity (which occurs when $\rho = \rho'$, $\phi = \phi'$ and $z = z'$) is solved using $J_{zz_{att}}(z, z' = z)(-jk_j)$ instead of

$\Big(J_{zz_{att}}(z,z')I_1 - J_{zz_{att}}(z,z'=z)I_1'\Big)$ at the singular point. In a similar manner, the integral that must be evaluated analytically for the second term of (6.4) can be written as

$$\int I_1 d\beta. \tag{6.8}$$

Again (6.8) comes from the substitution of (5.20) into the second term of (6.4). Rewriting (6.8) as

$$\int \Big(I_1 - I_1'\Big)d\beta + \int I_1' d\beta \tag{6.9}$$

the second integral $\int I_1' d\beta$ can be evaluated as

$$\int I_1' d\beta = \int \frac{1}{\sqrt{(\beta-\beta')^2 + (z-z')^2}} d\beta = \sinh^{-1}\Big(\frac{\beta-\beta'}{|z-z'|}\Big) \tag{6.10}$$

where (6.10) is obtained from (D.18). Note that the first integral in (6.9) is regular. However, during the numerical integration of $\Big(I_1 - I_1'\Big)$, $\Big(-jk_j\Big)$ is used when the numerical singularity occurs when $\rho = \rho'$, $\phi = \phi'$ and $z = z'$.

Regarding the mutual impedance expression between a $\phi-$ directed current mode and $J_{z_{att}}$, the related four-fold integral is given by

$$Z_{12\phi z_{att}} = \int\int\int\int J_\phi J_{z_{att}} G_{\phi z} dz dz' d\beta d\beta'. \tag{6.11}$$

Similar to the $Z_{12\phi z}$ calculations, first $G_{\phi z}$ is expressed as

$$G_{\phi z} = (-j)\frac{\partial}{\partial \phi}(-j)\frac{\partial}{\partial z'} G_{\phi z 2}, \tag{6.12}$$

where $G_{\phi z2}$ is obtained from (5.20) for $uv = \phi z$ case. Performing an integration by parts twice the mutual impedance expression is obtained as

$$\begin{aligned} Z_{12\phi z_{att}} \;=\; & \int\int\int\int (j)\frac{\partial J_\phi}{\partial \phi}(j)\frac{\partial J_{z_{att}}}{\partial z'} G_{\phi z2} dz dz' d\beta d\beta' \\ & + \int\int\int (j)\frac{\partial J_\phi}{\partial \phi}(j)\frac{1}{2l_{att}} G_{\phi z2} dz d\beta d\beta'. \end{aligned} \tag{6.13}$$

In (6.13), the second term is due to the definition of the attachment mode as discussed for $Z_{12zz_{att}}$ the case.

The spectral domain singularity $\Big(\log(|\bar{\rho}-\bar{\rho}'|) \approx \log(|\beta-\beta'|)\Big)$ exists and is the same for both terms of (6.13). The integrals that include the spectral domain singularity can be written as

$$\int J_{\phi 2}(\phi)\log(|\beta-\beta'|)d\beta \tag{6.14}$$

where $J_{\phi 2}(\phi) = (j)\frac{\partial J_\phi}{\partial \phi}$. Rewriting (6.14) as

$$\int [J_{\phi 2}(\phi) - J_{\phi 2}(\phi=\phi')]\log(|\beta-\beta'|)d\beta + J_{\phi 2}(\phi=\phi')\int \log(|\beta-\beta'|)d\beta, \tag{6.15}$$

the second integral in (6.15) is analytically evaluated using (C.67) whereas the first integral is regular and can be evaluated numerically. When β is equal to β' in the numerical evaluation, the $[J_{\phi 2}(\phi) - J_{\phi 2}(\phi=\phi')]\log(|\beta-\beta'|)$ term becomes zero in order to handle the numerical singularity (i.e., logarithmic singularity vanishes since it is multiplied by zero at the singular point). The remaining z, z' and β' integrals are evaluated numerically. On the other hand for the space domain singularity, substituting (5.23) into the first term of (6.13), the space domain singularity for the first term of (6.13) appears as

$$\int\int I_1' dz d\beta' \tag{6.16}$$

where I_1' is given in (5.22). In order to perform the two-fold integral given by (6.16) accurately and efficiently, first the integration with respect to z is evaluated analytically given by

$$\int \frac{1}{\sqrt{(\beta-\beta')^2+(z-z')^2}}dz = \sinh^{-1}\Big(\frac{z-z'}{|\beta-\beta'|}\Big). \tag{6.17}$$

Then, the β' integral is evaluated analytically as

$$\begin{aligned}&\int \sinh^{-1}(\frac{z-z'}{|\beta-\beta'|})d\beta' = \\ &= \left(\frac{|\beta'-\beta|}{z-z'}\sinh^{-1}(\frac{z-z'}{|\beta'-\beta|}) + \text{sign}(\frac{|\beta'-\beta|}{z-z'})\sinh^{-1}(\frac{|\beta'-\beta|}{z-z'})\right)\text{sign}(\beta-\beta')(z'-z).\end{aligned} \tag{6.18}$$

(6.18) solves the space domain singularity for the first term of (6.13). The remaining z and β' integrals are evaluated numerically. Substituting (5.20) into the

second term of (6.13) the space domain singularity for the second term of (6.13) appears as

$$\int J_{\phi z_{att}}(\phi) I_1 d\beta \tag{6.19}$$

where $J_{\phi z_{att}}(\phi) = (j)\frac{\partial J_\phi}{\partial \phi}(j)\frac{1}{2l_{att}}$ and I_1 is given in (3.17). Rewriting (6.19) as

$$\int \Big(J_{\phi z_{att}}(\phi) I_1 - J_{\phi z_{att}}(\phi = \phi') I_1' \Big) d\beta + J_{\phi z_{att}}(\phi = \phi') \int I_1' d\beta, \tag{6.20}$$

$\int I_1' d\beta$ is evaluated using (6.10). Remaining integrals are evaluated numerically using a Gaussian quadrature algorithm. In this numerical integration, $\Big(J_{\phi z_{att}}(\phi = \phi')(-jk_j) \Big)$ is used instead of the $\Big(J_{\phi z_{att}}(\phi) I_1 - J_{\phi z_{att}}(\phi = \phi') I_1' \Big)$ term in order to solve the numerical singularity when $\rho = \rho'$, $\phi = \phi'$ and $z = z'$.

Regarding the mutual impedance between the probe current and $J_{z_{att}}$, the related three-fold mutual impedance expression is given by

$$V_{z_{att}\rho} = -\int \int J_{z_{att}} \int G_{z\rho} d\rho' d\beta dz. \tag{6.21}$$

Similar to the $V_{z\rho}$ calculations, first the $G_{z\rho}$ is written as

$$G_{z\rho} = j\frac{\partial}{\partial z} G_{z\rho 2} \tag{6.22}$$

where $G_{z\rho 2}$ is obtained from (5.34). Performing an integration by parts, the expression becomes

$$V_{z_{att}\rho} = -\int \int (-j)\frac{\partial J_{z_{att}}}{\partial z} \int G_{z\rho 2} d\rho' d\beta dz. \tag{6.23}$$

Since $G_{z\rho 2}$ is an odd function with respect to z, the extra contribution that comes from the attachment mode definition (from upper and lower halves) is zero and (6.23) contains only one term. The spectral domain and the space domain singularities are solved using the procedure given in Sections 5.3.1 and 5.3.2, respectively.

Regarding the mutual impedance expression between a $\phi-$ directed current mode and $J_{\phi_{att}}$, the related four-fold integral is given by

$$Z_{12\phi\phi_{att}} = \int \int \int \int J_\phi J_{\phi_{att}} G_{\phi\phi} dz dz' d\beta d\beta'. \tag{6.24}$$

Similar the $Z_{12\phi\phi}$ calculations, first $G_{\phi\phi}$ is expressed as

$$G_{\phi\phi} = \frac{\partial^2 G_{\phi\phi 2}}{\partial\phi\partial\phi'}$$

where $G_{\phi\phi 2}$ is obtained from (5.20) for $uv = \phi\phi$ case. Performing an integration by parts twice the mutual impedance expression can be obtained as

$$\begin{aligned} Z_{12\phi\phi_{att}} &= \int\int\int\int \frac{\partial J_\phi}{\partial\phi}\frac{\partial J_{\phi_{att}}}{\partial\phi'} G_{\phi\phi 2} d\beta' d\beta dz dz' \\ &+ \int\int\int \frac{\partial J_\phi}{\partial\phi}\frac{1}{2z_{att}} G_{\phi\phi 2} dz dz' d\beta. \end{aligned} \tag{6.25}$$

In (6.25) the second term is due to the definition of the attachment mode at the probe location as discussed for $Z_{12zz_{att}}$ case.

The spectral domain singularity $\Big(\log(|\bar{\rho} - \bar{\rho}'|) \approx \log(|\beta - \beta'|)\Big)$ is common for both terms of (6.25) and the related integrals (that include the spectral domain singularity) can be written as

$$\int J_{\phi 2}(\phi)\log(|\beta - \beta'|)d\beta \tag{6.26}$$

where $J_{\phi 2}(\phi) = (j)\frac{\partial J_\phi}{\partial\phi}$. This integral is evaluated as explained in (6.15). On the other hand, the space domain singularity in the first term of (6.25) is coming from the substitution of (5.20) into the first term of (6.25) and is given by

$$\int\int J_{\phi 2}(\phi) I_1 d\beta dz' \tag{6.27}$$

where $J_{\phi 2}(\phi) = \frac{\partial J_\phi}{\partial\phi}$ and I_1 is given in (3.17). Rewriting (6.27) as

$$\int\int \Big(J_{\phi 2}(\phi)I_1 - J_{\phi 2}(\phi = \phi')I_1'\Big)d\beta dz' + J_{\phi 2}(\phi = \phi')\int\int I_1' d\beta dz', \tag{6.28}$$

where I_1' is given in (5.22), the second integral in (6.28) is analytically evaluated using (D.19). The remaining integrals (i.e., the first integral of (6.28) as well as the z and β' integrals) are evaluated numerically. In the numerical evaluation, the $\Big(J_{\phi 2}(\phi = \phi')(-jk_j)\Big)$ term is used instead of the $\Big(J_{\phi 2}(\phi)I_1 - J_{\phi 2}(\phi = \phi')I_1'\Big)$ term in order to handle the numerical singularity when $\rho = \rho'$, $\phi = \phi'$ and $z = z'$. Similarly, for the second part of (6.25), the singular integral related with the

space domain singularity comes as a result of substituting (5.20) into the second part of (6.25) and is given by

$$\int I_1 dz. \tag{6.29}$$

Rewriting (6.29) as

$$\int \Big(I_1 - I_1'\Big) dz + \int I_1' dz \tag{6.30}$$

the second integral is evaluated using (6.17). The remaining integrals are regular and can be evaluated numerically. However, in order to solve the numerical singularity, the $\Big(-jk_j\Big)$ term is used for the $\Big(I_1 - I_1'\Big)$ term when $\rho = \rho'$, $\phi = \phi'$ and $z = z'$ during the numerical integration.

Regarding the mutual impedance expression between a $z-$ directed current mode and $J_{\phi_{att}}$, the related four-fold integral is given by

$$Z_{12z\phi_{att}} = \int\int\int\int J_z J_{\phi_{att}} G_{z\phi} dz dz' d\beta d\beta'. \tag{6.31}$$

Similar to the $Z_{12z\phi_{att}}$ calculations, first $G_{z\phi}$ is written as

$$G_{z\phi} = (j)\frac{\partial}{\partial z}(j)\frac{\partial}{\partial \phi'} G_{z\phi 2}, \tag{6.32}$$

where $G_{z\phi 2}$ is obtained from (5.20) for $uv = z\phi$ case. Performing an integration by parts twice the mutual impedance expression is obtained as

$$\begin{aligned} Z_{12z\phi_{att}} \;=\; & \int\int\int\int (-j)\frac{\partial J_z}{\partial z}(-j)\frac{\partial J_{\phi_{att}}}{\partial \phi'} G_{z\phi 2} dz dz' d\beta d\beta' \\ & + \int\int\int (-j)\frac{\partial J_z}{\partial z}(-j)\frac{1}{2z_{att}} G_{z\phi 2} dz d\beta d\beta'. \end{aligned} \tag{6.33}$$

The second term in (6.33) is due the definition of the attachment mode as discussed for $Z_{12zz_{att}}$ case.

The spectral domain singularity is common for both terms of (6.33) and is evaluated analytically by taking the following integral

$$\int \log(|\beta - \beta'|) d\beta \tag{6.34}$$

in closed-form using (C.67). The space domain singularity for the first term of (6.33) is coming from the substitution of (5.23) into the first term of (6.33) and is given by

$$\int\int I_1' dz' d\beta. \tag{6.35}$$

It is evaluated analytically using (D.18) and (D.19). After the analytical evaluation of (6.35), the remaining z and β' integrals are evaluated numerically using a Gaussian quadrature algorithm. For the second term of (6.33), the singular integral comes from the substitution of (5.23) into (6.33) and is written as

$$\int I_1' d\beta. \tag{6.36}$$

(6.36) is analytically evaluated using (6.10) and the remaining z and β' integrals are evaluated numerically.

Finally, regarding the mutual impedance expression between the probe current and $J_{\phi_{att}}$, the related three-fold integral is given by

$$V_{\phi_{att}\rho} = -\int\int J_{\phi_{att}} \int G_{\phi\rho} d\rho' d\beta dz. \tag{6.37}$$

Similar to the $V_{\phi\rho}$ calculations, first $G_{\phi\rho}$ is written as

$$G_{\phi\rho} = -j\frac{\partial}{\partial\phi} G_{\phi\rho 2} \tag{6.38}$$

where $G_{\phi\rho 2}$ is obtained from (5.34). Performing an integration by parts, the expression becomes

$$V_{\phi_{att}\rho} = -\int\int (j)\frac{\partial J_{\phi_{att}}}{\partial\phi} \int G_{\phi\rho 2} d\rho' d\beta dz. \tag{6.39}$$

Similar to $G_{z\rho 2}$ case, since $G_{\phi\rho 2}$ is odd (this time with respect to ϕ), the extra contribution due to the definition of the attachment mode at the probe location does not exist. The spectral domain and the space domain singularities are solved using the procedure given in Sections 5.3.1 and 5.3.2, respectively.

6.2 Input Impedance Calculations

When the mutual impedance expressions related to the attachment mode, presented in Section 6.3, are included into the MoM matrix equation given by (1.7),

the resultant MoM matrix equation is given by

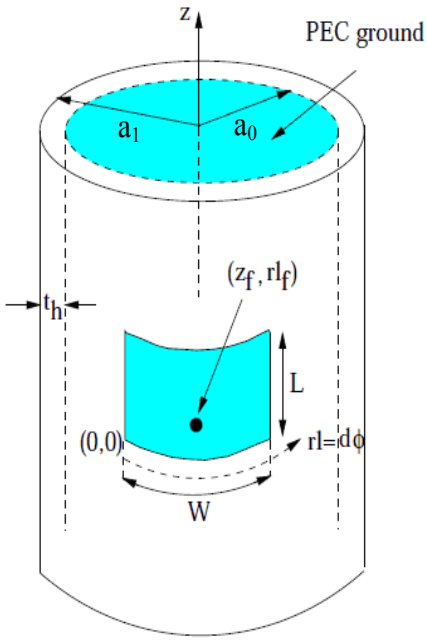

Figure 6.7: Patch antenna geometry which is excited with a TM_{01} mode

$$\begin{bmatrix} Z_{\phi_{att}\phi_{att}} & Z_{\phi_{att}z_{att}} & \underline{Z}_{\phi_{att}z} & \underline{Z}_{\phi_{att}\phi} \\ Z_{z_{att}\phi_{att}} & Z_{z_{att}z_{att}} & \underline{Z}_{z_{att}z} & \underline{Z}_{z_{att}\phi} \\ \underline{Z}_{z\phi_{att}} & \underline{Z}_{zz_{att}} & \underline{\underline{Z}}_{zz} & \underline{\underline{Z}}_{z\phi} \\ \underline{Z}_{\phi\phi_{att}} & \underline{Z}_{\phi z_{att}} & \underline{\underline{Z}}_{\phi z} & \underline{\underline{Z}}_{\phi\phi} \end{bmatrix} \begin{bmatrix} \alpha_0 \\ (1-\alpha_0) \\ \underline{I}_z \\ \underline{I}_\phi \end{bmatrix} = \begin{bmatrix} V_{\phi_{att}\rho} \\ V_{z_{att}\rho} \\ \underline{V}_{z\rho} \\ \underline{V}_{\phi\rho} \end{bmatrix} \tag{6.40}$$

for a single microstrip patch antenna, where α_0 is the magnitude of the attachment mode.

In (6.40) the dimensions of the submatrices are as follows: Making use of (1.6) $\underline{\underline{Z}}_{zz}$ is a $P \times P$ matrix, $\underline{\underline{Z}}_{z\phi}$ is a $P \times K$ matrix, $\underline{\underline{Z}}_{\phi z}$ is a $K \times P$ matrix, $\underline{\underline{Z}}_{\phi\phi}$ is a $K \times K$ matrix, $Z_{\phi_{att}\phi_{att}}$, $Z_{\phi_{att}z_{att}}$, $Z_{z_{att}\phi_{att}}$, $Z_{z_{att}z_{att}}$ are scalars, $\underline{Z}_{\phi_{att}z}$ and $\underline{Z}_{z_{att}z}$ are $1 \times P$ vectors, $\underline{Z}_{\phi_{att}\phi}$ and $\underline{Z}_{z_{att}\phi}$ are $1 \times K$ vectors, and finally $\underline{Z}_{z\phi_{att}}$ and $\underline{Z}_{zz_{att}}$ are $P \times 1$ vectors whereas $\underline{Z}_{\phi\phi_{att}}$ and $\underline{Z}_{\phi z_{att}}$ are $K \times 1$ vectors. Moreover in (6.40), $\underline{I_z}$ and $\underline{I_\phi}$ are $P \times 1$ and $K \times 1$ vectors. Similarly, $\underline{V}_{z\rho}$ and $\underline{V}_{\phi\rho}$ are also

$P \times 1$ and $K \times 1$ vectors, respectively. Finally, in (6.40) α_0, (1-α_0), $V_{\phi_{att}\rho}$ and $V_{z_{att}\rho}$ are scalars.

Since the amplitude of the probe current is equal to 1 ($I_0 = 1$), sum of the magnitudes of $z-$ and $\phi-$ directed attachment modes (the first two rows of the current vector given in the left hand side of (6.40)) is equal to 1. If only $\phi-$ directed attachment mode is defined α_0 is equal to 1, if only $z-$ directed attachment mode is defined α_0 is equal to 0 and if both $z-$ and $\phi-$ directed attachment modes are defined α_0 is equal to 0.5. Therefore, in the first two rows of (6.40) there is not any unknown and the matrix equation given in (6.40) can be cast into:

$$\begin{bmatrix} \underline{\underline{Z}}_{zz} & \underline{\underline{Z}}_{z\phi} \\ \underline{\underline{Z}}_{\phi z} & \underline{\underline{Z}}_{\phi\phi} \end{bmatrix} \begin{bmatrix} \underline{I}_z \\ \underline{I}_\phi \end{bmatrix} = \begin{bmatrix} \underline{V}_{z\rho} \\ \underline{V}_{\phi\rho} \end{bmatrix} - \begin{bmatrix} \alpha_0 \underline{Z}_{z\phi_{att}} + (1-\alpha_0)\underline{Z}_{zz_{att}} \\ \alpha_0 \underline{Z}_{\phi\phi_{att}} + (1-\alpha_0)\underline{Z}_{\phi z_{att}} \end{bmatrix}, \quad (6.41)$$

which can be expressed as

$$\underline{\underline{Z}}\,\underline{I} = (\underline{V} - \underline{V}_{att}). \quad (6.42)$$

The unknowns a_n's are solved using the inverse of $\underline{\underline{Z}}$ as

$$\underline{I} = \underline{\underline{Z}}^{-1}(\underline{V} - \underline{V}_{att}). \quad (6.43)$$

Once a_n's are determined, the current distribution on the antenna can be constructed. Since the magnitude of the probe current is equal to 1 ($I_0 = 1$), we know that

$$\int d\vartheta J_\rho \delta(\rho - p_e) = 1, \quad (6.44)$$

where p_e denotes the probe end and J_ρ is given in (5.24). Finally, the input impedance is defined as the total voltage at the feed point since the total current through the probe is 1A. Hence, the input impedance expression is given by

$$Z_{11} = \sum_{n=1}^{N} a_n V_\rho^n + \alpha_0 V_{\rho\phi_{att}} + (1-\alpha_0) V_{\rho z_{att}} \quad (6.45)$$

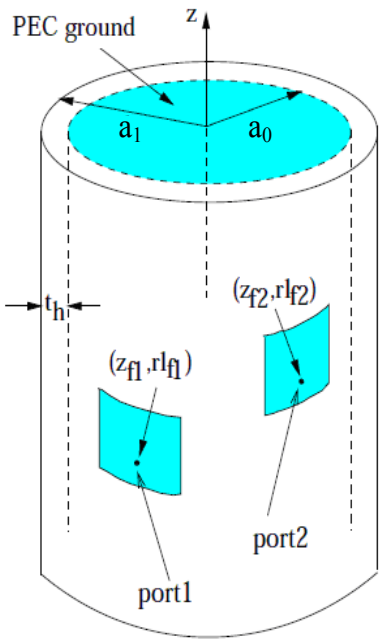

Figure 6.8: Mutual coupling geometry where two patch antennas are present on circular cylinder

where a_n (entries of $\underline{I}$) are the expansion mode coefficients found from the MoM procedure and V_ρ^n (simply the corresponding $V_{\rho z}$'s and $V_{\rho\phi}$'s) are the induced voltages on the probe due the current modes J_n. Similarly, $V_{\rho z_{att}}$ and $V_{\rho\phi_{att}}$ are the induced voltages on the probe due the attachment mode. The $V_{\rho v}$ terms can be obtained using Appendix F where v can be z, ϕ, z_{att} or ϕ_{att}.

6.3 Calculation of Mutual Coupling Between Two Antennas

The geometry used for the mutual coupling calculations between two antennas on a dielectric coated circular cylinder is shown in Fig.6.8. For each patch antenna N basis functions (P basis functions in $z-$ direction and K basis functions in $\phi-$ direction) are used. For the two-port configuration given in Fig.6.8, the input impedance of element one Z_{11} is calculated when port two is open. Similarly, the

mutual impedance Z_{21} is calculated when port two is open. The other parameters $Z_{12} = Z_{21}$ as a result of reciprocity theorem and $Z_{22} = Z_{11}$ because of the fact that two antennas are selected to be identical.

In order to calculate only the Z_{11} and Z_{21}, port two is left open and the attachment mode is defined only on patch one. After the current modes are defined on the patch antennas, using a Galerkin type testing, the following matrix equation is obtained.

$$\begin{bmatrix} Z_{\phi_{att}\phi_{att}} & Z_{\phi_{att}z_{att}} & \underline{Z}_{\phi_{att}z_1} & \underline{Z}_{\phi_{att}z_2} & \underline{Z}_{\phi_{att}\phi_1} & \underline{Z}_{\phi_{att}\phi_2} \\ Z_{z_{att}\phi_{att}} & Z_{z_{att}z_{att}} & \underline{Z}_{z_{att}z_1} & \underline{Z}_{z_{att}z_2} & \underline{Z}_{z_{att}\phi_1} & \underline{Z}_{z_{att}\phi_2} \\ \underline{Z}_{z_1\phi_{att}} & \underline{Z}_{z_1z_{att}} & \underline{\underline{Z}}_{z_1z_1} & \underline{\underline{Z}}_{z_1z_2} & \underline{\underline{Z}}_{z_1\phi_1} & \underline{\underline{Z}}_{z_1\phi_2} \\ \underline{Z}_{z_2\phi_{att}} & \underline{Z}_{z_2z_{att}} & \underline{\underline{Z}}_{z_2z_1} & \underline{\underline{Z}}_{z_2z_2} & \underline{\underline{Z}}_{z_2\phi_1} & \underline{\underline{Z}}_{z_2\phi_2} \\ \underline{Z}_{\phi_1\phi_{att}} & \underline{Z}_{\phi_1z_{att}} & \underline{\underline{Z}}_{\phi_1z_1} & \underline{\underline{Z}}_{\phi_1z_2} & \underline{\underline{Z}}_{\phi_1\phi_1} & \underline{\underline{Z}}_{\phi_1\phi_2} \\ \underline{Z}_{\phi_2\phi_{att}} & \underline{Z}_{\phi_2z_{att}} & \underline{\underline{Z}}_{\phi_2z_1} & \underline{\underline{Z}}_{\phi_2z_2} & \underline{\underline{Z}}_{\phi_2\phi_1} & \underline{\underline{Z}}_{\phi_2\phi_2} \end{bmatrix} \begin{bmatrix} \alpha_0 \\ (1-\alpha_0) \\ \underline{I_{z_1}} \\ \underline{I_{z_2}} \\ \underline{I_{\phi_1}} \\ \underline{I_{\phi_2}} \end{bmatrix} = \begin{bmatrix} V_{\phi_{att}\rho_1} \\ V_{z_{att}\rho_1} \\ \underline{V}_{z_1\rho_1} \\ \underline{V}_{z_2\rho_1} \\ \underline{V}_{\phi_1\rho_1} \\ \underline{V}_{\phi_2\rho_1} \end{bmatrix}. \tag{6.46}$$

In (6.46), the subscripts are written in such a way that $\underline{Z}_{z_1\phi_{att}}$ is the vector which gives the mutual impedance between the $\phi-$ directed attachment mode and the $z-$ directed current modes on patch one. Similarly, $\underline{\underline{Z}}_{\phi_2z_1}$ is the mutual impedance matrix between the $\phi-$ directed current modes on patch two and the $z-$ directed current modes on patch one. $\underline{V}_{z_2\rho_1}$ is the induced voltage vector on the $z-$ directed current modes on patch two due to the probe of patch one. All the other submatrices and vectors in (6.46) have similar meanings.

Similar to the input impedance calculations, since the amplitude of the probe current of patch one is equal to 1 ($I_0 = 1$), the summation of $z-$ and $\phi-$ directed attachment modes is equal to 1. If only $\phi-$ directed attachment mode is defined, α_0 is equal to 1, if only $z-$ directed attachment mode is defined, α_0 is equal to 0 and if both $z-$ and $\phi-$ directed attachment modes are defined, α_0 is equal to 0.5. Therefore, in the first two rows of (6.46) there is not any unknown and the matrix equation given in (6.46) can be cast into:

$$\begin{bmatrix} \underline{\underline{Z}}_{z_1z_1} & \underline{\underline{Z}}_{z_1z_2} & \underline{\underline{Z}}_{z_1\phi_1} & \underline{\underline{Z}}_{z_1\phi_2} \\ \underline{\underline{Z}}_{z_2z_1} & \underline{\underline{Z}}_{z_2z_2} & \underline{\underline{Z}}_{z_2\phi_1} & \underline{\underline{Z}}_{z_2\phi_2} \\ \underline{\underline{Z}}_{\phi_1z_1} & \underline{\underline{Z}}_{\phi_1z_2} & \underline{\underline{Z}}_{\phi_1\phi_1} & \underline{\underline{Z}}_{\phi_1\phi_2} \\ \underline{\underline{Z}}_{\phi_2z_1} & \underline{\underline{Z}}_{\phi_2z_2} & \underline{\underline{Z}}_{\phi_2\phi_1} & \underline{\underline{Z}}_{\phi_2\phi_2} \end{bmatrix} \begin{bmatrix} \underline{I_{z_1}} \\ \underline{I_{z_2}} \\ \underline{I_{\phi_1}} \\ \underline{I_{\phi_2}} \end{bmatrix} = \begin{bmatrix} \underline{V}_{z_1\rho_1} \\ \underline{V}_{z_2\rho_1} \\ \underline{V}_{\phi_1\rho_1} \\ \underline{V}_{\phi_2\rho_1} \end{bmatrix} - \begin{bmatrix} \alpha_0\underline{Z}_{z_1\phi_{att}} + (1-\alpha_0)\underline{Z}_{z_1z_{att}} \\ \alpha_0\underline{Z}_{z_2\phi_{att}} + (1-\alpha_0)\underline{Z}_{z_2z_{att}} \\ \alpha_0\underline{Z}_{\phi_1\phi_{att}} + (1-\alpha_0)\underline{Z}_{\phi_1z_{att}} \\ \alpha_0\underline{Z}_{\phi_2\phi_{att}} + (1-\alpha_0)\underline{Z}_{\phi_2z_{att}} \end{bmatrix} \tag{6.47}$$

which can be expressed as

$$\underline{\underline{Z}}\,\underline{I} = (\underline{V} - \underline{V}_{att}). \tag{6.48}$$

$\underline{I}$ in (6.48) is the current vector which contains the unknown coefficients of the current modes (for instance $\underline{I_{z_1}}$ is the vector which contains the amplitudes of the $z-$ directed current modes on patch one, $\underline{I_{\phi_2}}$ is used for the $\phi-$ directed current modes on patch two) defined as

$$\underline{I} = [a_1, a_2, a_3, ..., a_{2N}]^T, \tag{6.49}$$

and are calculated from

$$\underline{I} = \underline{\underline{Z}}^{-1}(\underline{V} - \underline{V}_{att}). \tag{6.50}$$

Similar to (6.45), the input impedance of patch one is defined as [(voltage at the probe of patch one)/1A]

$$Z_{11} = \sum_{n=1}^{2N} a_n V_{\rho_1}^n + \alpha_0 V_{\rho_1\phi_{att}} + (1-\alpha_0)V_{\rho_1 z_{att}} \tag{6.51}$$

where a_n's are the expansion mode coefficients found from (6.50) and $V_{\rho_1}^n$ (simply the corresponding $V_{\rho_1 z_1}$'s, $V_{\rho_1 z_2}$'s, $V_{\rho_1\phi_1}$'s and $V_{\rho_1\phi_2}$'s) are the induced voltages on the probe of patch one due to the current modes J_n. $V_{\rho_1 z_{att}}$ and $V_{\rho_1\phi_{att}}$ are the induced voltages on the probe of patch one due to the attachment mode.

Similarly, the mutual coupling between two antennas is defined as [(voltage at the probe of patch two)/1A]

$$Z_{21} = \sum_{n=1}^{2N} a_n V_{\rho_2}^n + \alpha_0 V_{\rho_2\phi_{att}} + (1-\alpha_0)V_{\rho_2 z_{att}} \tag{6.52}$$

where a_n's are the expansion mode coefficients found from (6.50) when port one is excited and port two is left open. $V_{\rho_2}^n$ (simply the corresponding $V_{\rho_2 z_1}$'s, $V_{\rho_2 z_2}$'s, $V_{\rho_2 \phi_1}$'s and $V_{\rho_2 \phi_2}$'s) are the induced voltages on the probe of patch two due to the current modes J_n. $V_{\rho_2 z_{att}}$ and $V_{\rho_2 \phi_{att}}$ are the induced voltages on the probe of patch two due to the attachment mode. Finally, the mutual coupling coefficient between two antennas can be calculated as follows:

$$S_{12} = \frac{2Z_{12}Z_0}{(Z_{11} + Z_0)(Z_{22} + Z_0) - Z_{12}Z_{21}} \tag{6.53}$$

where $Z_0 = 50$. In (6.53), $Z_{12} = Z_{21}$ as mentioned before due to reciprocity.

Chapter 7

Numerical Results

To assess the accuracy of the proposed CFGF representations together with the MoM procedure that uses the aforementioned attachment mode, numerical results in the form of input impedance of a single antenna and mutual coupling between two antennas are obtained and compared with the available results in literature and the results obtained from a commercial software CST Microwave Studio.

In all of the numerical results obtained via MoM with CFGF, piecewise sinusoidal (PWS) current modes are used as the expansion functions with the attachment mode which is consistent with PWS current modes.

In the course of obtaining the space domain CFGF representations, the following parameters are used for the GPOF implementation of the tangential components : $T' = 0.5$, $T_1 = 0.2$, $T_2 = 5$, $T_3 = 20$, $T_4 = 40$, $N' = 20$, $N_1 = 40$, $N_2 = 80$, $N_3 = 20$, $N_4 = 20$, $M' = 5$, $M_1 = 8$, $M_2 = 12$, $M_3 = 6$, $M_4 = 4$. On the other hand, for the probe-related components the values of the same parameters are as follows: $T' = 0.5$, $T_1 = 0.2$, $T_2 = 4$, $T_3 = 50$, $T_4 = 60$, $N' = 10$, $N_1 = 20$, $N_2 = 10$, $N_3 = 40$, $N_4 = 20$, $M' = 3$, $M_1 = 5$, $M_2 = 3$, $M_3 = 5$, $M_4 = 3$.

The first numerical example is given for a single rectangular microstrip patch mounted on a dielectric coated circular cylinder as shown in Fig. 7.1 with $a_0 = 20$ cm, $\epsilon_r = 2.32$, $t_h = a_1 - a_0 = 0.795$ mm. The length of the patch L is 3 cm,

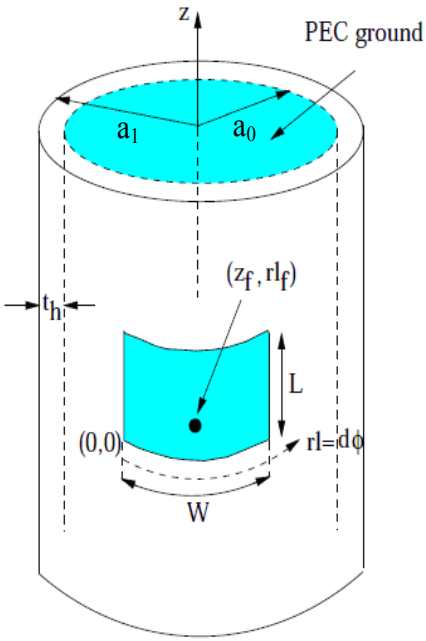

Figure 7.1: Probe-fed microstrip patch antenna on a dielectric coated PEC cylinder

and the width of the patch W is 4 cm. The antenna is excited with a TM_{01} mode and fed via a probe at the feed location (z_f,rl_f)=(0.5 cm,2 cm). The input impedance result (real and imaginary parts) obtained using CFGF is given in Fig. 7.2 with the result of CST Microwave Studio, and they are in good agreement. In obtaining the CFGF results, the conducting patch, on which the induced current exists, is divided into 10 subdomains along the $z-$ and $\phi-$ directions ($P = 90$, $K = 90$ and $N = 180$) and a $z-$ directed attachment mode with $z_{att} = z_a$ and $l_{att} = l_a$ (as explained in Section 6.3 where the $z-$ directed current mode has a dimension of $2z_a \times l_a$) is used. $\phi-$ directed attachment mode is not used for this example.

Another way to assess the accuracy of the MoM formulation is to perform a convergence test. Thus, a convergence test is performed for the first example. As the number of current modes used in the MoM solution is increased, the input impedance results converge to the $P = 90$, $K = 90$ case and do not change much if more current modes are used. As seen in Fig. 7.3 the input impedance results

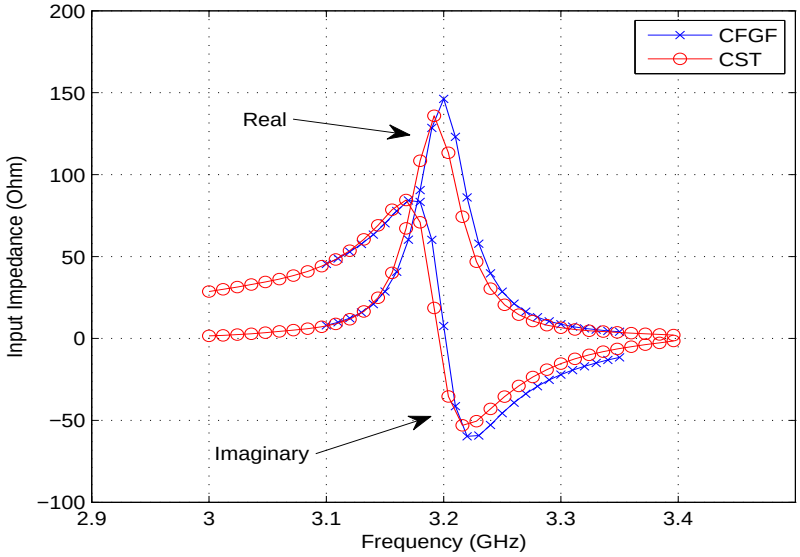

Figure 7.2: Input impedance versus frequency for a patch with the following parameters: $a_0 = 20$ cm, $\epsilon_r = 2.32$, $t_h = 0.795$ mm, $L = 3$ cm, $W = 4$ cm and (z_f,rl_f)=(0.5 cm,2 cm)

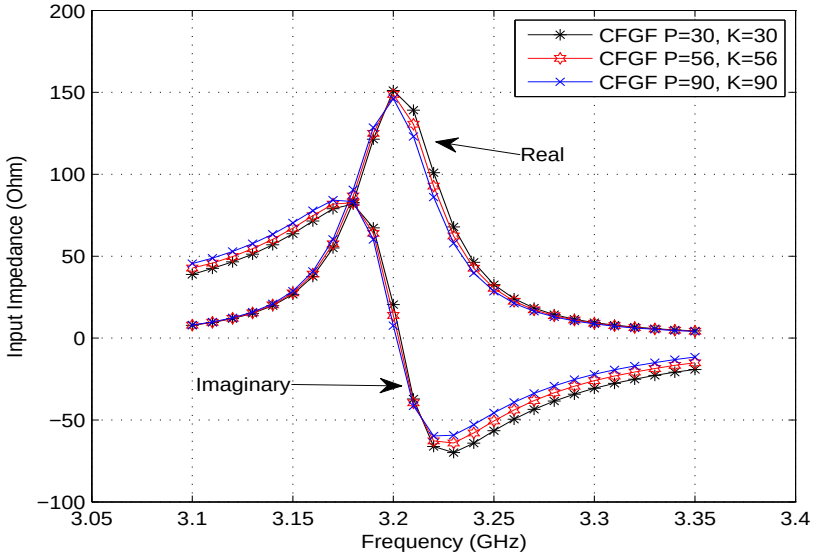

Figure 7.3: Input impedance versus frequency for different number of current modes for the patch given in Fig. 7.2

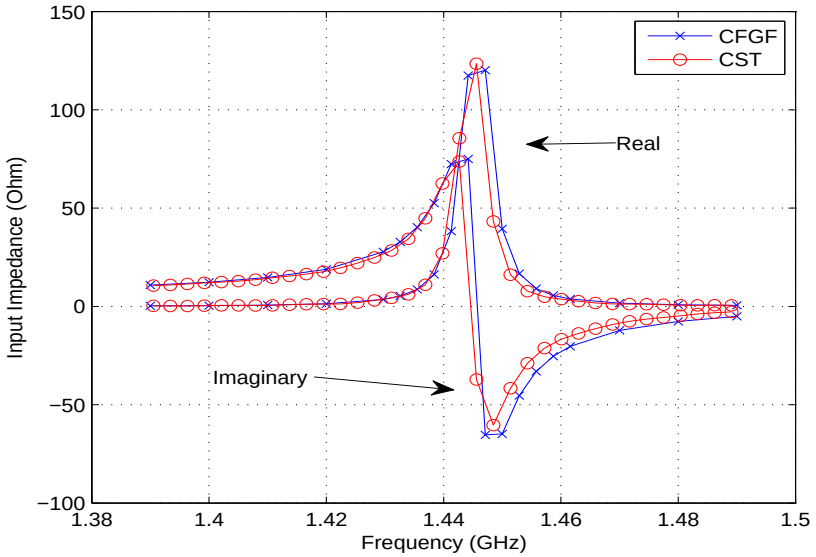

Figure 7.4: Input impedance versus frequency for a patch with the following parameters: $a_0 = 40$ cm, $\epsilon_r = 2.98$, $t_h = 0.762$ mm, $L = 6$ cm, $W = 4$ cm and (z_f,rl_f)=(2.1 cm,2 cm)

for $P = 30$, $K = 30$, $N = 60$; $P = 56$, $K = 56$, $N = 112$; $P = 90$, $K = 90$, $N = 180$ cases are very close to each other.

As the second example, a cylinder with the following parameters is used : $a_0 = 40$ cm, $\epsilon_r = 2.98$, $t_h = 0.762$ mm. The dimensions of the patch is L=6 cm, W=4 cm, yielding a resonance at 1.444 GHz where the TM_{01} mode is excited. Probe is located at (z_f,rl_f)=(2.1 cm,2 cm). The input impedance (real and imaginary parts) result obtained using the CFGF representations versus frequency for this antenna is given in Fig. 7.4 together with the results of CST Microwave Studio. In this example, the conducting patch is divided into 8 subdomains along the $z-$ and $\phi-$ directions ($P = 56$, $K = 56$, $N = 112$) and a $z-$ directed attachment mode with $z_{att} = z_a$ and $l_{att} = l_a$ (as explained in Section 6.3) is used. As seen in Fig. 7.4 excellent agreement is obtained.

The previous geometry with the same parameters is considered as the third example except the dielectric layer is considered to be lossy with $\tan\delta = 0.0045$. The input impedance result obtained using the CFGF representations versus

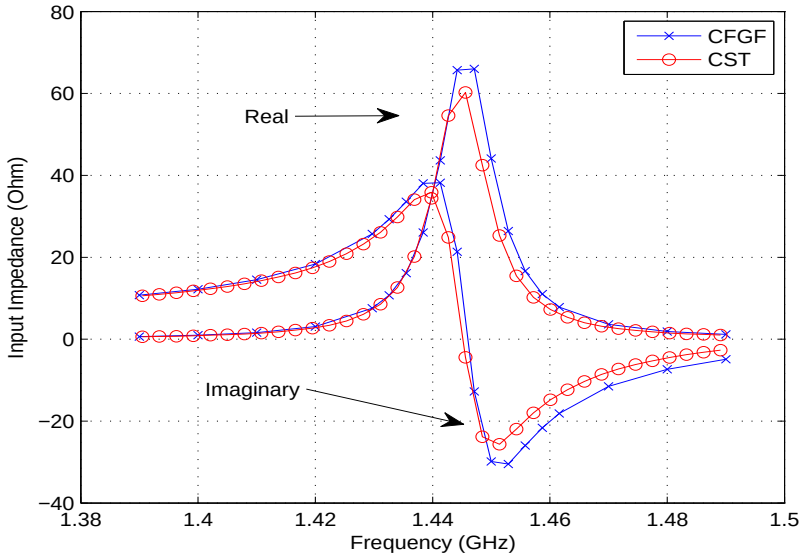

Figure 7.5: Input impedance versus frequency for a patch with the following parameters: $a_0 = 40$ cm, $\epsilon_r = 2.98$, $\tan\delta = 0.0045$, $t_h = 0.762$ mm, $L = 6$ cm, $W = 4$ cm and (z_f,rl_f)=(2.1 cm,2 cm)

frequency for this antenna is given in Fig. 7.5 with the result of CST Microwave Studio. In the CFGF result, the conducting patch is divided into 8 subdomains in both $z-$ and $\phi-$ directions ($P = 56$, $K = 56$, $N = 112$) and a $z-$ directed attachment mode with $z_{att} = z_a$ and $l_{att} = l_a$ is used. Similar to the previous case, very good agreement is obtained.

The next example has the same parameters with the first example (i.e., $a_0 = 20$ cm, $\epsilon_r = 2.32$, $t_h = 0.795$ mm and the dimensions of the patch is $L = 3$ cm, $W = 4$ cm) except the probe location, where the probe is located at (z_f,rl_f)=(1.5 cm,2.67 cm). Therefore, TM_{10} mode is excited. The microstrip patch antenna geometry is illustrated in Fig. 7.6. The input impedance result obtained using the CFGF representations versus frequency for this antenna is given in Fig. 7.7 with the result of CST Microwave Studio. In the CFGF result, the conducting patch is divided into 8 subdomains in both $z-$ and $\phi-$ directions ($P = 56$, $K = 56$, $N = 112$) and a $\phi-$ directed attachment mode ($z_{att} = z_a$ and $l_{att} = l_a$ where $z_a \times 2l_a$ is the dimension of the $\phi-$ directed current mode) is used. In this example, the $z-$ directed attachment mode is not used. As seen in Fig. 7.7, very

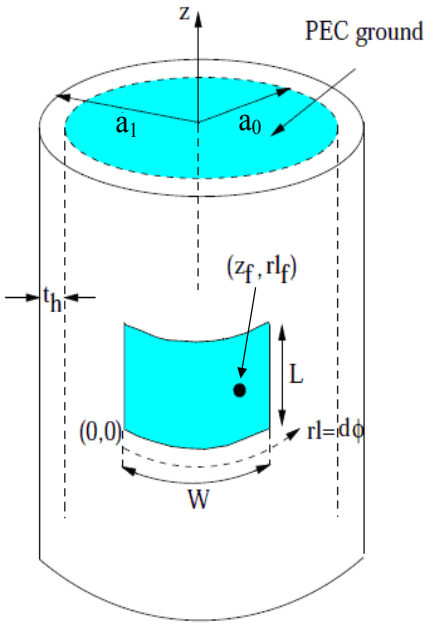

Figure 7.6: Microstrip patch antenna geometry which is excited with a TM_{10} mode

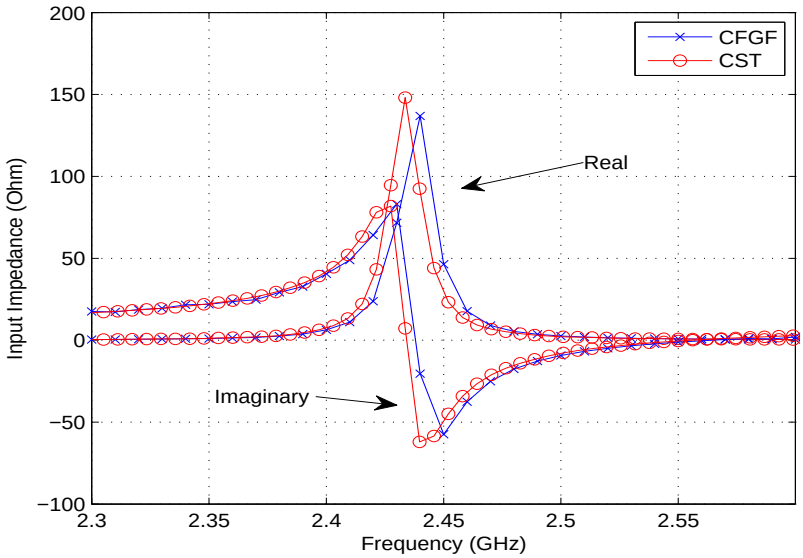

Figure 7.7: Input impedance versus frequency for a patch with the following parameters: $a_0 = 20$ cm, $\epsilon_r = 2.32$, $t_h = 0.795$ mm, $L = 3$ cm, $W = 4$ cm and (z_f,rl_f)=(1.5 cm,2.67 cm)

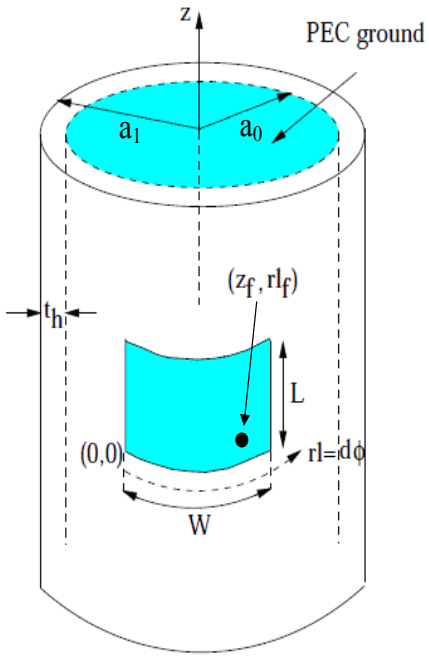

Figure 7.8: Microstrip patch antenna geometry where the probe is located at the corner of the antenna

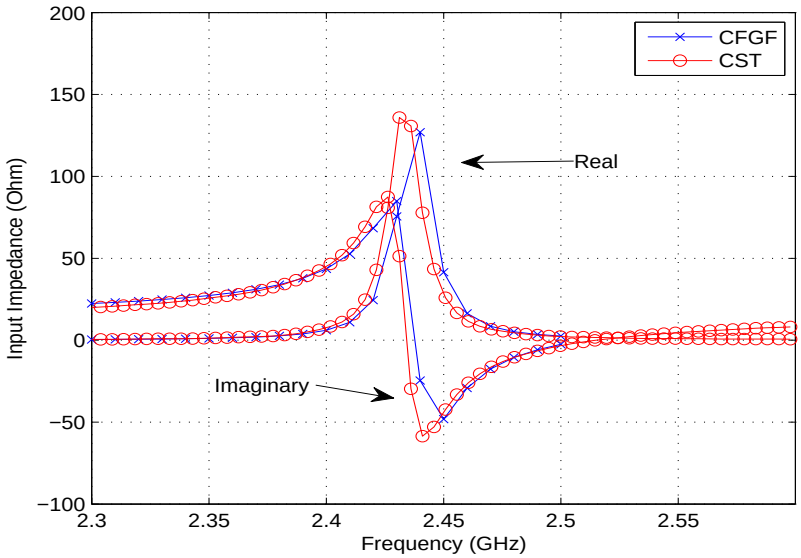

Figure 7.9: Input impedance versus frequency for a patch with the following parameters: $a_0 = 20$ cm, $\epsilon_r = 2.32$, $t_h = 0.795$ mm, $L = 3$ cm, $W = 4$ cm and (z_f,rl_f)=(0.05 cm,2.67 cm)

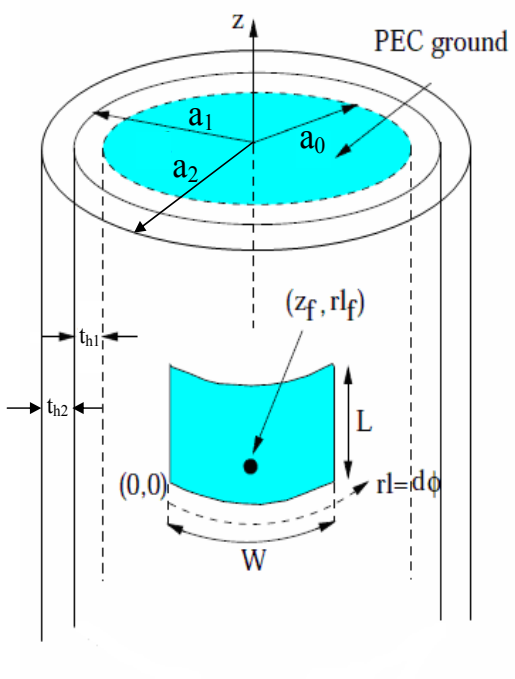

Figure 7.10: The patch antenna geometry where a substrate and a superstrate exist around PEC. Patch antenna is defined at the substrate-superstrate interface

good agreement is obtained.

The parameters for the next input impedance example are exactly the same with the previous example. The only difference is the location of the probe. The probe is located at (z_f,rl_f)=(0.05 cm,2.67 cm) where the probe is located at the corner of the patch antenna as seen in Fig. 7.8. The CFGF and CST Microwave Studio results are given in Fig. 7.9. CFGF results are obtained by dividing the conducting patch into 12 subdomains along the $z-$ and $\phi-$ directions ($P = 132$, $K = 132$, $N = 264$) and both $z-$ and $\phi-$ directed attachment modes are used where they have the same length with the $z-$ and $\phi-$ directed current modes while the widths of the attachment modes are twice that of the widths of the corresponding current modes. Similar to the previous cases, very good agreement is obtained.

As the last input impedance example, Fig. 7.10 depicts the microstrip patch

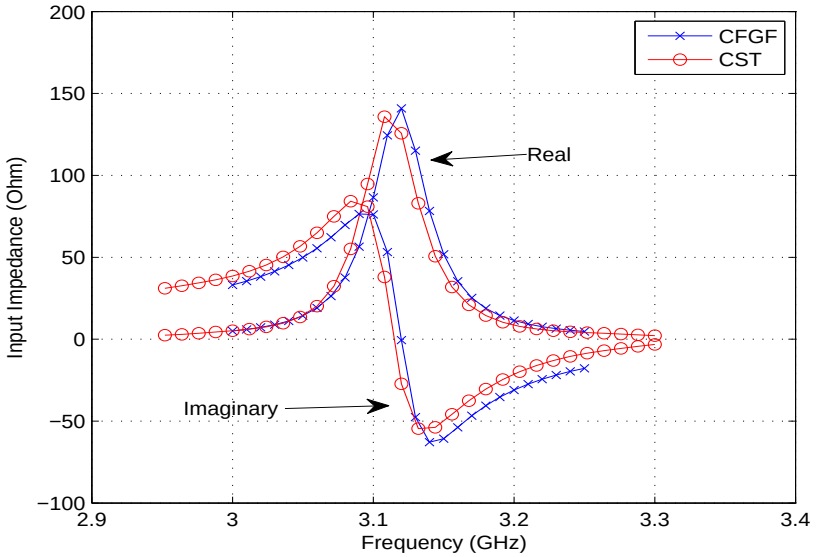

Figure 7.11: Input impedance versus frequency for a patch with the following parameters: $a_0 = 20$ cm, Substrate $\epsilon_r = 2.32$, $t_{h1} = 0.795$ mm, Superstrate $\epsilon_r = 2.98$, $t_{h2} = 0.762$ mm, $L = 3$ cm, $W = 4$ cm and (z_f,rl_f)=(0.5 cm,2 cm)

antenna geometry where a substrate and a superstrate are present. The patch antenna, with the parameters $W = 4$ cm and $L = 3$ cm, is located at the substrate-superstrate interface. Probe is located at (z_f,rl_f)=(0.5 cm,2 cm). Substrate has a thickness of 0.795 mm with $\epsilon_r = 2.32$ whereas the thickness of the superstrate layer is 0.762 mm and $\epsilon_r = 2.98$. The input impedance result obtained using the CFGF representations versus frequency for this antenna is given in Fig. 7.11 together with the CST Microwave Studio result. In the CFGF results the conducting patch is divided into 30 and 4 subdomains along the $z-$ and $\phi-$ directions, respectively, ($P = 174$, $K = 150$, $N = 324$) and a $z-$ directed attachment mode with $z_{att} = z_a$ and $l_{att} = l_a$ is used. In this example $\phi-$ directed attachment mode is not used. Excellent agreement is obtained as seen in Fig. 7.11.

Fig. 7.12 illustrates the geometry used for the mutual coupling calculations between two identical antennas along the E-plane. Note that the antennas shown in Fig. 7.12 are fed in such a way that the TM_{01} mode is excited resulting the $z-$ directed current on each patch being the dominant current mode. Therefore, the $z-$ direction on the cylinder is part of the E-plane and the $\phi-$ direction on

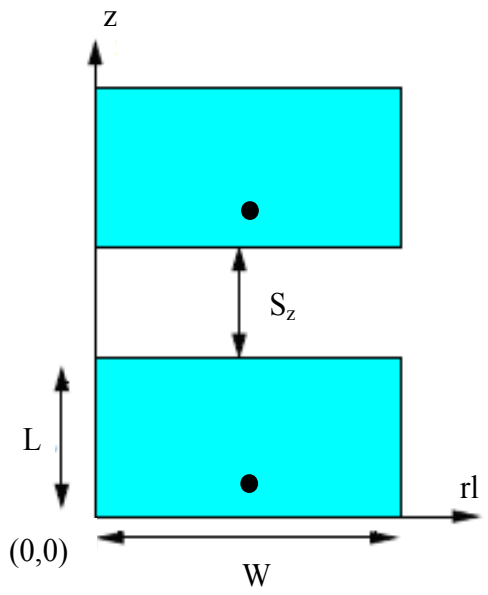

Figure 7.12: E-plane coupling geometry

the cylinder becomes part of the H-plane. Fig. 7.13 shows the E-plane coupling results at $f = 3.195$ GHz between the antennas whose parameters are defined in Fig. 7.2 except the probe location. Note that the probe location is now set to (z_f,rl_f)=(0.95 cm,2 cm), so that antennas are matched to 50 Ω at resonance. In the CFGF results, the conducting patch for each antenna is divided into 10 subdomains both in $z-$ and $\phi-$ directions ($P = 90$, $K = 90$, $N = 180$) and a $z-$ directed attachment mode ($z_{att} = z_a$ and $l_{att} = l_a$, no $\phi-$ directed attachment mode) is used. As seen in Fig. 7.13, very good agreement is achieved between the CFGF and CST Microwave Studio results. The E-plane coupling results for the geometry given in Fig. 7.12 (with the antenna parameters given in Fig. 7.4) is illustrated in Fig. 7.14 at the resonance frequency $f = 1.444$ GHz. In Fig. 7.14, the mutual coupling results are obtained by dividing the conducting patch for each antenna into 6 subdomains along the $z-$ and $\phi-$ directions ($P = 30$, $K = 30$, $N = 60$) and a $z-$ directed attachment mode with $z_{att} = z_a$ and $l_{att} = l_a$ ($\phi-$ directed attachment mode is not used) is used. Very good agreement is achieved between the CFGF and the CST Microwave Studio results. When the dielectric loss is introduced (as shown in the parameters given in Fig. 7.5) to the same example, the E-plane coupling results are given in Fig. 7.15. To obtain

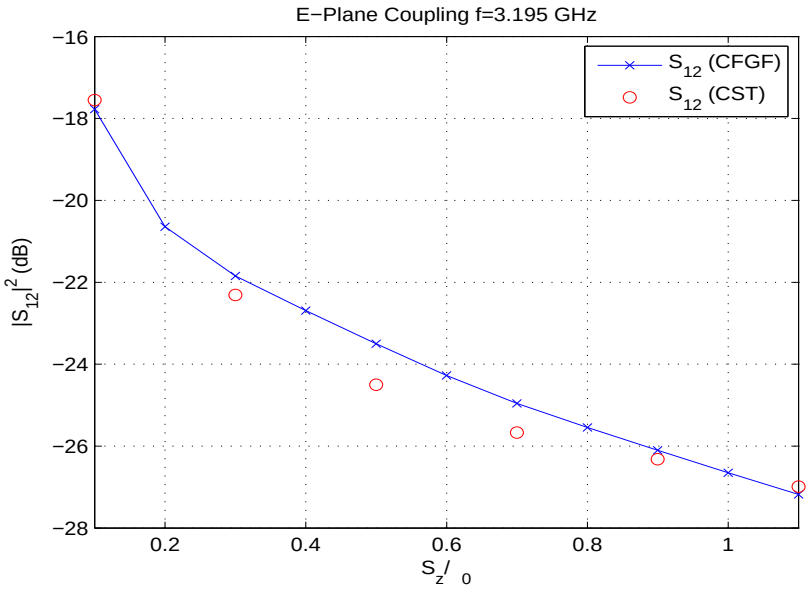

Figure 7.13: E-plane coupling results for patch antenna geometry given in Fig. 7.2 with (z_f, rl_f)=(0.95 cm,2 cm)

the CFGF results given in Fig. 7.15, the conducting patch for each antenna is divided into 12 subdomains in both $z-$ and $\phi-$ directions ($P = 132$, $K = 132$, $N = 264$) and a $z-$ directed attachment mode that has $z_{att} = z_a$ and $l_{att} = l_a$ (no $\phi-$ directed attachment mode) is used. In Fig. 7.15 the CFGF results are compared with the CST Microwave Studio and the measurement results available in the literature [33]. Notice that with the introduction of the dielectric loss, the coupling results decrease as expected. Also note that the agreement of all results are excellent.

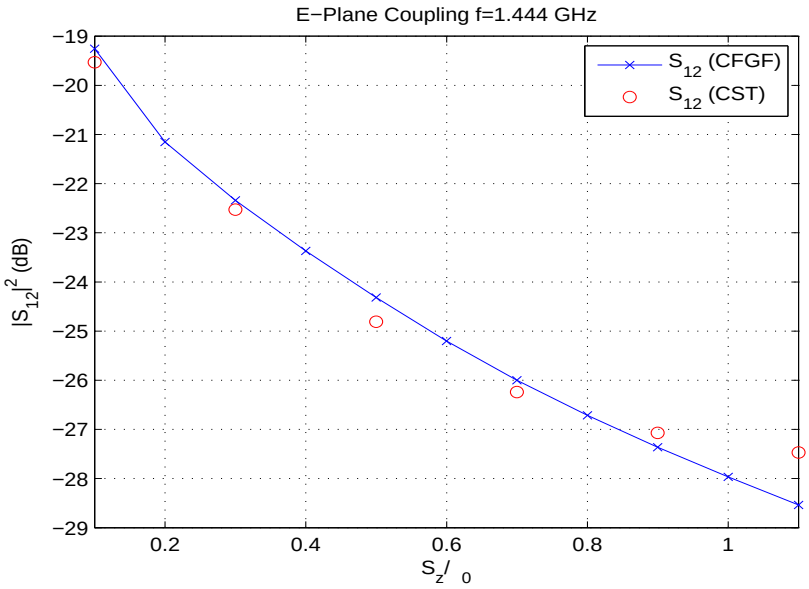

Figure 7.14: E-plane coupling results for patch antenna geometry given in Fig. 7.4

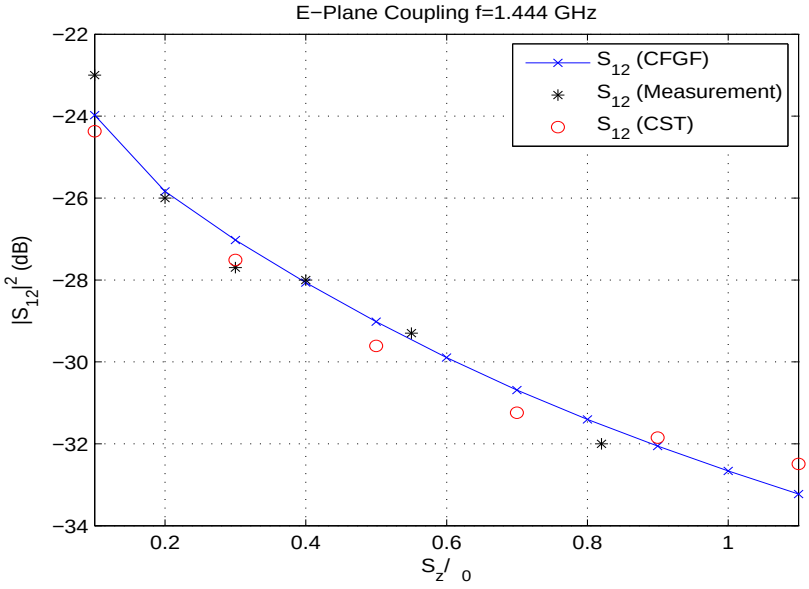

Figure 7.15: E-plane coupling results for patch antenna geometry given in Fig. 7.5

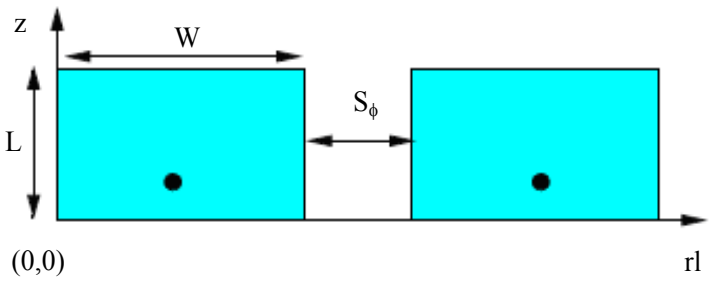

Figure 7.16: H-plane coupling geometry

Similar to the E-plane coupling case, Fig. 7.16 illustrates the geometry used for the mutual coupling calculations between two identical antennas along the H-plane. The H-plane coupling results are shown in Fig. 7.17-7.19 for the same patch antenna parameters given for the E-plane coupling calculations. In all the CFGF results related with the H-plane coupling, the conducting patch for each antenna is divided into 8 subdomains along the $z-$ and $\phi-$ directions ($P = 56$, $K = 56$, $N = 112$) and a $z-$ directed attachment mode ($z_{att} = z_a$ and $l_{att} = l_a$) is used. In the first two H-plane coupling results shown in Fig. 7.17 and Fig. 7.18, the CFGF results are compared with the CST Microwave Studio results where for the last example measurement results are compared to both CFGF and CST Microwave Studio results as shown in Fig. 7.19. In all these results, excellent agreement is achieved.

Note that in all mutual coupling results, the mutual coupling along the H-plane is stronger than that of the E-plane for small separations but it decreases faster than the E-plane coupling as the separation increases. Hence, the H-plane coupling is weaker than the E-plane coupling for large separations. The main reason is that along the H-plane the main coupling mechanism is the space waves. However, space waves reduce by $1/s$ (s: separation) for the fields. The surface waves are very weak along this plane due to the TM_{01} excitation of the antennas. On the other hand, the main coupling mechanism along the E-plane is the surface waves (space wave coupling is very weak). Because surface waves decay with $1/\sqrt{s}$, the decay of the mutual coupling along the E-plane is slower.

Finally, regarding the efficiency of the developed hybrid MoM/CFGF code, in

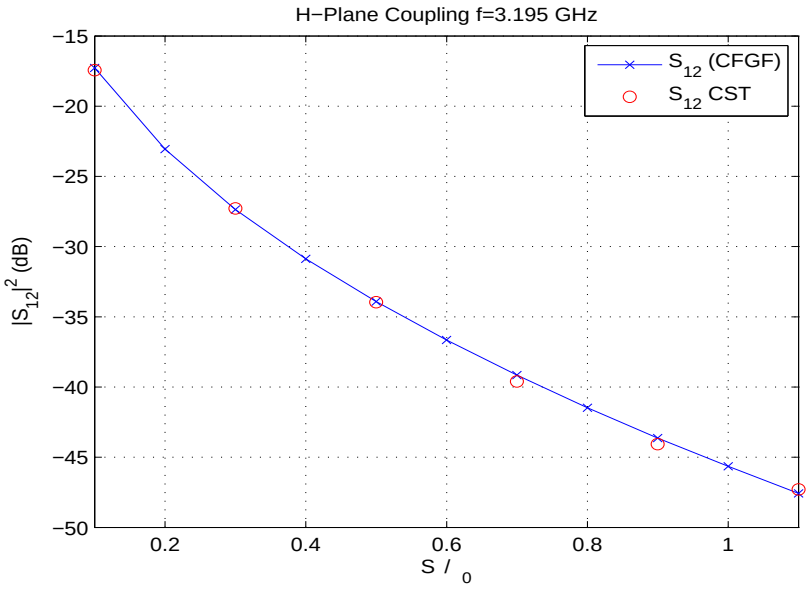

Figure 7.17: H-plane coupling results for patch antenna geometry given in Fig. 7.2 with (z_f,rl_f)=(0.95 cm,2 cm)

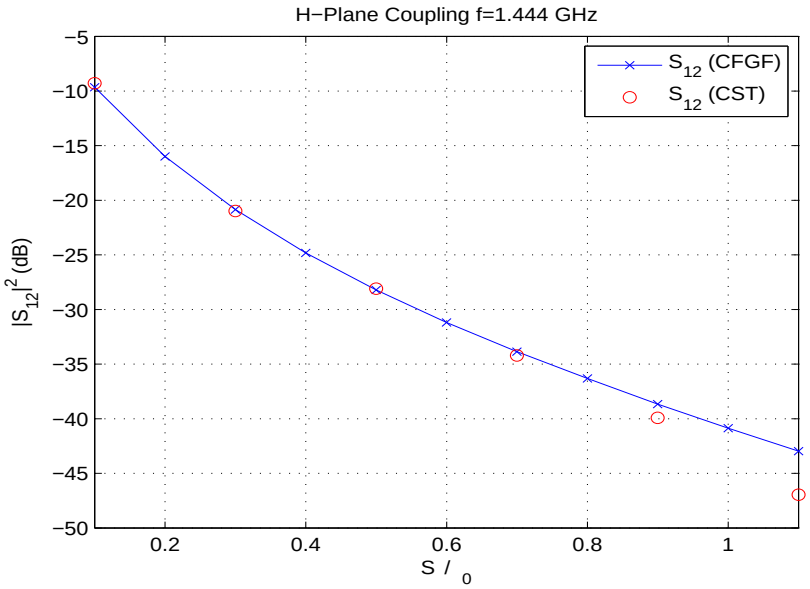

Figure 7.18: H-plane coupling results for patch antenna geometry given in Fig. 7.4

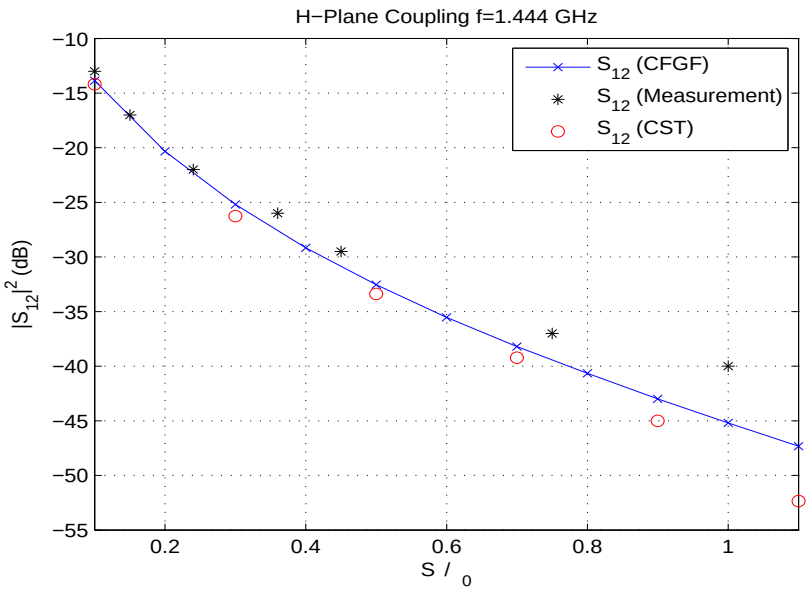

Figure 7.19: H-plane coupling results for patch antenna geometry given in Fig. 7.5

the course of obtaining the input impedance and mutual coupling results (using CFGF) given in this chapter, Matlab codes are written and executed on a standard desktop personal computer (PC). The CPU time for the evaluation of CFGF and the solution of the MoM formulation is in the order of minutes. On the other hand, most of the simulation time is to obtain the mutual impedance terms which include two-fold or four-fold integrals. Besides, the simulations done with CST Microwave Studio are repeated by increasing the number of mesh cells until the input impedance and mutual coupling results converge. The converged number of mesh cells used in the CST Microwave Studio is in the order of tens of millions and hence, special computers (work stations) with multi cores and RAM values in the order of 10 GB, are used to handle the increased workload. Since the Matlab codes for CFGF and the simulations on CST Microwave Studio are run on different computers with different number of cores, it is not easy to compare the CPU time of both procedures. But, although the Matlab codes are not fully optimized in terms of CPU time and executed on a standard desktop PC, the CPU time of both procedures is very near to each other.

Chapter 8

Conclusions

Novel CFGF representations, which constitute the kernel of an EFIE for cylindrically stratified media, are developed. The developed CFGF representations are used in an efficient and accurate hybrid MoM/Green's function method in the space domain for the analysis of antennas and arrays in the cylindrically stratified media. The analysis and design of the microstrip antennas mounted on aircraft, spacecraft and mobile communication applications can be made using the proposed hybrid MoM/Green's function method in this dissertation.

The accuracy and efficiency of the hybrid method strongly depend on the computation of the novel Green's function representations which are the kernel of the integral equation solved via MoM for the unknown equivalent currents induced on the microstrip patch antennas. In the course of obtaining the novel CFGF representations in the space domain, first the conventional spectral domain Green's function representations used for the radiation/scattering problems [18], are written in such a form that all the Hankel (or Bessel) functions are in the form of ratio with another Hankel (or Bessel) function. Then, the Debye representations are defined for the ratio terms using the Debye expressions of Hankel (or Bessel) functions available in the literature. Since when $\rho = \rho'$, the summation over the cylindrical eigenmodes is slowly convergent in the spectral domain, in the evaluation of the summation for large n values the Debye representations are used when necessary. Therefore, possible overflow or underflow

problems in the evaluation of the summation are handled in the spectral domain. As the second step, in order to accelerate the summation an envelope extraction with respect to n is applied using the series expansion of the zeroth-order Hankel function. Similarly, using the properties of the zeroth-order Hankel function, an envelope extraction with respect to k_z is applied in order to have a fast decaying spectral expression. After the envelope extractions (with respect to n and k_z), the spectral domain Green's function representation is obtained in the most accurate and efficient form with a fast convergent summation and a fast decaying spectral behaviour. The space domain Green's function representations are obtained in closed-form as a sum of the complex images using DCIM after the spectral domain counterparts are approximated as complex exponentials of k_z using GPOF. In order to increase the accuracy for $\rho = \rho'$ case, a new integration path is defined in the implementation of GPOF in this dissertation. The CFGF representations given in this dissertation are valid and accurate for all possible ρ and ρ' values. The CFGF representations obtained in this dissertation for the probe-related components are presented for the first time in the open literature.

In order to use CFGF representations in the mutual impedance calculations for the MoM procedure, the derivatives on the CFGF representations with respect to z, z', ϕ and ϕ' are treated separately and they are transferred onto the current modes in the mutual impedance calculations. By this way, the mutual impedance calculations become less singular. In the evaluation of the mutual impedance, there are two singularities. The first singularity is due to the argument of the zeroth-order Hankel function in the spectral domain and it is solved by analytical treatment using the small argument approximation of the Hankel function. Similarly the second singularity, which occurs in the space domain when the source and observation points are on top of each other, is again solved analytically.

To increase the accuracy of the MoM analysis of the antennas, probe-fed excitations are modeled by implementing an attachment mode that is consistent with the PWS current modes that are used as the expansion functions. The attachment mode is defined carefully in order to increase the accuracy of the proposed hybrid method. Numerical results in the form of input impedance of

various microstrip antennas as well as mutual coupling between two microstrip antennas are presented by comparing the results obtained using these novel CFGF representations with the available results in the literature as well as the results obtained from the CST Microwave Studio. Excellent agreement achieved which assures the accuracy of the developed CFGF representations. As a result, the developed CFGF representations can safely be used in the MoM-based analysis of microstrip antennas/arrays and printed circuits on multilayered cylindrical structures.

As the next step, the hybrid MoM/Green's function method can be optimised in terms of the CPU time. Besides, the CFGF representations can be obtained for the magnetic sources and then the analysis of aperture coupled patch antennas where a slot is present can be possible for cylindrically stratified media.

Appendix A

Debye Approximations

In order to calculate the Green's function representations without any overflow or underflow problems, the Green's function representations are written in the form of ratios. The ratios obtained at the final expressions are $\frac{J_n'(z_1)}{J_n(z_2)}$, $\frac{H_n^{'(2)}(z_1)}{H_n^{(2)}(z_2)}$ and $\frac{H_n^{(2)}(z_1)}{H_n^{(2)}(z_2)}\frac{J_n(z_2)}{J_n(z_1)}$. Also the multiplication terms $H_n^{(2)}(z_1)J_n(z_2)$ and $H_n^{(2)}(z_1)J_n'(z_2)$ exist in the Green's function representations and these terms are also treated as the ratio terms. Making use of the Debye representation of each cylindrical function and its derivative [34], the Debye expressions for the following terms are derived:

The first ratio term is $\frac{J_n'(z_1)}{J_n(z_2)}$ and the following debye expression is defined

$$\frac{J_n'(z_1)}{J_n(z_2)} \approx \frac{e^{(s_1-s_2)}}{z_1}(n^2-z_1^2)^{0.25}(n^2-z_2^2)^{0.25}\frac{1-\frac{9}{24\sqrt{n^2-z_1^2}}+\frac{7n^2}{24(\sqrt{n^2-z_1^2})^3}}{1+\frac{3}{24\sqrt{n^2-z_1^2}}-\frac{5n^2}{24(\sqrt{n^2-z_1^2})^3}} \tag{A.1}$$

where

$$s_1 = \sqrt{n^2-z_1^2} - |n|\cosh^{-1}(\frac{|n|}{z_1}) \tag{A.2}$$

and

$$s_2 = \sqrt{n^2-z_2^2} - |n|\cosh^{-1}(\frac{|n|}{z_2}). \tag{A.3}$$

The following debye expression is used for the second ratio term which is

$\frac{H_n^{'(2)}(z_1)}{H_n^{(2)}(z_2)}$,

$$\frac{H_n^{'(2)}(z_1)}{H_n^{(2)}(z_2)} \approx -\frac{e^{(s_2-s_1)}}{z_1}(n^2-z_1^2)^{0.25}(n^2-z_2^2)^{0.25}\frac{1+\frac{3}{24\sqrt{n^2-z_1^2}}-\frac{5n^2}{24(\sqrt{n^2-z_1^2})^3})}{1-\frac{9}{24\sqrt{n^2-z_1^2}}+\frac{7n^2}{24(\sqrt{n^2-z_1^2})^3}}. \quad \text{(A.4)}$$

Finally, for the last ratio term $(\frac{H_n^{(2)}(z_1)}{H_n^{(2)}(z_2)}\frac{J_n(z_2)}{J_n(z_1)})$, the following debye expression is defined as

$$\frac{H_n^{(2)}(z_1)}{H_n^{(2)}(z_2)}\frac{J_n(z_2)}{J_n(z_1)} \approx e^{2(s_2-s_1)}. \quad \text{(A.5)}$$

Using debye approximations, the first multiplication term $H_n^{(2)}(z_1)J_n(z_2)$ can be computed as

$$H_n^{(2)}(z_1)J_n(z_2) \approx \frac{j}{\pi}\frac{1}{(n^2-z_1^2)^{0.25}}\frac{1}{(n^2-z_2^2)^{0.25}}e^{(s_2-s_1)}. \quad \text{(A.6)}$$

The other multiplication term $H_n^{(2)}(z_1)J_n'(z_2)$ is written as

$$H_n^{(2)}(z_1)J_n'(z_2) \approx \frac{j}{\pi z_2}\frac{(n^2-z_2^2)^{0.25}}{(n^2-z_1^2)^{0.25}}e^{(s_2-s_1)}. \quad \text{(A.7)}$$

Appendix B

Generalized Pencil of Function (GPOF) Method

The generalized pencil of function method is used to approximate the spectral domain Green's function representations with complex exponentials. Since this method is an important step in approximating the Green's function representations, it is explained in detail in this appendix.

Similar to the Prony method and its variants [35]-[36], the pencil of function (POF) method [37] can be used to extract the poles of an electromagnetics (EM) system, where the poles are found from the solution of a generalized eigenvalue problem. On the other hand, the generalized pencil of function method is a generalization to the POF method and it is used to estimate the poles of an EM system from its transient response [32]. The GPOF method is more robust and less noise sensitive, compared to the Prony method.

An EM transient signal with N samples y_k , can be approximated in terms of complex exponentials as,

$$y_k = \sum_{i=1}^{M} b_i e^{s_i \delta t k} = \sum_{i=1}^{M} b_i z_i^k \qquad k = 0, 1, ..., N-1 \tag{B.1}$$

where b_i are the complex residues, s_i are the complex poles, and δt is the sampling interval. The method can be briefly explained as follows:

1. The following matrices are constructed,

$$\underline{\underline{Y_1}} = \left[\begin{array}{c} \underline{y}_0, \underline{y}_1, ..., \underline{y}_{L-1} \end{array} \right] \tag{B.2}$$

$$\underline{\underline{Y_2}} = \left[\begin{array}{c} \underline{y}_1, \underline{y}_2, ..., \underline{y}_L \end{array} \right] \tag{B.3}$$

where

$$\underline{y}_i = \left[\begin{array}{c} y_i, y_{i+1}, ..., y_{i+N-L-1} \end{array} \right]^T \tag{B.4}$$

and L is the pencil parameter, and its optimal choice is around $L = N/2$ [32].

2. Find a $\underline{\underline{Z}}$ matrix (after applying the singular value decomposition (SVD) to $\underline{\underline{Y}}_1$),

$$SVD(\underline{\underline{Y}}_1) = \underline{\underline{U}}\,\underline{\underline{S}}\,\underline{\underline{V}}^H \tag{B.5}$$

where $\underline{\underline{U}}$, $\underline{\underline{S}}$ and $\underline{\underline{V}}^H$ are $(N-L)\times(N-L)$, $(N-L)\times L$ and $L\times L$ matrices, respectively. The superscript H denotes the complex conjugate transpose of a matrix. Note that in this study the optimal choice of L is chosen, which is $L = N/2$. As a result of this choice $\underline{\underline{S}}$ is now a diagonal matrix. Let $\underline{\underline{S}}_t$ be the $M\times M$ matrix (M is determined from the number of complex exponentials and $M \leq L$) which includes the largest diagonal terms of $\underline{\underline{S}}$ in the decaying order. Then, taking the corresponding rows and columns of $\underline{\underline{U}}$ and $\underline{\underline{V}}$, two new matrices $\underline{\underline{U}}_t$ and $\underline{\underline{V}}_t$, respectively, are formed both of which are $L\times M$ matrices. Using $\underline{\underline{U}}_t$ and $\underline{\underline{V}}_t$ together with $\underline{\underline{S}}_t$, $\underline{\underline{Y}}_1$ is written as

$$\underline{\underline{Y}}_1 = \underline{\underline{U}}_t \underline{\underline{S}}_t \underline{\underline{V}}_t^H. \tag{B.6}$$

Finally, the $\underline{\underline{Z}}$ matrix is defined as

$$\underline{\underline{Z}} = \underline{\underline{S}}_t^{-1} \underline{\underline{U}}_t^H \underline{\underline{Y}}_2 \underline{\underline{V}}_t. \tag{B.7}$$

3. The poles of the system are obtained as

$$s_i = \frac{\log z_i}{\delta t} \qquad i = 1, 2, \cdots, M \tag{B.8}$$

where z_i's are the eigenvalues of the $\underline{\underline{Z}}$ matrix.

4. The residues are found from the least-squares solution of the following system.

$$\begin{bmatrix} 1 & 1 & \cdots & 1 \\ z_1 & z_2 & \cdots & z_M \\ \cdot & \cdot & \cdots & \cdot \\ \cdot & \cdot & \cdots & \cdot \\ \cdot & \cdot & \cdots & \cdot \\ z_1^{N-1} & z_2^{N-1} & \cdots & z_M^{N-1} \end{bmatrix} \begin{bmatrix} b_1 \\ b_2 \\ \cdot \\ \cdot \\ \cdot \\ b_M \end{bmatrix} = \begin{bmatrix} y_0 \\ y_1 \\ \cdot \\ \cdot \\ \cdot \\ y_{N-1} \end{bmatrix} \tag{B.9}$$

that can be expressed as

$$\underline{\underline{A}}\ \underline{b} = \underline{y} \tag{B.10}$$

so the b_i's are found by using the pseudo-inverse of $\underline{\underline{A}}$ as $\underline{b} = \underline{\underline{A}}^{+}\underline{y}$.

Appendix C

Mutual Impedance Calculations (zz case)

C.1 General Procedure For Mutual Impedance Calculations

The mutual impedance expression between two $z-$ directed current modes is written as [see (5.8)],

$$Z_{12zz} = \int\int\int\int J_z J_{z'} G_{zz} dz dz' d\beta d\beta' \tag{C.1}$$

where $\beta = \rho\phi$, $\beta' = \rho'\phi'$, $d\beta = \rho d\phi$ and $d\beta' = \rho' d\phi'$. Because the $k_{\rho_j}^2$ term in the spectral domain corresponds to $(k_j^2 - \frac{\partial^2}{\partial z \partial z'})$ in the space domain, the expression for the Green's function representation for G_{zz} can be expressed as

$$G_{zz} \;\; = \;\; (k_j^2 - \frac{\partial^2}{\partial z \partial z'}) G_{zz2}. \tag{C.2}$$

Performing an integration by parts twice on (C.2) (also note that the current modes are differentiable and zero at the end points), (C.1) becomes

$$Z_{12zz} = \int\int\int\int \Big(k_0^2 J_z J_{z'} G_{zz2} - \frac{\partial J_z}{\partial z} \frac{\partial J_{z'}}{\partial z'} G_{zz2} \Big) dz dz' d\beta d\beta'. \tag{C.3}$$

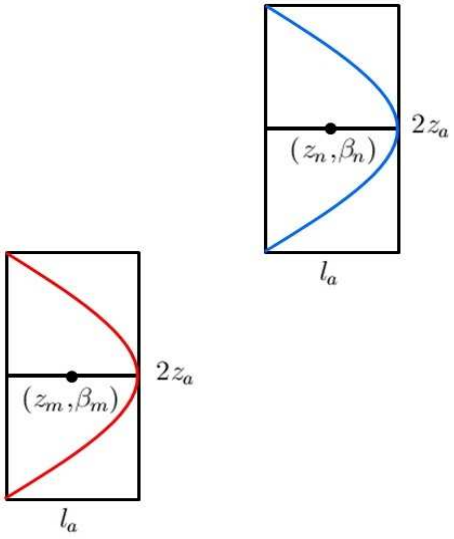

Figure C.1: PWS current modes in the $z-$ direction

The numerical evaluation of the four-fold integral given in (C.3) is a time consuming calculation especially for the problematic cases when there is a space domain singularity (i.e., source and observation points are on top of each other. This situation corresponds to current modes being on the top of each other, self-term in MoM, or partially overlapping with each other, overlapping terms in MoM).

The evaluation of the four-fold mutual impedance integrals are performed in a similar way as explained in [38]. The starting point of this evaluation process is (C.1). When there is no **singularity** in (C.1), the goal is to reduce this four-fold integral into a two-fold integral as explained in [38]. Briefly, the mutual impedance expression between two $z-$ directed current modes (with dimensions $2z_a \mathrm{x} l_a$) centered at the points (z_m,β_m) and (z_n,β_n) (as illustrated in Fig. C.1) can be rewritten from (C.1) as

$$Z_{12zz} = \int_{\beta_m-l_a/2}^{\beta_m+l_a/2}\int_{\beta_n-l_a/2}^{\beta_n+l_a/2}\int_{z_m-z_a}^{z_m+z_a}\int_{z_n-z_a}^{z_n+z_a} G_{zz}\frac{\sin(k_a(z_a-|z-z_n|))}{l_a\sin(k_a z_a)} \frac{\sin(k_a(z_a-|z'-z_m|))}{l_a\sin(k_a z_a)} dz dz' d\beta d\beta'. \quad \text{(C.4)}$$

As the first step the $\beta - \beta'$ domain is mapped to the $\tau - \psi$ domain by applying the following change of variables :

$$\tau = \frac{1}{\sqrt{2}}(\beta' - \beta) \tag{C.5}$$

$$\psi = \frac{1}{\sqrt{2}}(\beta' + \beta) \tag{C.6}$$

$$d\beta' d\beta = d\tau d\psi \tag{C.7}$$

where the details are given in [38].

As a result of this step, the new integral variables are supposed to be τ and ψ. However, noticing that ψ does not occur in the integrand, the ψ integral turns out to be the end point contributions which are functions of only τ. Therefore, the resultant three-fold integral is given by

$$\begin{aligned} Z_{12zz} &= \int_{\tau_0}^{\tau_2} T_{zz}(\tau) \int_{z_m - z_a}^{z_m + z_a} \int_{z_n - z_a}^{z_n + z_a} G_{zz} \frac{\sin(k_a(z_a - |z - z_n|))}{l_a \sin(k_a z_a)} \\ &\quad \frac{\sin(k_a(z_a - |z' - z_m|))}{l_a \sin(k_a z_a)} dz dz' d\tau \end{aligned} \tag{C.8}$$

where

$$T_{zz}(\tau) = \begin{cases} -2\tau + (l_a + \beta_s)\sqrt{2} & \tau_1 \leq \tau < \tau_2 \\ 2\tau + (l_a - \beta_s)\sqrt{2} & \tau_0 \leq \tau < \tau_1 \end{cases} \tag{C.9}$$

with

$$\tau_0 = \frac{\beta_s - l_a}{\sqrt{2}} \tag{C.10}$$

$$\tau_1 = \frac{\beta_s}{\sqrt{2}} \tag{C.11}$$

$$\tau_2 = \frac{\beta_s + l_a}{\sqrt{2}} \tag{C.12}$$

and $\beta_s = \beta_m - \beta_n$.

As the next step, after transferring the space derivatives in (C.2) onto the basis and testing current modes [see (C.3)], the $z - z'$ domain is mapped to the $u - v$ domain in similar way (see [38] for details) by using the following change

of variables :

$$v = \frac{1}{\sqrt{2}}(z' - z) \tag{C.13}$$

$$u = \frac{1}{\sqrt{2}}(z' + z) \tag{C.14}$$

$$dz'dz = dvdu. \tag{C.15}$$

As a result of this step, the new integral variables are u and v but similar to $\tau - \psi$ case, u does not occur in the integrand. Consequently, the final two-fold mutual impedance expression for the zz case is written as

$$Z_{12zz} = (\frac{1}{l_a \sin(k_a z_a)})^2 \int_{\tau_0}^{\tau_2} T_{zz}(\tau)\{I_{v1} + I_{v2} + I_{v3}\}d\tau \tag{C.16}$$

where I_{v1}, I_{v2} and I_{v3} are defined as

$$I_{v1} = 2\int_{v_1}^{v_3} \Big\{ \cos[k_a(z_s - v\sqrt{2})]V_1^{zz}(v)(k_0^2 - k_a^2)G_{zz2} + V_2^{zz}(v)(k_0^2 + k_a^2)G_{zz2} \Big\} dv \tag{C.17}$$

$$I_{v2} = \int_{v_2}^{v_4} \Big\{ \cos[k_a(2z_a + z_s - v\sqrt{2})]V_3^{zz}(v)(k_0^2 - k_a^2)G_{zz2} + V_4^{zz}(v)(k_0^2 + k_a^2)G_{zz2} \Big\} dv \tag{C.18}$$

$$I_{v3} = \int_{v_0}^{v_2} \Big\{ \cos[k_a(2z_a - z_s + v\sqrt{2})]V_5^{zz}(v)(k_0^2 - k_a^2)G_{zz2} + V_6^{zz}(v)(k_0^2 + k_a^2)G_{zz2} \Big\} dv \tag{C.19}$$

with

$$V_1^{zz}(v) = \begin{cases} v - \frac{z_s - z_a}{\sqrt{2}} & v_1 < v < v_2 \\ -v + \frac{z_s + z_a}{\sqrt{2}} & v_2 < v < v_3 \end{cases} \tag{C.20}$$

$$V_2^{zz}(v) = \begin{cases} \frac{\cos(k_a z_a)}{k_a\sqrt{2}} \sin[k_a(-v\sqrt{2} - z_a + z_s)] & v_1 < v < v_2 \\ \frac{\cos(k_a z_a)}{k_a\sqrt{2}} \sin[k_a(v\sqrt{2} - z_a - z_s)] & v_2 < v < v_3 \end{cases} \tag{C.21}$$

$$V_3^{zz}(v) = \begin{cases} \frac{z_s - v\sqrt{2}}{\sqrt{2}} & v_2 < v < v_3 \\ \frac{-2z_a - z_s + v\sqrt{2}}{\sqrt{2}} & v_3 < v < v_4 \end{cases} \tag{C.22}$$

$$V_4^{zz}(v) = \begin{cases} -\frac{\sin\left[k_a(z_s - v\sqrt{2})\right]}{k_a\sqrt{2}} & v_2 < v < v_3 \\ \frac{\sin\left[k_a(2z_a + z_s - v\sqrt{2})\right]}{k_a\sqrt{2}} & v_3 < v < v_4 \end{cases} \tag{C.23}$$

$$V_5^{zz}(v) = \begin{cases} \frac{-2z_a + z_s - v\sqrt{2}}{\sqrt{2}} & v_0 < v < v_1 \\ \frac{-z_s + v\sqrt{2}}{\sqrt{2}} & v_1 < v < v_2 \end{cases} \tag{C.24}$$

$$V_6^{zz}(v) = \begin{cases} \frac{\sin\left[k_a(2z_a - z_s + v\sqrt{2})\right]}{k_a\sqrt{2}} & v_0 < v < v_1 \\ \frac{\sin\left[k_a(z_s - v\sqrt{2})\right]}{k_a\sqrt{2}} & v_1 < v < v_2 \end{cases} \tag{C.25}$$

and

$$v_0 = \frac{z_s - 2z_a}{\sqrt{2}} \tag{C.26}$$

$$v_1 = \frac{z_s - z_a}{\sqrt{2}} \tag{C.27}$$

$$v_2 = \frac{z_s}{\sqrt{2}} \tag{C.28}$$

$$v_3 = \frac{z_s + z_a}{\sqrt{2}} \tag{C.29}$$

$$v_4 = \frac{z_s + 2z_a}{\sqrt{2}}. \tag{C.30}$$

Finally $z_s = z_m - z_n$.

C.2 Overlapping Term

In the space domain MoM analysis of microstrip antennas/arrays, singularity occurs when the two PWS current modes partially overlap with each other. The problematic mutual impedance expression, when two $z-$ directed current modes partially overlap with each other (overlapping term), is the last term of (5.23) which can be written as

$$Z_{12zz} = \int_{-l_a/2}^{l_a/2}\int_{-l_a/2}^{l_a/2}\int_{0}^{2z_a}\int_{-z_a}^{z_a} \frac{1}{s}\Big(k_0^2 J_z J_{z'} - \frac{\partial J_z}{\partial z}\frac{\partial J'_z}{\partial z'}\Big) dz dz' d\beta d\beta' \tag{C.31}$$

where

$$\frac{1}{s} = \frac{1}{\sqrt{(\beta-\beta')^2+(z-z')^2}}. \tag{C.32}$$

Note that the constant $[-\frac{j}{4\pi\omega\epsilon_j}C_{uv}(k_{z\infty})]$ is not included. Furthermore, (C.31) is obtained after performing an integration by parts twice. Performing the change of variables defined in (C.5)-(C.6) and evaluating the ψ and τ integrals analytically (see [38] for the details of analytical integration of $\tau-$ integral), the Z_{12zz} is given by

$$\begin{aligned} Z_{12zz} \;=\; & \int_0^{2z_a}\int_{-z_a}^{z_a}\left(t_3\cos\Big[k_a(2z_a-|z'-z_a|-|z|)\Big]+t_4\cos\Big[k_a(|z'-z_a|-|z|)\Big]\right) \\ & \left(2l_a\left[\log(\frac{l_a}{\sqrt{2}}+\sqrt{(\frac{z'-z}{\sqrt{2}})^2+\frac{l_a^2}{2}})-\log\Big|\frac{z'-z}{\sqrt{2}}\Big|\right]\right. \\ & \left.-2\sqrt{2}\left[\sqrt{\Big(\frac{z'-z}{\sqrt{2}}\Big)^2+\frac{l_a^2}{2}}-\Big|\frac{z'-z}{\sqrt{2}}\Big|\right]\right)dzdz' \end{aligned} \tag{C.33}$$

where

$$t_3 = K\Big[-\frac{k_0^2}{2}-\frac{k_a^2}{2}\text{sign}(z)\text{sign}(z'-z_a)\Big], \tag{C.34}$$

$$t_4 = K\Big[\frac{k_0^2}{2}-\frac{k_a^2}{2}\text{sign}(z)\text{sign}(z'-z_a)\Big] \tag{C.35}$$

and

$$K = \frac{1}{\Big[l_a\sin(k_a z_a)\Big]^2}. \tag{C.36}$$

Then, performing the change of variables defined in (C.13)-(C.14), the two dimensional integral with respect to z and z' can be written as a one dimensional integral as the integration with respect to u is evaluated analytically. Finally, for the resultant $v-$ domain integral, we perform a final change of variable given by

$$\alpha = \frac{v}{z_a\sqrt{2}} \tag{C.37}$$

$$d\alpha = \frac{dv}{z_a\sqrt{2}}, \tag{C.38}$$

so that the integration interval can be normalized to (0, 1.5). After arranging and regrouping the resultant terms, the final integral expression is obtained as

$$\begin{aligned} Z_{12zz} &= \int_0^{0.5} \Bigg\{ t_5 \sin(2k_a z_a \alpha) + t_6(1-2\alpha)\cos(2k_a z_a \alpha) \\ &\quad + t_7 \alpha \cos\Big[k_a z_a (1-2\alpha)\Big] + t_8 \sin\Big[k_a z_a (1-2\alpha)\Big] \Bigg\} H^r(\alpha) d\alpha \\ &\quad \int_{0.5}^{1} \Bigg\{ t_5 \sin\Big[2k_a z_a (1-\alpha)\Big] - t_9(1-2\alpha)\cos\Big[k_a z_a (3-2\alpha)\Big] \\ &\quad + t_7(1-\alpha)\cos\Big[k_a z_a (1-2\alpha)\Big] - t_{10}\sin\Big[k_a z_a (1-2\alpha)\Big] \Bigg\} H(\alpha) d\alpha \\ &\quad \int_{1}^{1.5} \Bigg\{ t_9(3-2\alpha)\cos\Big[k_a z_a (3-2\alpha)\Big] + t_{10}\sin\Big[k_a z_a (3-2\alpha)\Big] \Bigg\} H(\alpha) d\alpha \\ &\quad + I_{p1} \end{aligned} \tag{C.39}$$

where

$$H^r(\alpha) = \frac{l_a}{\sqrt{2}}\Big[\log\Big(\frac{l_a}{2} + \sqrt{z_a^2\alpha^2 + \frac{l_a^2}{2}}\Big) - \log(z_a)\Big] - \sqrt{2}\Big[\sqrt{z_a^2\alpha^2 + \frac{l_a^2}{2}} - z_a\alpha\Big] \tag{C.40}$$

and

$$H(\alpha) = \frac{l_a}{\sqrt{2}}\Big[\log\Big(\frac{l_a}{2} + \sqrt{z_a^2\alpha^2 + \frac{l_a^2}{2}}\Big) - \log(z_a\alpha)\Big] - \sqrt{2}\Big[\sqrt{z_a^2\alpha^2 + \frac{l_a^2}{2}} - z_a\alpha\Big]. \tag{C.41}$$

I_{p1} is defined as

$$\begin{aligned} I_{p1} &= -\frac{l_a}{\sqrt{2}}\Bigg\{\kappa_1\Big[\delta_1\log(\delta_1) - \delta_1\Big] + \kappa_2\Big[\frac{\delta_1^2}{2}\log(\delta_1) - \frac{\delta_1^2}{4}\Big] + \kappa_3\Big[\frac{\delta_1^3}{3}\log(\delta_1) - \frac{\delta_1^3}{9}\Big]\Bigg\} \\ &\quad -\frac{l_a}{\sqrt{2}}\int_{\delta_1}^{0.5} \Bigg\{ t_5 \sin(2k_a z_a \alpha) + t_6(1-2\alpha)\cos(2k_a z_a \alpha) \\ &\quad + t_7 \alpha \cos\Big[k_a z_a (1-2\alpha)\Big] + t_8 \sin\Big[k_a z_a (1-2\alpha)\Big] \Bigg\} \log(\alpha) d\alpha \end{aligned} \tag{C.42}$$

and δ_1 is a small number which is chosen as $(2k_a z_a \delta_1) << 1$. The other parameters are defined as

$$\kappa_1 = t_6 + t_8 \sin(k_a z_a) \tag{C.43}$$

$$\kappa_2 = 2t_5 k_a z_a - 2t_6 + t_7 \cos(k_a z_a) - 2t_8 k_a z_a \cos(k_a z_a) \tag{C.44}$$

$$\kappa_3 = 2t_7 k_a z_a \sin(k_a z_a) \tag{C.45}$$

$$t_5 = \frac{8\sqrt{2} z_a}{k_a} \cos(k_a z_a) t_{3+} \tag{C.46}$$

$$t_6 = 8\sqrt{2} z_a^2 \cos(k_a z_a) t_{3-} \tag{C.47}$$

$$t_7 = 16\sqrt{2} z_a^2 t_{4+} \tag{C.48}$$

$$t_8 = \frac{8\sqrt{2} z_a}{k_a} t_{4-} \tag{C.49}$$

$$t_9 = 4\sqrt{2} z_a^2 t_{3-} \tag{C.50}$$

$$t_{10} = \frac{4\sqrt{2} z_a}{k_a} t_{4-}. \tag{C.51}$$

In this expressions, t_{3+} and t_{4+} mean that $\text{sign}(z)\text{sign}(z' - z_a)$ is positive where t_{3-} and t_{4-} mean that $\text{sign}(z)\text{sign}(z' - z_a)$ is negative. The integral given by (C.39) can be computed numerically in a very easy way using a simple Gaussian quadrature integration scheme. Finally, it should be mentioned that all the details of this section (for its planar counterpart) can be found in [38].

C.3 Self Term

In the space domain MoM analysis of microstrip antennas/arrays, singularity exists for the self term case which occurs when two PWS current modes are on top of each other. Similar to the overlapping term explained in the previous section (C.2), the singular part of the self impedance, Z_{12zz}, integral can be written as

$$Z_{12zz} = \int_{-l_a/2}^{l_a/2} \int_{-l_a/2}^{l_a/2} \int_{-z_a}^{z_a} \int_{-z_a}^{z_a} \frac{1}{s} \Big(k_0^2 J_z J_{z'} - \frac{\partial J_z}{\partial z} \frac{\partial J'_z}{\partial z'} \Big) dz dz' d\beta d\beta'. \tag{C.52}$$

Notice that the expression is the same as (C.31)-(C.32) except the integration limits in the $z - z'$ domain. Performing the change of variable defined in (C.5)-(C.6) and evaluating the τ and ψ integrals in closed-form as explained in [38],

Z_{12zz} is given by

$$\begin{aligned} Z_{12zz} &= \int_{-z_a}^{z_a}\int_{-z_a}^{z_a}\Bigg\{c_1\cos\Big[k_a(2z_a-|z'|-|z|)\Big]+c_2\cos\Big[k_a(|z'|-|z|)\Big]\Bigg\} \\ &\quad \Bigg(2l_a\Bigg[\log\Big(\frac{l_a}{\sqrt{2}}+\sqrt{\Big(\frac{z'-z}{\sqrt{2}}\Big)^2+\frac{l_a^2}{2}}\Big)-\log\Big|\frac{z'-z}{\sqrt{2}}\Big|\Bigg] \\ &\quad -2\sqrt{2}\Bigg[\sqrt{\Big(\frac{z'-z}{\sqrt{2}}\Big)^2+\frac{l_a^2}{2}}-\Big|\frac{z'-z}{\sqrt{2}}\Big|\Bigg]\Bigg)dzdz' \end{aligned} \tag{C.53}$$

where

$$c_1 = K\Big[-\frac{k_0^2}{2}-\frac{k_a^2}{2}\text{sign}(z)\text{sign}(z')\Big], \tag{C.54}$$

$$c_2 = K\Big[\frac{k_0^2}{2}-\frac{k_a^2}{2}\text{sign}(z)\text{sign}(z')\Big], \tag{C.55}$$

and K is defined in (C.36). Then, first (C.13)-(C.14) are applied to move from $z-z'$ domain to $u-v$ domain, then the $u-$ domain integration is performed analytically and finally performing the change of variables given by (C.37)-(C.38) for the $v-$ domain integration, the final Z_{12zz} expression is given by

$$\begin{aligned} Z_{12zz} &= \int_0^{0.5}\Bigg\{c_3\sin\Big[k_a z_a(1-2\alpha)\Big]+c_4\alpha\cos\Big[k_a 2z_a(1-\alpha)\Big] \\ &\quad +c_5(1-2\alpha)\cos(2k_a z_a\alpha)+c_6\sin(2k_a z_a\alpha)\Bigg\}H^r(\alpha)d\alpha \\ &\quad \int_{0.5}^1\Bigg\{c_4(1-\alpha)\cos\Big[2k_a z_a(1-\alpha)\Big]+c_6\sin\Big[2k_a z_a(1-\alpha)\Big]\Bigg\}H(\alpha)d\alpha \\ &\quad +I_{p2} \end{aligned} \tag{C.56}$$

where $H^r(\alpha)$, $H(\alpha)$ are given in (C.40) and (C.41). I_{p2} in (C.56) is defined as

$$\begin{aligned} I_{p2} &= -\frac{l_a}{\sqrt{2}}\Bigg\{d_1\Big[\delta_2\log(\delta_2)-\delta_2\Big]+d_2\Big[\frac{\delta_2^2}{2}\log(\delta_2)-\frac{\delta_2^2}{4}\Big]+d_3\Big[\frac{\delta_2^3}{3}\log(\delta_2)-\frac{\delta_2^3}{9}\Big]\Bigg\} \\ &\quad -\frac{l_a}{\sqrt{2}}\int_{\delta_2}^{0.5}\Bigg\{c_3\sin\Big[k_a z_a(1-2\alpha)\Big]+c_4\alpha\cos\Big[k_a 2z_a(1-\alpha)\Big] \\ &\quad +c_5(1-2\alpha)\cos(2k_a z_a\alpha)+c_6\sin(2k_a z_a\alpha)\Bigg\}\log(\alpha)d\alpha \end{aligned} \tag{C.57}$$

and δ_2 is a small number where $(2k_a z_a \delta_2) << 1$. The other parameters are given as

$$d_1 = c_3 \sin(k_a z_a) + c_5 \tag{C.58}$$

$$d_2 = -2c_3 k_a z_a \cos(k_a z_a) + c_4 \cos(2k_a z_a) - 2c_5 + 2c_6 k_a z_a \tag{C.59}$$

$$d_3 = 2c_4 k_a z_a \sin(2k_a z_a) \tag{C.60}$$

$$c_3 = \frac{z_a 16\sqrt{2}}{k_a} \cos(k_a z_a) c_{1+} \tag{C.61}$$

$$c_4 = z_a^2 16\sqrt{2} c_{1-} \tag{C.62}$$

$$c_5 = z_a^2 16\sqrt{2} c_{2+} \tag{C.63}$$

$$c_6 = \frac{z_a 8\sqrt{2}}{k_a} c_{2-}. \tag{C.64}$$

Similar to the overlapping case, c_{1+} and c_{2+} mean that $\text{sign}(z)\text{sign}(z')$ is positive and c_{2-} mean that $\text{sign}(z)\text{sign}(z')$ is negative. The integral given by (C.56) can be computed numerically using a simple Gaussian quadrature integration scheme. Similar to the overlapping case, all details of this section (for its planar counterpart) can be seen in [38].

C.4 Spectral Domain Singularity

Substituting (5.20) into (5.10) and performing the IFTs, the singular part of the mutual impedance expression due to the spectral domain singularity appears as

$$\begin{aligned} Z_{12zz} &= \int\int\int\int \Big(k_0^2 J_z J_{z'} C^{zz}(z,z') \log(|\beta - \beta'|) \\ &- \frac{\partial J_z}{\partial z} \frac{\partial J_{z'}}{\partial z'} C^{zz}(z,z') \log(|\beta - \beta'|) \Big) dz dz' d\beta d\beta' \end{aligned} \tag{C.65}$$

where $C^{zz}(z,z')$ is an expression which is a function of z and z' only. Therefore, the mutual impedance expression is rewritten as

$$Z_{12zz} = \int\int \Big(k_0^2 J_z J_{z'} C^{zz}(z,z') - \frac{\partial J_z}{\partial z} \frac{\partial J_{z'}}{\partial z'} C^{zz}(z,z') \Big) \int\int \log(|\beta - \beta'|) d\beta d\beta' dz dz'. \tag{C.66}$$

In the analytic evaluation of (C.66), the result of $\int \log(|\beta - \beta'|)d\beta$ which is given by

$$\int \log(|\beta - \beta'|)d\beta = \beta \log(|\beta' - \beta|) - \log(|\beta - \beta'|)\beta' - \beta \tag{C.67}$$

and the result of $\int\int \log(|\beta - \beta'|)d\beta d\beta'$ which is given by

$$\int\int \log(|\beta - \beta'|)d\beta d\beta' = -\frac{\beta'^2 \log(|\beta' - \beta|)}{2} + \beta\beta' \log(|\beta' - \beta|)$$
$$+\frac{\beta^2 \log(|\beta' - \beta|) + \frac{\beta'^2 + 2\beta\beta'}{2}}{2} - \beta(\beta \log(|\beta' - \beta|) + \beta') - \beta\beta' \tag{C.68}$$

are used. Using (C.68), the singular β and β' integrals in (C.66) are evaluated analytically. z and z' integrals in (C.66) are evaluated using the v integral [after it is applied to (C.66) as it is given in (C.16)] in order to reduce the integral to a one-fold integral. Note that in the evaluation of (C.65), when using the v integral (to evaluate z and z' integrals) as given in (C.16), the τ integral (C.16) is not considered since the β and β' integrals are already evaluated using (C.68).

Appendix D

Mutual Impedance Calculations ($z\phi = \phi z$ case)

D.1 General Procedure For Mutual Impedance Calculations

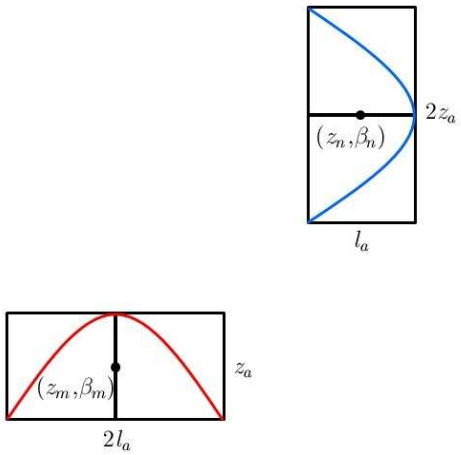

Figure D.1: Current modes in the $z-$ and $\phi-$ directions

Similar to the zz case, the mutual impedance expression between a $z-$ and a $\phi-$ directed current modes (shown in Fig. D.1) is written [see (5.8)] as

$$Z_{12z\phi} = \int\int\int\int J_z J_{\phi'} G_{z\phi} dz dz' d\beta d\beta'. \tag{D.1}$$

The $z\phi = \phi z$ components of the Green's function representation in the space domain can be written as follows:

$$G_{z\phi} = j\frac{\partial}{\partial z} j\frac{\partial}{\partial \phi'} G_{z\phi 2}. \tag{D.2}$$

Performing an integration by parts twice on (D.2) together with the PWS current modes, the mutual impedance expression is obtained as

$$Z_{12z\phi} = \int\int\int\int (-j)\frac{\partial J_z}{\partial z}(-j)\frac{\partial J_{\phi'}}{\partial \phi'} G_{z\phi 2} dz dz' d\beta d\beta'. \tag{D.3}$$

When there is no singularity, this four-fold mutual impedance integral is reduced to a two-fold integral as follows (the details for this part (for its planar counterpart) can be found in [38]): The mutual impedance expression between a $z-$ and a $\phi-$ directed current modes (with the size and location parameters as depicted in Fig. D.1) is rewritten from (D.1) as

$$\begin{aligned} Z_{12z\phi} &= \int_{\beta_m - l_a}^{\beta_m + l_a} \int_{\beta_n - l_a/2}^{\beta_n + l_a/2} \int_{z_m - z_a/2}^{z_m + z_a/2} \int_{z_n - z_a}^{z_n + z_a} G_{z\phi} \frac{\sin(k_a(z_a - |z - z_n|))}{l_a \sin(k_a z_a)} \\ &\quad \frac{\sin(k_a(l_a - |\beta' - \beta_m|))}{z_a \sin(k_a l_a)} dz dz' d\beta d\beta'. \end{aligned} \tag{D.4}$$

After transferring the spatial derivatives [see (D.2)] onto the basis and testing functions [see (D.3)], and following the same procedure given in Appendix C.1, the $z - z'$ domain is mapped to the $u - v$ domain given by (C.13)-(C.15) [38]. As a result of this step, the following three-fold integral expression is obtained:

$$\begin{aligned} Z_{12z\phi} &= [\frac{k_a}{\sqrt{2} z_a \sin(k_a l_a)}] \int_{\beta_m - l_a}^{\beta_m + l_a} \int_{\beta_n - l_a/2}^{\beta_n + l_a/2} \cos[k_a(l_a - |\beta' - \beta_m|)] \\ &\quad \text{sign}(\beta' - \beta_m) \{ \int_{v_0^{z\phi}}^{v_3^{z\phi}} V^{z\phi}(v) G_{z\phi 2} dv \} d\beta d\beta' \end{aligned} \tag{D.5}$$

where

$$V^{z\phi}(v) = \begin{cases} -\sin[k_a(1.5 z_a - z_s + v\sqrt{2})] & v_0^{z\phi} < v < v_1^{z\phi} \\ 2\cos(\frac{k_a z_a}{2}) \sin[k_a(v\sqrt{2} - z_s)] & v_1^{z\phi} < v < v_2^{z\phi} \\ \sin[k_a(1.5 z_a + z_s - v\sqrt{2})] & v_2^{z\phi} < v < v_3^{z\phi} \end{cases} \tag{D.6}$$

with

$$v_0^{z\phi} = \frac{z_s - 1.5z_a}{\sqrt{2}} \tag{D.7}$$

$$v_1^{z\phi} = \frac{z_s - 0.5z_a}{\sqrt{2}} \tag{D.8}$$

$$v_2^{z\phi} = \frac{z_s + 0.5z_a}{\sqrt{2}} \tag{D.9}$$

$$v_3^{z\phi} = \frac{z_s + 1.5z_a}{\sqrt{2}} \tag{D.10}$$

and $z_s = z_m - z_n$. As the next step, converting the $\beta - \beta'$ domain integration into a $\tau - \psi$ domain integration using the change of variables given by (C.5)-(C.7) (see [38] for details), the final two-fold mutual impedance integral expression for $z\phi = \phi z$ case becomes

$$Z_{12z\phi} = \left(\frac{2}{z_a l_a \sin(k_a z_a) \sin(k_a l_a)}\right) \int_{\tau_0^{z\phi}}^{\tau_3^{z\phi}} T_{z\phi}(\tau) \left\{ \int_{v_0^{z\phi}}^{v_3^{z\phi}} V^{z\phi}(v) G_{z\phi 2} dv \right\} d\tau \tag{D.11}$$

where

$$T^{z\phi}(\tau) = \begin{cases} -\sin\left[k_a\left(\frac{3l_a}{2} - \beta_s + \tau\sqrt{2}\right)\right] & \tau_0^{z\phi} < \tau < \tau_1^{z\phi} \\ -2\cos\left(\frac{k_a l_a}{2}\right)\sin\left[k_a(\beta_s - \tau\sqrt{2})\right] & \tau_1^{z\phi} < \tau < \tau_2^{z\phi} \\ \sin\left[k_a\left(\frac{3l_a}{2} + \beta_s - \tau\sqrt{2}\right)\right] & \tau_2^{z\phi} < \tau < \tau_3^{z\phi} \end{cases} \tag{D.12}$$

with

$$\tau_0^{z\phi} = \frac{\beta_s - \frac{3l_a}{2}}{\sqrt{2}} \tag{D.13}$$

$$\tau_1^{z\phi} = \frac{\beta_s - \frac{l_a}{2}}{\sqrt{2}} \tag{D.14}$$

$$\tau_2^{z\phi} = \frac{\beta_s + \frac{l_a}{2}}{\sqrt{2}} \tag{D.15}$$

$$\tau_3^{z\phi} = \frac{\beta_s + \frac{3l_a}{2}}{\sqrt{2}} \tag{D.16}$$

and $\beta_s = \beta_m - \beta_n$.

D.2 Overlapping Term

In the course of evaluating the mutual impedance integral for the $z\phi$ case, the most singular situation is the overlapping case since the self term case does not exist for the $z\phi$ case. Similar to the zz case, the singular part for $Z_{12z\phi}$ is coming from the last term of (5.23) when (5.23) is substituted into (D.3). Ignoring the constants, the singular term can be written as

$$Z_{12z\phi} = \int_0^{2l_a}\int_0^{l_a}\int_0^{z_a}\int_0^{2z_a} \frac{\partial J_z}{\partial z}\frac{\partial J_{\phi'}}{\partial \phi'}\frac{1}{\sqrt{(\beta-\beta')^2+(z-z')^2}}dzdz'd\beta d\beta'. \quad \text{(D.17)}$$

In order to perform the four-fold integral given by (D.17) accurately and efficiently, first the integration with respect to z' is evaluated analytically given by

$$\int \frac{1}{\sqrt{(\beta-\beta')^2+(z-z')^2}}dz' = \sinh^{-1}\Big(\frac{z'-z}{|\beta-\beta'|}\Big) = \operatorname{csch}^{-1}\Big(\frac{|\beta-\beta'|}{z'-z}\Big). \quad \text{(D.18)}$$

Then, the β integral is evaluated analytically as given by

$$\begin{aligned}&\int \sinh^{-1}(\frac{z'-z}{|\beta-\beta'|})d\beta = I_{z\phi}(\beta,\beta',z,z') = \\ &= \left(\frac{|\beta-\beta'|}{z'-z}\sinh^{-1}(\frac{z'-z}{|\beta-\beta'|}) + \operatorname{sign}(\frac{|\beta-\beta'|}{z'-z})\sinh^{-1}(\frac{|\beta-\beta'|}{z'-z})\right)\operatorname{sign}(\beta'-\beta)(z-z').\end{aligned} \quad \text{(D.19)}$$

As a result of these steps, the mutual impedance integral given by (D.17) is now a two-fold integral given by

$$\begin{aligned}Z_{12z\phi} \;=\; &\int_0^{2l_a}\int_0^{2z_a}\frac{\partial J_z}{\partial z}\frac{\partial J_{\phi'}}{\partial \phi'}\Big[\Big(I_{z\phi}(l_a,\beta',z,2z_a)-I_{z\phi}(l_a,\beta',z,0)\Big)\\ &-\Big(I_{z\phi}(0,\beta',z,2z_a)-I_{z\phi}(0,\beta',z,0)\Big)\Big]dzd\beta\end{aligned} \quad \text{(D.20)}$$

where $I_{z\phi}(\beta,\beta',z,z')$ is given in (D.19).

(D.20) can be evaluated in an efficient way using a simple Gaussian quadrature algorithm and can be used for all cases that a possible singularity occurs (partially overlapping, touching through a corner or an edge, etc.).

D.3 Spectral Domain Singularity

Substituting (5.20) into (5.11) for $uv = z\phi$ $(= \phi z)$ and performing the IFTs, the singular part of the mutual impedance expression due to the spectral domain singularity appears as

$$Z_{12z\phi} = \int\int\int\int (-j)\frac{\partial J_z}{\partial z}(-j)\frac{\partial J_{\phi'}}{\partial \phi'}\log(|\beta - \beta'|)dzdz'd\beta d\beta' \qquad \text{(D.21)}$$

where the constants are not included. Singular part is the same as that of the zz case. Hence, (C.67) is used for the evaluation of the β integral. Then, the v integral (τ integral is not considered) given in (D.11) is used for the z and z' integrals in (D.21). Finally, the remaining β' and v integrals (v integral is obtained for (D.21) as given in (D.11)) are evaluated as two-fold integrals using a simple Gaussian quadrature algorithm.

Appendix E

Mutual Impedance Calculations ($\phi\phi$ case)

E.1 General Procedure for Mutual Impedance Calculations

Similar to the zz case, the mutual impedance calculation between two $\phi-$ directed current modes can be expressed as [see (5.8)]

$$Z_{12\phi\phi} = \int\int\int\int J_{\phi} J_{\phi'} G_{\phi\phi} dz dz' d\beta d\beta'. \tag{E.1}$$

Noticing that n^2 in the spectral domain corresponds to derivative with respect to ϕ and ϕ' in the space domain, the expression for the Green's function representation $G_{\phi\phi}$ can be written as

$$G_{\phi\phi} = \frac{\partial^2 G_{\phi\phi 2}}{\partial\phi\partial\phi'}. \tag{E.2}$$

Performing an integration by parts twice on (E.2) (also note that PWS current modes are differentiable and zero at the end points), the final mutual impedance expression becomes

$$Z_{12\phi\phi} = \int\int\int\int \frac{\partial J_{\phi}}{\partial\phi}\frac{\partial J_{\phi'}}{\partial\phi'} G_{\phi\phi 2} dz dz' d\beta d\beta'. \tag{E.3}$$

This four-fold integral for the $\phi\phi$ case can be reduced to a two-fold integral using the same methodology given for the zz case as explained in Appendix C.1. In the course of obtaining the final expressions for the $\phi\phi$ case z is changed by β and z' is changed by β'. Consequently, the final two-fold mutual impedance integral for the $\phi\phi$ case can be expressed as

$$Z_{12\phi\phi} = (\frac{1}{z_a \sin(k_a l_a)})^2 \int_{\tau_0}^{\tau_2} T_{\phi\phi}(\tau)\{I_{v1} + I_{v2} + I_{v3}\}d\tau \tag{E.4}$$

where

$$T_{\phi\phi}(\tau) = \begin{cases} -2\tau + (z_a + z_s)\sqrt{2} & \tau_1 \leq \tau < \tau_2 \\ 2\tau + (z_a - z_s)\sqrt{2} & \tau_0 \leq \tau < \tau_1 \end{cases} \tag{E.5}$$

with

$$\tau_0 = \frac{z_s - z_a}{\sqrt{2}} \tag{E.6}$$

$$\tau_1 = \frac{z_s}{\sqrt{2}} \tag{E.7}$$

$$\tau_2 = \frac{z_s + z_a}{\sqrt{2}} \tag{E.8}$$

and $z_s = z_m - z_n$ as defined in Appendix C. Furthermore, in (E.4) I_{v1}, I_{v2} and I_{v3} are defined as

$$I_{v1} = 2\int_{v_1}^{v_3} \Big\{ \cos[k_a(\beta_s - v\sqrt{2})]V_1^{\phi\phi}(v)G_{\phi\phi 2} + V_2^{\phi\phi}(v)G_{\phi\phi 2} \Big\} dv \tag{E.9}$$

$$I_{v2} = \int_{v_2}^{v_4} \Big\{ \cos[k_a(2l_a + \beta_s - v\sqrt{2})]V_3^{\phi\phi}(v)G_{\phi\phi 2} + V_4^{\phi\phi}(v)G_{\phi\phi 2} \Big\} dv \tag{E.10}$$

$$I_{v3} = \int_{v_0}^{v_2} \Big\{ \cos[k_a(2l_a - \beta_s + v\sqrt{2})]V_5^{\phi\phi}(v)G_{\phi\phi 2} + V_6^{\phi\phi}(v)G_{\phi\phi 2} \Big\} dv \tag{E.11}$$

with

$$V_1^{\phi\phi}(v) = \begin{cases} v - \frac{\beta_s - l_a}{\sqrt{2}} & v_1 < v < v_2 \\ -v + \frac{\beta_s + l_a}{\sqrt{2}} & v_2 < v < v_3 \end{cases} \tag{E.12}$$

$$V_2^{\phi\phi}(v) = \begin{cases} \frac{\cos(k_a l_a)}{k_a\sqrt{2}} \sin\left[k_a(-v\sqrt{2} - l_a + \beta_s)\right] & v_1 < v < v_2 \\ \frac{\cos(k_a l_a)}{k_a\sqrt{2}} \sin\left[k_a(v\sqrt{2} - l_a - \beta_s)\right] & v_2 < v < v_3 \end{cases} \tag{E.13}$$

$$V_3^{\phi\phi}(v) = \begin{cases} \frac{\beta_s - v\sqrt{2}}{\sqrt{2}} & v_2 < v < v_3 \\ \frac{-2l_a - \beta_s + v\sqrt{2}}{\sqrt{2}} & v_3 < v < v_4 \end{cases} \tag{E.14}$$

$$V_4^{\phi\phi}(v) = \begin{cases} -\frac{\sin\left[k_a(\beta_s - v\sqrt{2})\right]}{k_a\sqrt{2}} & v_2 < v < v_3 \\ \frac{\sin\left[k_a(2l_a + \beta_s - v\sqrt{2})\right]}{k_a\sqrt{2}} & v_3 < v < v_4 \end{cases} \tag{E.15}$$

$$V_5^{\phi\phi}(v) = \begin{cases} \frac{-2l_a + \beta_s - v\sqrt{2}}{\sqrt{2}} & v_0 < v < v_1 \\ \frac{-\beta_s + v\sqrt{2}}{\sqrt{2}} & v_1 < v < v_2 \end{cases} \tag{E.16}$$

$$V_6^{\phi\phi}(v) = \begin{cases} \frac{\sin\left[k_a(2l_a - \beta_s + v\sqrt{2})\right]}{k_a\sqrt{2}} & v_0 < v < v_1 \\ \frac{\sin\left[k_a(\beta_s - v\sqrt{2})\right]}{k_a\sqrt{2}} & v_1 < v < v_2 \end{cases} \tag{E.17}$$

and

$$v_0 = \frac{\beta_s - 2l_a}{\sqrt{2}} \tag{E.18}$$

$$v_1 = \frac{\beta_s - l_a}{\sqrt{2}} \tag{E.19}$$

$$v_2 = \frac{\beta_s}{\sqrt{2}} \tag{E.20}$$

$$v_3 = \frac{\beta_s + l_a}{\sqrt{2}} \tag{E.21}$$

$$v_4 = \frac{\beta_s + 2l_a}{\sqrt{2}}. \tag{E.22}$$

Finally $\beta_s = \beta_m - \beta_n$ as defined in Appendix C.1.

E.2 Overlapping Term

Similar to the zz case, the singular part of the mutual impedance expression, when two $\phi-$ directed current modes partially overlap with each other, is the last term of (5.23) which can be written as

$$Z_{12\phi\phi} = \int_0^{2l_a} \int_{-l_a}^{l_a} \int_{-z_a/2}^{z_a/2} \int_{-z_a/2}^{z_a/2} \frac{1}{s} \frac{\partial J_\phi}{\partial \phi} \frac{\partial J_{\phi'}}{\partial \phi'} dz dz' d\beta d\beta'. \tag{E.23}$$

where $\frac{1}{s}$ is defined in (C.32). For the $\phi\phi$ case, the corresponding integral given in (C.33) is obtained as

$$\begin{aligned} Z_{12\phi\phi} \;=\; & \int_0^{2l_a} \int_{-l_a}^{l_a} \left(t_3 \cos\Big[k_a(2l_a - |\beta' - l_a| - |\beta|)\Big] + t_4 \cos\Big[k_a(|\beta' - l_a| - |\beta|)\Big] \right) \\ & \left(2z_a \left[\log\Big(\frac{z_a}{\sqrt{2}} + \sqrt{(\frac{\beta' - \beta}{\sqrt{2}})^2 + \frac{z_a^2}{2}}\Big) - \log\Big|\frac{\beta' - \beta}{\sqrt{2}}\Big| \right] \right. \\ & \left. -2\sqrt{2}\left[\sqrt{\Big(\frac{\beta' - \beta}{\sqrt{2}}\Big)^2 + \frac{z_a^2}{2}} - \Big|\frac{\beta' - \beta}{\sqrt{2}}\Big| \right] \right) d\beta d\beta' \end{aligned} \tag{E.24}$$

where

$$t_3 = K\Big[\text{sign}(\beta)\text{sign}(\beta' - l_a)\Big] \tag{E.25}$$

$$t_4 = K\Big[\text{sign}(\beta)\text{sign}(\beta' - l_a)\Big] \tag{E.26}$$

$$K = \frac{-k_a \rho}{2\Big[z_a \sin(k_a l_a)\Big]^2}. \tag{E.27}$$

Following the same methodology given in Appendix C.2 and making use of [38] for the details, the final integral expression is given by

$$\begin{aligned} Z_{12\phi\phi} \;=\; & \int_0^{0.5} \Big\{ t_5 \sin(2k_a l_a \alpha) + t_6(1 - 2\alpha)\cos(2k_a l_a \alpha) \\ & + t_7 \alpha \cos\Big[k_a l_a(1 - 2\alpha)\Big] + t_8 \sin\Big[k_a l_a(1 - 2\alpha)\Big] \Big\} H^r(\alpha) d\alpha \\ & \int_{0.5}^{1} \Big\{ t_5 \sin\Big[2k_a l_a(1 - \alpha)\Big] - t_9(1 - 2\alpha)\cos\Big[k_a l_a(3 - 2\alpha)\Big] \end{aligned}$$

$$+t_7(1-\alpha)\cos\Big[k_a l_a(1-2\alpha)\Big] - t_{10}\sin\Big[k_a l_a(1-2\alpha)\Big]\Bigg\}H(\alpha)d\alpha$$
$$\int_1^{1.5}\Bigg\{t_9(3-2\alpha)\cos\Big[k_a l_a(3-2\alpha)\Big] + t_{10}\sin\Big[k_a l_a(3-2\alpha)\Big]\Bigg\}H(\alpha)d\alpha$$
$$+I_{p1} \tag{E.28}$$

where

$$H^r(\alpha) = \frac{z_a}{\sqrt{2}}\Big[\log\Big(\frac{z_a}{2}+\sqrt{l_a^2\alpha^2+\frac{z_a^2}{2}}\Big) - \log(l_a)\Big] - \sqrt{2}\Big[\sqrt{l_a^2\alpha^2+\frac{z_a^2}{2}} - l_a\alpha\Big] \tag{E.29}$$

and

$$H(\alpha) = \frac{z_a}{\sqrt{2}}\Big[\log\Big(\frac{z_a}{2}+\sqrt{l_a^2\alpha^2+\frac{z_a^2}{2}}\Big) - \log(l_a\alpha)\Big] - \sqrt{2}\Big[\sqrt{l_a^2\alpha^2+\frac{z_a^2}{2}} - l_a\alpha\Big]. \tag{E.30}$$

I_{p1} in (E.24) is defined as

$$\begin{aligned} I_{p1} &= -\frac{z_a}{\sqrt{2}}\Bigg\{\kappa_1\Big[\delta_1\log(\delta_1)-\delta_1\Big] + \kappa_2\Big[\frac{\delta_1^2}{2}\log(\delta_1) - \frac{\delta_1^2}{4}\Big] + \kappa_3\Big[\frac{\delta_1^3}{3}\log(\delta_1) - \frac{\delta_1^3}{9}\Big]\Bigg\} \\ &\quad -\frac{z_a}{\sqrt{2}}\int_{\delta_1}^{0.5}\Bigg\{t_5\sin(2k_a l_a\alpha) + t_6(1-2\alpha)\cos(2k_a l_a\alpha) \\ &\quad +t_7\alpha\cos\Big[k_a l_a(1-2\alpha)\Big] + t_8\sin\Big[k_a l_a(1-2\alpha)\Big]\Bigg\}\log(\alpha)d\alpha \end{aligned} \tag{E.31}$$

and δ_1 is a small number which is chosen as $(2k_a l_a\delta_1) << 1$. The other parameters in (E.24)-(E.31) are defined as

$$\kappa_1 = t_6 + t_8\sin(k_a l_a) \tag{E.32}$$
$$\kappa_2 = 2t_5 k_a l_a - 2t_6 + t_7\cos(k_a l_a) - 2t_8 k_a l_a\cos(k_a l_a) \tag{E.33}$$
$$\kappa_3 = 2t_7 k_a l_a\sin(k_a l_a) \tag{E.34}$$
$$t_5 = \frac{8\sqrt{2}l_a}{k_a}\cos(k_a l_a)t_{3+} \tag{E.35}$$
$$t_6 = 8\sqrt{2}l_a^2\cos(k_a l_a)t_{3-}$$

$$t_7 = 16\sqrt{2}l_a^2 t_{4+} \tag{E.36}$$

$$t_8 = \frac{8\sqrt{2}l_a}{k_a} t_{4-} \tag{E.37}$$

$$t_9 = 4\sqrt{2}l_a^2 t_{3-} \tag{E.38}$$

$$t_{10} = \frac{4\sqrt{2}l_a}{k_a} t_{4-}. \tag{E.39}$$

In this expressions, t_{3+} and t_{4+} mean that $\text{sign}(\beta)\text{sign}(\beta' - l_a)$ is positive where t_{3-} and t_{4-} mean that $\text{sign}(\beta)\text{sign}(\beta' - l_a)$ is negative.

E.3 Self Term

Similar to the zz case, explained in Appendix C.3, the singular part of the self impedance (i.e., mutual impedance when source and field points overlap with each other), $Z_{12\phi\phi}$, integral can be written as

$$Z_{12\phi\phi} = \int_{-l_a}^{l_a}\int_{-l_a}^{l_a}\int_{-z_a/2}^{z_a/2}\int_{-z_a/2}^{z_a/2} \frac{1}{s}\frac{\partial J_\phi}{\partial \phi}\frac{\partial J_{\phi'}}{\partial \phi'} dz dz' d\beta d\beta'. \tag{E.40}$$

Following the same methodology given in Appendix C.2 and C.3 and making use of [38] for the details, the final integral expression is given by

$$\begin{aligned} Z_{12\phi\phi} \;=\; & \int_0^{0.5} \Big\{ c_3 \sin\Big[k_a l_a(1-2\alpha)\Big] + c_4\alpha\cos\Big[k_a 2l_a(1-\alpha)\Big] \\ & + c_5(1-2\alpha)\cos(2k_a l_a\alpha) + c_6\sin(2k_a l_a\alpha)\Big\} H^r(\alpha)d\alpha \\ & \int_{0.5}^{1} \Big\{ c_4(1-\alpha)\cos\Big[2k_a l_a(1-\alpha)\Big] + c_6\sin\Big[2k_a l_a(1-\alpha)\Big]\Big\} H(\alpha)d\alpha \\ & + I_{p2} \end{aligned} \tag{E.41}$$

with

$$\begin{aligned} I_{p2} \;=\; & -\frac{z_a}{\sqrt{2}}\Big\{ d_1\Big[\delta_2\log(\delta_2) - \delta_2\Big] + d_2\Big[\frac{\delta_2^2}{2}\log(\delta_2) - \frac{\delta_2^2}{4}\Big] + d_3\Big[\frac{\delta_2^3}{3}\log(\delta_2) - \frac{\delta_2^3}{9}\Big]\Big\} \\ & -\frac{z_a}{\sqrt{2}}\int_{\delta_2}^{0.5} \Big\{ c_3\sin\Big[k_a l_a(1-2\alpha)\Big] + c_4\alpha\cos\Big[k_a 2l_a(1-\alpha)\Big] \\ & + c_5(1-2\alpha)\cos(2k_a l_a\alpha) + c_6\sin(2k_a l_a\alpha)\Big\}\log(\alpha)d\alpha \end{aligned} \tag{E.42}$$

In (E.42), δ_2 is a small number where $(2k_a z_a \delta_2) << 1$. The other parameters in (E.41)-(E.42) are given as

$$d_1 = c_3 \sin(k_a l_a) + c_5 \tag{E.43}$$

$$d_2 = -2c_3 k_a l_a \cos(k_a l_a) + c_4 \cos(2k_a l_a) - 2c_5 + 2c_6 k_a l_a \tag{E.44}$$

$$d_3 = 2c_4 k_a l_a \sin(2k_a l_a) \tag{E.45}$$

$$c_3 = \frac{l_a 16\sqrt{2}}{k_a} \cos(k_a l_a) c_{1+} \tag{E.46}$$

$$c_4 = l_a^2 16\sqrt{2} c_{1-} \tag{E.47}$$

$$c_5 = l_a^2 16\sqrt{2} c_{2+} \tag{E.48}$$

$$c_6 = \frac{l_a 8\sqrt{2}}{k_a} c_{2-} \tag{E.49}$$

$$c_1 = K\Big[\text{sign}(\beta)\text{sign}(\beta')\Big] \tag{E.50}$$

$$c_2 = K\Big[\text{sign}(\beta)\text{sign}(\beta')\Big]. \tag{E.51}$$

Similar to the overlapping case, c_{1+} and c_{2+} mean that $\text{sign}(\beta)\text{sign}(\beta')$ is positive. Also c_{1-} and c_{2-} mean that $\text{sign}(\beta)\text{sign}(\beta')$ is negative. $H^r(\alpha)$ and $H(\alpha)$ are given in (E.29) and (E.30), respectively.

E.4 Spectral Domain Singularity

Substituting (5.20) into (5.12) for $uv = \phi\phi$ and performing the IFTs, the singular part of the mutual impedance expression due to the spectral domain singularity appears as

$$Z_{12\phi\phi} = \int\int\int\int \frac{\partial J_\phi}{\partial \phi} \frac{\partial J_{\phi'}}{\partial \phi'} \log(|\beta - \beta'|) dz dz' d\beta d\beta' \tag{E.52}$$

where the constants are not included. Since the spectral domain singularity is related with $(\beta - \beta')$ and the current modes are dependent on ϕ and ϕ' (or β and β') the solution for the spectral domain singularity given for the zz case can not be used for the $\phi\phi$ case. Therefore, let the center points of the $J_{\phi'}$ and J_ϕ current modes (both of them have dimensions $2l_a \times z_a$) be at β_m, z_m and β_n, z_n, respectively. The spectral domain singularity in (E.52) appears in two different

cases. In the first case, the singularity appears when $\beta_m - \beta_n = l_a$ regardless of $z_m - z_n$. For this case (E.52) can be written as

$$Z_{12\phi\phi} = \int_0^{2l_a} \int_{-l_a}^{l_a} \int\int \frac{\partial J_\phi}{\partial \phi} \frac{\partial J_{\phi'}}{\partial \phi'} \log(|\beta - \beta'|) dz dz' d\beta d\beta'. \tag{E.53}$$

Performing the z and z' integrals (the integrand does not depend on z and z' and the width of both current modes are z_a), (E.53) is reduced to

$$\begin{aligned} Z_{12\phi\phi} &= \int_0^{2l_a} \int_{-l_a}^{l_a} \left(t_3 \cos\Big[k_a(2l_a - |\beta' - l_a| - |\beta|)\Big] + t_4 \cos\Big[k_a(|\beta' - l_a| - |\beta|)\Big] \right) \\ &\quad \left(z_a^2 \log(|\beta - \beta'|) \right) d\beta d\beta' \end{aligned} \tag{E.54}$$

where t_3 and t_4 are defined in (E.25) and (E.26). Note that (E.54) is similar to (E.24). In (E.24), the corresponding integrand for $z_a^2 \log(|\beta - \beta'|)$ term is

$$\begin{aligned} H_t &= \left(2z_a \left[\log\Big(\frac{z_a}{\sqrt{2}} + \sqrt{(\frac{\beta' - \beta}{\sqrt{2}})^2 + \frac{z_a^2}{2}}\Big) - \log\Big|\frac{\beta' - \beta}{\sqrt{2}}\Big| \right] \right. \\ &\quad \left. -2\sqrt{2}\left[\sqrt{\Big(\frac{\beta' - \beta}{\sqrt{2}}\Big)^2 + \frac{z_a^2}{2}} - \Big|\frac{\beta' - \beta}{\sqrt{2}}\Big| \right] \right). \end{aligned} \tag{E.55}$$

Using (C.37) and (C.13) (also changing z, z', z_a and l_a for the zz case with β, β', l_a and z_a is necessary), when $2l_a\alpha$ is substituted instead of $\beta' - \beta$ in (E.55), the following is obtained.

$$H_t|_{(\beta' - \beta) = 2l_a\alpha} = 2\sqrt{2} H(\alpha) \tag{E.56}$$

where $H(\alpha)$ is given in (E.30). Therefore, for the $z_a^2 \log(|\beta - \beta'|)$ term, the corresponding $H(\alpha)$ and $H^r(\alpha)$ expressions (substituting $2l_a\alpha$ instead of $\beta' - \beta$) can be defined as

$$H(\alpha) = \frac{z_a^2}{\sqrt{2}} \log(2l_a\alpha) \tag{E.57}$$

$$H^r(\alpha) = \frac{z_a^2}{\sqrt{2}} \log(2l_a). \tag{E.58}$$

As a result, for the numerical evaluation of (E.53) or (E.54), the expression given in (E.28) is used with the $H(\alpha)$ and $H^r(\alpha)$ expressions given in (E.57) and (E.58).

The spectral singularity also appears when $\beta_m = \beta_n$ (the second case) as given in the following expression

$$Z_{12\phi\phi} = \int_{-l_a}^{l_a} \int_{-l_a}^{l_a} \int\int \frac{\partial J_\phi}{\partial \phi} \frac{\partial J_{\phi'}}{\partial \phi'} \log(|\beta - \beta'|) dz dz' d\beta d\beta'. \tag{E.59}$$

As explained for the $\beta_m - \beta_n = l_a$ case, in the course of the numerical evaluation of (E.59), (E.41) is used with the $H(\alpha)$ and $H^r(\alpha)$ expressions given in (E.57) and (E.58), respectively.

Appendix F

Even and Odd Properties of Green's Functions and Mutual Impedance

In this dissertation, even and odd properties of the Green's function components are used in order to increase the efficiency of the computation procedure. Table F.1 depicts the even and odd properties of the components of the spectral and the space domain Green's function representations with respect to k_z or $\Delta z = (z - z')$ and $\Delta\phi = (\phi - \phi')$, respectively. In the spectral domain, the summation with

	$k_z/\Delta z$	$n/\Delta\phi$
$\tilde{G}_{zz}/G_{zz}$	even	even
$\tilde{G}_{z\phi}/G_{z\phi}$	odd	odd
$\tilde{G}_{\phi z}/G_{\phi z}$	odd	odd
$\tilde{G}_{\phi\phi}/G_{\phi\phi}$	even	even
$\tilde{G}_{z\rho}/G_{z\rho}$	odd	even
$\tilde{G}_{\phi\rho}/G_{\phi\rho}$	even	odd
$\tilde{G}_{\rho z}/G_{\rho z}$	odd	even
$\tilde{G}_{\rho\phi}/G_{\rho\phi}$	even	odd

Table F.1: Even and odd properties of the components of the spectral and the space domain Green's function representations

	$\Delta z, \Delta\phi$	$-\Delta z, \Delta\phi$	$\Delta z, -\Delta\phi$	$-\Delta z, -\Delta\phi$
Z_{12zz}	a_{zz}	a_{zz}	a_{zz}	a_{zz}
$Z_{12z\phi}$	$a_{z\phi}$	$-a_{z\phi}$	$-a_{z\phi}$	$a_{z\phi}$
$Z_{12\phi z}$	$a_{z\phi}$	$-a_{z\phi}$	$-a_{z\phi}$	$a_{z\phi}$
$Z_{12\phi\phi}$	$a_{\phi\phi}$	$a_{\phi\phi}$	$a_{\phi\phi}$	$a_{\phi\phi}$
$V_{z\rho}$	$a_{z\rho}$	$-a_{z\rho}$	$a_{z\rho}$	$-a_{z\rho}$
$V_{\rho z}$	$-a_{z\rho}$	$a_{z\rho}$	$-a_{z\rho}$	$a_{z\rho}$
$V_{\phi\rho}$	$a_{\phi\rho}$	$a_{\phi\rho}$	$-a_{\phi\rho}$	$-a_{\phi\rho}$
$V_{\rho\phi}$	$-a_{\phi\rho}$	$-a_{\phi\rho}$	$a_{\phi\rho}$	$a_{\phi\rho}$

Table F.2: Even and odd properties of mutual impedance

respect to the cylindrical eigenmodes n that ranged from $-\infty$ to ∞ are folded to range from 0 to ∞ using the third column of Table F.1. Similarly, in the course of obtaining the space domain Green's function representations the k_z integral is evaluated over the range from 0 to ∞ using Table F.1. In Table F.1, the even and odd properties of the space domain Green's functions are also given for the sake of completeness.

In the MoM analysis of antennas or arrays, Table F.2 is used in order to obtain the impedance matrix and the voltage vector efficiently. In Table F.2, the even and odd properties of the mutual impedances are given. In the MoM analysis, only one of the four different (Δz, $\Delta\phi$) combinations is computed. For the other combinations, Table F.2 is used in order to increase the efficiency of the MoM analysis.

Bibliography

[1] D. M. Pozar, "Input impedance and mutual coupling of rectangular microstrip antennas," *IEEE Trans. Antennas Propagat.*, vol. 30, pp. 1191–1196, 1984.

[2] J. R. Mosig, "Arbitrarily shaped microstrip structures and their analysis with a mixed-potential integral equation," *IEEE Trans. Microwave Theory Tech.*, vol. 36, pp. 314–323, 1988.

[3] Y. L. Chow, J. J. Yang, D. F. Fang, and G. E. Howard, "A closed-form spatial Green's function for the thick microstrip substrate," *IEEE Trans. Microwave Theory Tech.*, vol. 39, pp. 588–592, 1991.

[4] M. I. Aksun and R. Mittra, "Derivation of closed-form Green's functions for a general microstrip geometry," *IEEE Trans. Microwave Theory Tech.*, vol. 40, pp. 2055–2062, 1992.

[5] G. Dural and M. I. Aksun, "Closed-form Green's functions for general sources and stratified media," *IEEE Trans. Microwave Theory Tech.*, vol. 43, pp. 1545–1552, 1995.

[6] M. I. Aksun, "A robust approach for the derivation of closed-form Green's functions," *IEEE Trans. Microwave Theory Tech.*, vol. 44, pp. 651–658, 1996.

[7] M. I. Aksun and G. Dural, "Clarification of issues on the closed-form Green's functions in stratified media," *IEEE Trans. Antennas Propagat.*, vol. 53, pp. 3644–3653, 2005.

[8] J. R. Lovell and W. C. Chew, "Response of a point source in a multicylindrically layered medium," *IEEE Trans. Geosci. Remote Sensing*, vol. TGRS-25, pp. 850–858, 1987.

[9] L. W. Pearson, "A construction of the fields radiated by z-directed point sources of current in the presence of a cylindrically layered obstacle," *Radio Sci.*, vol. 21, pp. 559–569, 1986.

[10] K. Naishadham and L. B. Felsen, "Dispersion of waves guided along a cylindrical substrate-superstrate layered medium," *IEEE Trans. Antennas Propagat.*, vol. 41, pp. 304–313, 1993.

[11] Z. Xiang and Y. Lu, "Electromagnetic dyadic Green's function in cylindrically multilayered media," *IEEE Trans. Microwave Theory Tech.*, vol. 44, pp. 614–621, 1996.

[12] P. S. Kildal, S. Rengarajan, and A. Moldsvor, "Analysis of nearly cylindrical antennas and scattering problems using a spectrum of two-dimensional solutions," *IEEE Trans. Antennas Propagat.*, vol. 44, pp. 1183–1192, 1996.

[13] P. S. Kildal, Z. Sipus, and M. Johansson, "Analysis of antennas on a curved multilayer structure by using the G1DMULT routine," *IEEE APS International Symposium and URSI Radio Science Meeting Digest*, vol. 3, pp. 1500–1503, 1997.

[14] W. C. Chew, *Waves and Fields in Inhomogeneous Media.* New York: Van Nostrand Reinhold, 1990.

[15] K. L. Wong, *Design of Nonplanar Microstrip Antennas and Transmission Lines.* New York: John Wiley & Sons, Inc, 1999.

[16] L. Josefsson and P. Persson, *Conformal Array Antenna Theory and Design.* New Jersey: John Wiley & Sons, Inc, 2006.

[17] Ç. Tokgöz, "Derivation of closed-form Green's functions for cylindrically stratified media," Master's thesis, Middle East Technical Univ. Dept. Elect. Electron. Eng., 1997.

[18] Ç. Tokgöz and G. Dural, "Closed-form Green's functions for cylindrically stratified media," *IEEE Trans. Microwave Theory Tech.*, vol. 48, pp. 40–49, 2000.

[19] J. Sun, C. F. Wang, L. W. Li, and M. S. Leong, "A complete set of spatial-domain dyadic Green's function components for cylindrically stratified media in fast computational form," *J. of Electromagn. Waves and Appl.*, vol. 16, pp. 1491–1509, 2002.

[20] R. C. Acar and G. Dural, "Comments on a complete set of spatial-domain dyadic Green's function components for cylindrically stratified media in fast computational form," *J. of Electromagn. Waves and Appl.*, vol. 18, pp. 1389–1394, 2004.

[21] J. Sun, C. F. Wang, L. W. Li, and M. S. Leong, "Reply to comments on a complete set of spatial-domain dyadic Green's function components for cylindrically stratified media in fast computational form," *J. of Electromagn. Waves and Appl.*, vol. 18, pp. 1395–1398, 2004.

[22] M. He and X. Xu, "Closed-form solutions for analysis of cylindrically conformal microstrip antennas with arbitrary radii," *IEEE Trans. Antennas Propagat.*, vol. 53, pp. 518–525, 2005.

[23] J. Sun, C. F. Wang, L. W. Li, and M. S. Leong, "Further improvement for fast computation of mixed potential Green's functions for cylindrically stratified media," *IEEE Trans. Antennas Propagat.*, vol. 52, pp. 3026–3036, 2004.

[24] R. C. Acar and G. Dural, "Complete set of closed-form Green's functions for cylindrically layered media," *IEEE AP-S International Symposium and USNC/URSI National Radio Science and AMEREM Meetings*, vol. -, pp. –, 2006.

[25] S. Karan, V. B. Erturk, and A. Altintas, "Closed-form Green's function representations in cylindrically stratified media for method of moments applications," *European Conference on Antennas and Propagation*, vol. -, pp. –, 2006.

[26] S. Karan, "Closed-form Green's functions in cylindrically stratified media for method of moments applications," Master's thesis, Bilkent Univ. Dept. Elect. Electron. Eng., 2006.

[27] S. Karan, V. B. Erturk, and A. Altintas, "Closed form Green's function representations in cylindrically stratified media for method of moments applications," *IEEE Trans. Antennas Propagat.*, vol. 57, pp. 1158–1166, 2009.

[28] J. Wu, S. K. Khamas, and G. G. Cook, "An efficient asymptotic extraction approach for the Green's functions of conformal antennas in multilayered cylindrical media," *IEEE Trans. Antennas Propagat.*, vol. 58, pp. 3737–3742, 2010.

[29] E. H. Newman, "An overview of the hybrid MM/Green's function method in electromagnetics," *Proc. IEEE*, vol. 76, pp. 270–282, 1988.

[30] V. B. Erturk and R. G. Rojas, "Efficient analysis of input impedance and mutual coupling of microstrip antennas mounted on large coated cylinders," *IEEE Trans. Antennas Propagat.*, vol. 51, pp. 739–749, 2003.

[31] V. B. Erturk, *Efficient hybrid MoM/Green's function technique to analyze conformal microstrip antennas and arrays*. PhD thesis, The Ohio-State University Dept. of Electrical Engineering, 2000.

[32] Y. Hua and T. K. Sarkar, "Generalized pencil-of-function method for extracting poles of an EM system from its transient response," *IEEE Trans. Antennas Propagat.*, vol. 37, pp. 229–234, 1989.

[33] C. Y. Huang and Y. T. Chang, "Curvature effects on the mutual coupling of cylindrical-rectangular microstrip antennas," *Electron. Lett.*, vol. 33, pp. 1108–1109, 1997.

[34] M. Abramowitz and I. A. Stegun, *Handbook of Mathematical Functions with Formulas, Graphs, and Mathematical Tables*. Washington, D.C., 1970.

[35] M. L. V. Blaricum and R.Mittra, "A technique for extracting the poles and residues of a system directly from its transient response," *IEEE Trans. Antennas Propagat.*, vol. AP-23, pp. 777–781, 1975.

[36] M. L. V. Blaricum and R. Mittra, "Problem and solutions associated with prony's method for processing transient data," *IEEE Trans. Antennas Propagat.*, vol. AP-26, pp. 174–182, 1978.

[37] V. K. Jain, T. K. Sarkar, and D. D. Weiner, "Rational modeling by pencil-of-function method," *IEEE Trans. on Acoust ., Sppech, Signal Processing*, vol. ASSP-31, pp. 564–573, 1983.

[38] O. Bakir, "Investigation of finite phased arrays of printed antennas on planar and cylindrical grounded dielectric slabs," Master's thesis, Bilkent Univ. Dept. Elect. Electron. Eng., 2006.